



**MONTCLAIR STATE**  
UNIVERSITY

Montclair State University  
**Montclair State University Digital  
Commons**

---

Theses, Dissertations and Culminating Projects

---

7-2010

## Rock Magnetic and Remanence Properties of Both Synthetic Martian Basaltic Intrusions and Dropstones Along the East Antarctic Margin, to Aid in the Understanding of the Carriers of Crustal Magnetic Anomalies

David Michael Cuomo Jr.  
*Montclair State University*

Follow this and additional works at: <https://digitalcommons.montclair.edu/etd>



Part of the [Earth Sciences Commons](#), and the [Environmental Sciences Commons](#)

---

### Recommended Citation

Cuomo, David Michael Jr., "Rock Magnetic and Remanence Properties of Both Synthetic Martian Basaltic Intrusions and Dropstones Along the East Antarctic Margin, to Aid in the Understanding of the Carriers of Crustal Magnetic Anomalies" (2010). *Theses, Dissertations and Culminating Projects*. 806.  
<https://digitalcommons.montclair.edu/etd/806>

This Thesis is brought to you for free and open access by Montclair State University Digital Commons. It has been accepted for inclusion in Theses, Dissertations and Culminating Projects by an authorized administrator of Montclair State University Digital Commons. For more information, please contact [digitalcommons@montclair.edu](mailto:digitalcommons@montclair.edu).

MONTCLAIR STATE UNIVERSITY

Rock magnetic and remanence properties of synthetic Martian basalts and dropstones from the East Antarctic margin: Understanding the carriers of crustal magnetic anomalies

by

David Michael Cuomo Jr

A Master's Thesis Submitted to the Faculty of  
Montclair State University


In Partial Fulfillment of the Requirements  
For the Degree of  
Master of Science

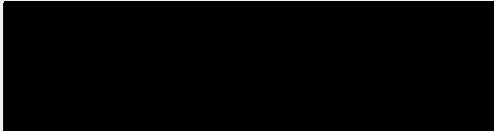
July 2010

College/School College of Science and Mathematics

Thesis Committee:

Department Earth & Environmental Studies


  
Dr. Stefanie Brachfeld  
Thesis Sponsor

  
Dr. Robert Prezant  
Dean

  
Dr. Sandra Passchier  
Committee Member

8/2/10  
Date

  
Dr. Matthew Goring  
Committee Member

  
Dr. Matthew L. Goring  
Chair of  
Earth and Environmental Studies

ROCK MAGNETIC AND REMANENCE PROPERTIES OF BOTH SYNTHETIC MARTIAN  
BASALTIC INTRUSTIONS AND DROPSTONES ALONG THE EAST ANTARCTIC  
MARGIN, TO AID IN THE UNDERSTANDING OF THE CARRIERS OF CRUSTAL  
MAGNETIC ANOMALIES

A THESIS

Submitted in partial fulfillment of the requirements  
for the degree of Masters of Science

by

DAVID MICHAEL CUOMO JR

Montclair State University

Montclair, NJ

2010

Copyright © 2010 by *David Michael Cuomo Jr.* All rights reserved.

## TABLE OF CONTENTS

### **Chapter 1: Rock Magnetic and Remanence Properties of Synthetic Martian Basaltic Intrusions: Implications for Mars crustal anomalies**

<b>INTRODUCTION</b>	<b>1 - 3</b>
<b>METHODS</b>	<b>3 - 7</b>
Petrologic Methods	3
Sample Nomenclature	4
Magnetic Susceptibility	5
Remanent Magnetization Measurements	6
Magnetic Hysteresis	6
Thermo-magnetic Measurements	7
<b>RESULTS</b>	<b>8 - 13</b>
Petrologic and Chemical Description of Iron Oxides	8
Magnetic Susceptibility	10
Magnetic Remanence	10
Anhyseretic Remanent Magnetization	10
Magnetic Hysteresis	11
Curie Point Determination	12
<b>DISCUSSION</b>	<b>13 - 20</b>
<b>CONCLUSIONS</b>	<b>20 - 21</b>
<b>REFERENCES</b>	<b>22 - 24</b>
Chapter 1 Figures	25 - 38
Chapter 1 Tables	39 - 41

## **Chapter 2: Rock Magnetic and Remanence Properties of East Antarctic Dropstones: to aid the interpretation of Antarctic magnetic studies**

<b>INTRODUCTION</b>	<b>42 - 44</b>
<b>METHODS</b>	<b>44 - 65</b>
Sample Nomenclature	44
Optical Microscopy	45
Electron Microscopy	45
Magnetic Susceptibility	46
Magnetic Remanence Measurements	47
Magnetic Hysteresis	47
Magnetic susceptibility as a function of Temperature	48
<b>RESULTS</b>	<b>48 - 63</b>
Meta-Granites of MacRobertson Land	48
Prydz Bay Amphibolite	50
Prydz Bay Quartz Alkali Feldspar Syenite	51
Prydz Bay Meta Granite	52
Prydz Bay Orthopyroxene Granite	54
Prydz Bay Quartzite	56
George V Coast Metapelites	57
George V Coast Meta Granite	62
George V Coast Mafic Igneous	63
<b>DISCUSSION</b>	<b>65 - 72</b>
<b>CONCLUSIONS</b>	<b>72 - 74</b>
<b>REFERENCES</b>	<b>74</b>
Chapter 2 Figures	75 - 92
Chapter 2 Tables	93 - 94

Appendix 1: Petrography of Dropstones of the  
East Antarctic Margin

95-113

## ACKNOWLEDGEMENTS

We would like to acknowledge Lisa Tatsumi Petrochilos and Julia Hammer for the synthesis and petrographic analysis of the Martian analogs. Julie Bowles for her input on the interpretation of Mars analogs. Ken Kodama for kindly letting us use his facilities for NRM and ARM demag measurements of the Mars basalts and Dennis Kent for allowing us to use his facilities for remanence measurements of the Antarctic samples.

I am very grateful for the support of my fellow graduate students and family. I am grateful for the members of my committee and professors that provided edits and insight into this thesis. For Matthew Gorrington for providing me a home in his office and valuable conversation about research. And I am especially grateful for my advisor Stefanie Brachfeld, for introducing me to the subject of rock magnetism, teaching me how to conduct scientific research, and displaying an enormous amount of patience while I learned and grew throughout this process.

This research is supported by NASA award# NAG5-12486 and MFR04-0000-0021, and NSF award# 0348274.



## ABSTRACT

This thesis examines potential carriers of magnetic anomalies found in remote areas where direct sampling is impossible. The areas examined are the southern hemisphere of Mars and the East Antarctic Margin. We examine the rock magnetic and remanence properties of synthetic Mars basalts and Antarctic dropstones, to predict the type and intensity of anomaly they would produce.

The anomalies measured within the Martian crust are entirely remanent magnetization and are remarkably orders of magnitude stronger than the strongest terrestrial anomaly. Two basalt compositions denoted M-type and T-type, deemed relevant to the crust of Mars, were synthesized to examine contrasts in rock magnetic and remanence properties following identical thermal histories and oxygen fugacity conditions. We examine the magnetic mineral assemblages produced and assess if they are efficient remanence carriers. The composition denoted T-type is rich in Al and poor in Fe, reflecting constraints provided by thermal emission spectroscopy that the Martian crust is somewhat terrestrial in character. The M-type composition is poor in Al and rich in Fe, reflecting the composition of basaltic liquid in equilibrium with Martian meteorite phase assemblages. The two compositions are identical with respect to MgO, SiO<sub>2</sub>, and TiO<sub>2</sub>. Batches of each composition were cooled from above 1200 °C to 1070 °C at 4 °C/h and annealed at 1070°C for 100 h, then quenched. Samples were then held at 650°C for periods ranging from 21 to 158 days under quartz-fayalite-magnetite (QFM) *f*O<sub>2</sub> buffer conditions, then quenched. The experimental conditions are germane to shallow igneous intrusions, which might be a significant volumetric fraction of the Martian crust and potential carriers of crustal magnetic anomalies, and provide an important contrast to a previous set of fast-cooled (3-230 °C/h) basalts our group performed on the same two compositions.

M-type samples contain Fe-Ti-Al-Mg oxide grains 40-50 µm in diameter with skeletal and equant euhedral morphologies. T-type samples contain equant euhedral Fe-Ti-Al-Mg oxides with grain diameters ranging from 15-30 µm as well as elongated anhedral ilmenite grains. For M-type samples both the starting material and the samples annealed at 650 °C have narrow multidomain hysteresis loops. T-type starting materials and samples annealed at 650 °C have pseudo single domain (PSD) hysteresis loops, but the annealed samples plot lower and to the right within the PSD field on a Day plot, indicating coarser magnetic grains. Alternating field demagnetization of anhysteretic remanent magnetization (ARM) shows median destructive fields < 10 mT. M-type samples exhibited higher magnetic susceptibility and intensity of remanence than T-type samples. Both M-type and T-type samples carry an intense natural remanent magnetization (NRM). The NRM is inferred to be a thermoremanent magnetization (TRM) acquired during quenching and air-cooling after the 650 °C anneal. NRM values range from 0.03 to 170 mA<sup>2</sup>/kg for M-type samples and 0.005 to 47 mA<sup>2</sup>/kg for T-type samples, values comparable to those observed in rapidly cooled synthetic basalts of the same chemical composition. However, the slow-cooled samples have a much "softer" coercivity spectrum. The multi-domain magnetic mineral assemblage suggests that while intrusions generated by slow-cooled basaltic melts are capable of carrying intense TRMs they may be less stable over geologic time.

The second portion of this study presents a catalog of the magnetic and petrographic properties of dropstones collected by United States Antarctic Program cruise NBP01-01. These dropstones provide direct samples of the subglacial geology and provide a range of susceptibility values, intensity of natural remanent magnetization, and description of the carriers of magnetization, which can help in the interpretation of magnetic anomaly surveys. Samples were collected in three main regions along the East Antarctic Margin, including the George V Coast, Prydz Bay, and MacRobertson Land. The samples are examined and classified optically through thin section analysis, and characterized magnetically through magnetic susceptibility, natural remanent magnetization, magnetic hysteresis, scanning electron microscopy and thermomagnetic measurements. The potential for each sample to generate a dominant induced or remnant magnetization was calculated using the Königsberger ratio,  $Q$ ; where  $Q = \text{Total Remnant Magnetization} / \text{Total Induced Magnetization}$ . The majority of magnetic minerals are found in low abundances (<1%) in granitic and metamorphic rocks and displayed  $Q$  values less than 1, suggesting they would produce induced dominated anomalies. The exception to this are two mafic igneous rocks, vesicular basalt and dolerite, that possess single domain magnetic minerals and recorded remanences several orders of magnitude higher than other east Antarctic rock types.

# **Rock Magnetic and Remanence Properties of Synthetic Martian Basaltic Intrusions: Implications for Mars crustal anomalies**

## **INTRODUCTION**

The following study investigates igneous analogs created to examine the carriers of magnetization found in the southern hemisphere of Mars. The Mars Global Surveyor MAG/ER experiment measured the highly cratered southern hemisphere of Mars to possess a distinct, intense magnetization (Acuña et al., 1998, 1999). This is of interest as Mars currently does not have a geodynamo field that could induce crustal magnetization. Therefore, the magnetic signal measured is entirely a remanent magnetization, and the intensity of remanence is remarkably more than 10 times stronger than terrestrial anomalies (Acuña, et. al. 1998, 1999 and references therein). Impact crater size-frequency distributions estimate the age of the crust surrounding the anomalies to be at least 4 Ga. This suggests that the rocks have cooled through their Curie temperature sometime in the early Martian history, when it most likely had a dynamo system creating a planetary magnetic field.

The intensity of the ancient Martian magnetic field is seen in Martian meteorite ALH84001. Meteorite ALH84001, which contains single domain particles dated at roughly 4 Ga, carry a remanence that suggest a field intensity to be within an order of magnitude of the present day Earth (Weiss, et al. 2002, Antretter, et al., 2003). In this respect, the magnetic mineral assemblage found within rocks of the southern hemisphere must be extremely efficient recorders of magnetic fields and also be 'magnetically hard' enough to remain stable over long geologic time scales. Several magnetic mineral assemblages have been proposed to explain the carrier of remanent magnetization. These

include but are not limited to: decomposition of siderite into magnetite (Scott and Fuller, 2004), the presence of multidomain hematite as the recorder (Dunlop and Kletetschka, 2001), and exsolution features subdividing multidomain (MD) grains into stable single domain (SSD) regions, i.e., lamellar magnetism (McEnroe et al., 2004). This study examines the magnetic properties of igneous analogs thought to bracket the chemistry of the Martian crust and is the third in a series of experimental studies to explain the Martian anomalies; previous work simulate rapidly cooled lavas and were performed by Brachfeld and Hammer (2006) and Bowles et al., (2009).

In this experiment, rocks of proposed Martian composition were synthesized experiencing variable annealing periods ranging from 21 to 158 days in an effort to simulate the crystallization of shallow igneous intrusions, which may be a significant volumetric fraction of the Martian crust and potential carriers of crustal magnetic anomalies. The original motivation of annealing the material was to produce spinel oxide exsolution. This type of exsolution results in compositional unmixing of titanium-rich and titanium-poor sections within titanomagnetite crystals. Magnetically the individual regions behave in a single domain or pseudo-single domain like manner and are optimal recorders of planetary fields (Evans and Wayman, 1974) and therefore they can be considered as a candidate for the intensely magnetic igneous bodies on Mars. Preliminary magnetic and microscopy results showed no evidence of compositional unmixing due to not ideal oxidizing conditions (Tatsumi-Petrochilos, 2010). Accordingly, the goal of this study was changed to the focus on properties of slow-cooled shallow igneous intrusions of Martian composition, and provided an opportunity for a comparison to early

experiments of rocks synthesized with similar chemistry but cooled more rapidly (Brachfeld and Hammer, 2006, and Bowles et al., 2009).

Two rock compositions were created, denoted T-type and M-type, chemically reflecting constraints of the thermal emission spectroscopy (TES) and Shergotty-Nahkla-Chassigny (SNC) meteorite assemblages, respectively. The two starting compositions can be thought of as end members that bracket proposed chemical compositions of an Fe-rich igneous Martian crust. The composition denoted T-type is rich in Al and poor in Fe (Fe/Al atomic ratio of 0.4), modeled on Thermal Emission Spectrometer (TES) data that suggests the Martian crust is terrestrial in character (Hamilton et. al. 2001). The M-type composition is richer in Fe and has lower concentration of Al (Fe/Al atomic ratio of 1.4), in equilibrium with SNC Martian meteorite phase assemblages (Treiman, 1993). The two compositions are identical with respect to MgO, SiO<sub>2</sub>, and TiO<sub>2</sub>.

This study focuses on the magnetic properties of these basalts as a function of anneal time and starting composition; which includes the magnetic mineralogy, chemistry, grain morphology, texture, rock magnetic, and remanence properties. We assess which scenario creates the most efficient magnetic recorder, and whether that recording assemblage is stable enough to hold that remanence over geologic time, as well as compare the recording abilities to more quickly cooled analogs.

## **METHODS**

### **Petrologic Methods**

All petrologic aspects of this study, including synthesis of the samples, reflected light petrography, and electron microprobe analysis were performed at the University of

Hawaii Experimental Petrology Lab by Lisa Tatsumi-Petrochilos, under the advisement of Dr. Julia Hammer. Methods used in sample synthesis and microanalysis are described in detail in Tatsumi-Petrochilos, (2010). Chemical composition and electron backscatter imaging were performed on a JEOL JXA 8500F Hyperprobe at the University of Hawaii. Differentiation between oxidation states of iron was calculated using methods by Droop, 1987.

Sample synthesis was performed on two starting materials. Each composition was cooled from  $> 1200\text{ }^{\circ}\text{C}$  to  $1070\text{ }^{\circ}\text{C}$  at  $4\text{ }^{\circ}\text{C/h}$  and annealed at  $1070\text{ }^{\circ}\text{C}$  for 100 h, then quenched. Samples were then held at  $650\text{ }^{\circ}\text{C}$  for periods ranging from 21 to 158 days under quartz-fayalite-magnetite (QFM)  $f\text{O}_2$  buffer conditions, and then quenched again.

### **Sample Nomenclature**

After synthesis, samples were broken into chips and split into equal proportions. Half was reserved for petrographic and chemical analysis, while the remainder was sent to Montclair State University for magnetic analysis. Sample names were used to represent the experimental conditions at which the sample was created. M-type samples, based on the chemistry of the Martian SNC meteorites, are denoted with the prefix “MAm” in their sample names, following an earlier naming scheme (Hammer, 2006). T-type samples, based on the TES data, use the prefix “MB2,” following the naming scheme used in Bowels, et al., 2009. The suffix at the end of the sample name is related to the duration for which the sample was annealed before quenched. Generally speaking, the larger the number the greater the amount of time the sample was allowed to anneal, with E-09 being 21 days and E-13 being 158 days. Letters present after the anneal period

distinguish a particular chip within a split of the material used for analysis. The integrity of individual chip letters was kept for all measurements, for example, ARM demagnetization spectra and magnetic hysteresis data displayed for chip MAm E-12a is the same chip measured in the two methods. An explanation of sample codes, compositions, and anneal times is described in Table 1.

### **Magnetic Measurements**

Magnetic measurements were performed in order of low to high applied field: magnetic susceptibility, alternating field (AF) demagnetization of anhysteretic remanent magnetization (ARM), induced magnetization vs. applied field curves (magnetic hysteresis loops), and Curie temperature determination via induced magnetization as a function of temperature. Analyses were performed on either individual chips of material within each anneal period or cumulate chips representing an entire annealing period. Cumulative measurements were taken in an effort to deal with the heterogeneity of the material. Throughout this thesis we use mass normalized units, which is appropriate due to the small size of these chips each having a mass of roughly 10 mg.

### **Magnetic Susceptibility**

Typically three chips per anneal period were measured for magnetic susceptibility on a KLY-4 Kappabridge under a 300 A/m applied field and a frequency of 920 Hz. Each chip was measured three times and magnetic susceptibility values were normalized by mass.

## **Remanent Magnetization Measurements**

Magnetic remanence measurements including natural remanent magnetization (NRM) and anhysteretic remanent magnetization (ARM) were measured at the paleomagnetism laboratory at Lehigh University. The two heaviest chips were chosen to represent each sample for measurement. Individual chips were placed on the lid of a 2-cm standard plastic cube with silicon grease. Natural remanent magnetization (NRM) without any treatment was first measured on a 2G 755 superconducting magnetometer. The samples were then demagnetized in 3 directions in a 100 mT peak alternating field and the intensity of remanence was measured again.

After NRM measurements, an ARM was imparted using a Schonstedt GSD-5 AF demagnetizer. Two magnetic fields were present during magnetization. The samples were subjected to an alternating decaying field of 100 mT in the presence of a steady 98  $\mu$ T DC bias field meant to impart ARM. The anhysteretic remanence acquired was measured using the 2G magnetometer and then erased using an alternating field demagnetizer in line with the 2G 755 superconducting magnetometer. Samples were stepwise demagnetized in 10 mT increments from 0 to 50 mT.

## **Magnetic Hysteresis**

Magnetic hysteresis loops were measured on a Princeton Measurement Corp. 3900-04C vibrating sample magnetometer (VSM). Due to the samples' heterogeneous nature two methods were used, one involving the measurement of individual chips attached to a plastic mount with silicon grease and the other using multiple chips packed into a gelatin capsule with fibro fax quartz cotton, then placed inside a drinking straw.



The latter of these measurements was performed in an effort to increase signal strength, overcome chip heterogeneity, and provide a more representative description of the annealing product. Hysteresis loops and parameters mentioned in the results section are the product of this method. Loops were obtained using a 1 T peak applied field. Induced magnetization was normalized by mass and the paramagnetic and diamagnetic contributions were subtracted using the high field slope above 0.7 T. Coercivity of remanence ( $H_{cr}$ ) was measured by inducing an isothermal remanent magnetization in a 1-T field and then DC demagnetizing the remanence in field increments of 10 mT up to 100 mT.

### **Thermo-magnetic Measurements**

Moment as a function of temperature curves were measured on a Princeton Measurement Corp. 3900-04C vibrating sample magnetometer (VSM). Magnetic moment was measured in a 50 mT applied field; chosen to minimize paramagnetic contributions that increase in high fields. Measurements were taken continuously from 30 - 700 °C in an inert flowing helium gas atmosphere. Both the heating and cooling curves were obtained and normalized by mass. Curie temperatures were calculated using the intersection of tangent lines of maximum slope method (Grommé et al., 1969).

Curie temperatures were also used to estimate a depth to the Curie isotherm or the depth at which magnetic material no longer records a remanent magnetization. This was calculated using proposed thermal gradients of 5, 10, 15, 20 and 25 K/km and an estimated Martian surface temperature of 220 K.

## RESULTS

### Petrologic and Chemical Description of Iron Oxides

All petrologic results including the description of the samples' mineralogy, electron microanalysis (summarized below), and a complete chemical and shape description of the Fe-oxides present can be found in Tatsumi-Petrochilos (2010). Here we present only a portion of the petrologic results, as this study focuses on the magnetic aspects of these samples.

M-type samples in all anneal durations were composed of clinopyroxene, glass, plagioclase, and titanomagnetite. There are two populations of titanomagnetite grains present in M-type samples. The majority of titanomagnetite grains were euhedral and equant. These grains are generally ~30-80  $\mu\text{m}$  in diameter and have a tendency to contain melt inclusions. The subordinate population of titanomagnetite grains are rounded and equant, are ~5-15  $\mu\text{m}$  in diameter, and commonly occur in clusters. With increasing anneal time the composition of titanomagnetite approaches endmember magnetite, showing a decrease in impurities of MgO and  $\text{TiO}_2$ . The median composition of titanomagnetite in order of increasing anneal time are as follows:  $\text{Mt}_{49}\text{Usp}_{35}\text{Mgf}_9\text{Hc}_7$ ,  $\text{Mt}_{50}\text{Usp}_{35}\text{Mgf}_8\text{Hc}_7$ ,  $\text{Mt}_{51}\text{Usp}_{34}\text{Mgf}_8\text{Hc}_7$ ,  $\text{Mt}_{49}\text{Usp}_{36}\text{Mgf}_8\text{Hc}_7$ , and  $\text{Mt}_{53}\text{Usp}_{32}\text{Mgf}_8\text{Hc}_7$  (where Mt: Magnetite  $\text{Fe}_3\text{O}_4$ , Usp: ulvöspinel  $\text{TiFe}^{2+}_2\text{O}_4$ , Mgf: magnesioferrite  $\text{MgFe}^{3+}_2\text{O}_4$ , and Hc: hercynite  $\text{Fe}^{2+}\text{Al}_2\text{O}_4$ ).

T-type samples contain plagioclase, clinopyroxene, glass, olivine, and two iron oxide phases of titanomagnetite, and ilmenite. Titanomagnetite grains are euhedral, equant, and ~5-10  $\mu\text{m}$  in diameter. Ilmenite grains are euhedral and elongated ~5-30  $\mu\text{m}$  in length. Titanomagnetite grains created from T-type starting reagents differ from those

of M-type samples in that they commonly contain Cr impurities. Similar to their M-type counterparts, titanomagnetite grains display a general decrease in MgO and TiO<sub>2</sub> with increasing anneal time, however the change is not as apparent due to the high amount of Cr occupying cation vacancies. Sample MB2 E-11, annealed for 48 days, contains grains with Chromium-rich cores with titanomagnetite rims. No other samples display this texture. Therefore in this respect we find the Cr-rich cores to be a product of the starting material, not of the annealing process. In order of increasing anneal time titanomagnetite compositions are Mt<sub>14</sub>Usp<sub>47</sub>Mgf<sub>25</sub>Hc<sub>8</sub>Chr<sub>6</sub>, Mt<sub>21</sub>Usp<sub>48</sub>Mgf<sub>22</sub>Hc<sub>7</sub>Chr<sub>2</sub>, Mt<sub>15</sub>Usp<sub>50</sub>Mgf<sub>22</sub>Hc<sub>7</sub>Chr<sub>6</sub>, Mt<sub>21</sub>Usp<sub>47</sub>Mgf<sub>21</sub>Hc<sub>8</sub>Chr<sub>3</sub>, and Mt<sub>16</sub>Usp<sub>50</sub>Mgf<sub>22</sub>Hc<sub>7</sub>Chr<sub>5</sub> (where, Mt: Magnetite Fe<sub>3</sub>O<sub>4</sub>, Usp: ulvöspinel TiFe<sup>2+</sup><sub>2</sub>O<sub>4</sub>, Mgf: magnesioferrite MgFe<sup>3+</sup><sub>2</sub>O<sub>4</sub>, Hc: hercynite Fe<sup>2+</sup>Al<sub>2</sub>O<sub>4</sub>, Chr: chromite Fe<sup>2+</sup>Cr<sub>2</sub>O<sub>4</sub>). Ilmenite grains are of Hem<sub>12</sub>Ilm<sub>68</sub>Gk<sub>20</sub>, Hem<sub>13</sub>Ilm<sub>68</sub>Gk<sub>19</sub>, Hem<sub>8</sub>Ilm<sub>74</sub>Gk<sub>18</sub>, Hem<sub>13</sub>Ilm<sub>69</sub>Gk<sub>18</sub>, and Hem<sub>2</sub>Ilm<sub>81</sub>Gk<sub>17</sub> composition, in the order of increasing annealing time (where, Hem: hematite Fe<sub>2</sub>O<sub>3</sub>, Ilm: ilmenite FeTiO<sub>3</sub>, and Gk: geikielite MgTiO<sub>3</sub>).

Notably, the texture of glass found within these samples significantly changed with increasing time annealed, however it was not quantified (Tatsumi-Petrochilos 2010). The textural change appears to be a progression trend of glass recrystallization, a process known as devitrification. The devitrified parts of glass appear in the BSE image as colloform aggregates of fibrous crystals, and the amount increases with anneal time. Figures 1 and 2 display a representative sample of electron backscatter images of Fe-Oxide minerals found within the Martian analogs.

## **Magnetic Susceptibility**

Magnetic susceptibility was first measured in order to obtain a preliminary estimation of the amount and general type of ferromagnetic material present in these rocks. Magnetic susceptibility values were on the order of  $10^{-6}$  -  $10^{-5}$  m<sup>3</sup>/kg for M-type samples and  $10^{-7}$  -  $10^{-6}$  m<sup>3</sup>/kg for T-type samples. M-type samples show a higher magnetic susceptibility than T-type, which can be attributed to the higher concentration of iron within the starting material, leading to greater abundance of magnetic material (Figure 3). No systematic behavior was seen as a function of time annealed. Table 2 displays the susceptibility values measured as well as some selected magnetic parameters, which are later described in the sections below.

## **Magnetic Remanence**

All samples possess a natural remanent magnetization (NRM) believed to be a single component of thermal remanence (TRM) obtained during the final quench. The laboratory magnetic field was approximately 35  $\mu$ T (Julie Bowles, email communication, 2009). NRM values range from 8.67 – 169.72 mAm<sup>2</sup>/kg for M-type samples and 7.04 - 47.13 mAm<sup>2</sup>/kg for T-type (Figure 4). T-type samples display values comparable to the TRM induced in rapidly cooled samples of the same composition by Brachfeld and Hammer, 2006 and Bowles et al., 2009. We observed no systematic behavior between the NRM intensity and time annealed.

## **Anhyseretic Remanent Magnetization**

All samples acquired an anhyseretic remanence with intensities of roughly 21 - 42 mAm<sup>2</sup>/kg. M-type samples recorded stronger anhyseretic remanence relative to T-

type samples. ARM values ranged from 0.04 – 238.85  $\text{mAm}^2/\text{kg}$  for M-type samples and 0.09 – 16.96  $\text{mAm}^2/\text{kg}$  for T-type samples (Figure 5). The ARM was step-wise demagnetized and measured after each demagnetization step, a method that measures the sample's coercivity spectrum. The majority of the material displayed soft coercivity spectra with median destructive fields (MDF) of roughly 10 mT, erasing one half of the acquired ARM. In most cases alternating fields of 30 mT completely erased the ARM below the detection limit of the magnetometer. However there were some anomalous samples annealed for longer durations that have harder coercivity spectra. One M-type chip with a 158 anneal period displayed an MDF higher than 30 mT, and 4 T-type chips with annealing periods of 32, 48, 111, and 158 days displayed MDFs higher than 30 mT (Figure 6).

### **Magnetic Hysteresis**

Magnetic hysteresis loops agree with ARM demagnetization data that suggest magnetic minerals with an overall low coercivity spectrum. Loops appear narrow suggesting multidomain grains (Figures 7, 8). Table 2 displays the hysteresis parameters saturation magnetization ( $M_s$ ), remanent magnetization ( $M_r$ ), coercive force ( $H_c$ ), and coercivity of remanence ( $H_{cr}$ ). These materials were plotted on a 'Day Plot' (Day et al., 1977) to display relative hysteresis parameters and estimate the material's magnetic domain state (Figure 9).

Generally these samples plot in the multi-domain (MD) or pseudo-single domain (PSD) regions of a 'Day Plot.' M-type samples exhibit higher saturation magnetization ( $M_s$ ) and remanent magnetization ( $M_r$ ). However coercive force ( $H_c$ ) and the coercivity of remanence ( $H_{cr}$ ) are lower than that of T-type samples. T-type samples behave more

PSD-like than M-type samples, these samples plot in the multidomain (MD) and pseudo single domain (PSD) regions of a 'Day Plot' (Day et. al. 1977) (Figure 9a). There appears to be movement to more PSD type grains with increasing anneal time, most evident in T-type samples. In comparison to more rapidly cooled samples of Brachfeld and Hammer, 2006 these rocks behave much more multidomain (figure 9b).

### **Curie Point Determination**

Magnetic moment as a function of temperature was measured to provide further insight into the chemistry of the magnetic mineral present and the depth in the crust to which these minerals would remain magnetic. M-type samples display generally reversible heating and cooling curves with Curie temperatures between 285 and 405 °C. This agrees with mineral chemistry data that suggest a carrier of titanium-rich titanomagnetite. The starting material for M-type samples has a higher Curie point of 355 °C. The final anneal duration of 158 days displays a lower Curie point of 310 °C and curves that are less reversible (Figure 10, 11).

T-type samples have lower Curie temperatures, between 165 - 215 °C, suggesting the magnetic carriers of ilmenite and titanomagnetite to be very rich in impurities, as there is generally an inverse relationship between impurities and Curie temperature (Dunlop and Özdemir, 1997). The T-type curves are less reversible than M-type samples, with cooling curves generally having higher magnetic moments than the heating curves, but still showing the originally Curie point. This suggests an alteration at high temperatures of some of the magnetic material present, possibly the decomposition of titanomaghemite into titanium-rich and titanium-poor phases.

Curie temperatures also provide estimations of the depth in the crust that is magnetized, providing a depth to the Curie isotherm using a given geothermal gradient. Using the Curie temperatures measured and an array of geothermal gradients from 5-25 K/km. an estimated depth to the Curie isotherm is displayed in Figure 12.

## **DISCUSSION**

The intense magnetic anomalies within regions of the Southern Hemisphere of Mars are found to have intensities up to 1000 nT at satellite altitude, consisting entirely of remanent magnetization (Acuña et al., 1999). This remarkable intensity is an order of magnitude stronger than the strongest terrestrial anomaly, which is 10 nT at satellite altitude (Acuña et al., 1999). TES satellite data and SNC meteorite phase assemblages suggest the Martian crust to be basaltic in composition. This would make it most probable that the anomalies are carried by a thermoremanent magnetization, a magnetic signal gained when rocks cool through their Curie temperature in the presence of a magnetic field. For this reason we examine possible candidates for the carriers of magnetization by creating analogs of iron-rich magmas and test their recording ability. This experiment focuses on material that have experienced variable annealing periods ranging from 21 to 158 days, most comparable to that of a shallow igneous intrusion.

It was the intention of annealing the material to create small-unmixed zones of pure magnetite within a titanomagnetite matrix, a form of spinel oxide exsolution that was experimentally created in preliminary runs prior to our experiment by Bowles et al., 2010. The magnetite regions found within this material are single domain, meaning they are uniformly magnetized and possess a stable single domain thermoremanent

magnetization, which can potentially hold pristine records of magnetic fields. They are extremely efficient magnetic recorders in terrestrial rocks, hence, a likely candidate for the carrier of the Martian magnetic anomalies. However, exsolution was not achieved in the experiments presented here, and the goal of the study was changed to modeling shallow igneous intrusions of Martian-like composition.

We estimate the domain state of the material by examining the samples' coercivity spectrum. A material's coercivity can be determined from the stability of remanent magnetization during alternating field or DC demagnetization, or from magnetization vs. applied field curves. The materials' coercivity shows the ease of moving domain walls vs. the difficulty of rotating moments away from the easy axis of magnetization in an SSD particle. In this study, this was performed using methods of magnetic hysteresis, which measure the materials response to a changing strong applied field, and AF demagnetization of ARM, measuring the magnetic remanence's response to a step-wise increasing alternating field.

To model the crust of Mars, experiments were performed on two rock compositions, denoted M-type and T-type. Chemically the starting reagents for these materials vary only with respect to Fe and Al, and contain identical concentrations of SiO<sub>2</sub>, MnO, MgO, CrO and TiO<sub>2</sub>. Both compositions were successful in synthesizing magnetic material. All samples recorded a thermal remanence from the laboratory magnetic field (approximately 35  $\mu$ T) during synthesis. The remanence acquired was roughly 65 mAm<sup>2</sup>/kg, values more intense than terrestrial basalts or plutonic rocks. Hysteresis parameter ratios of saturation remanence to saturation magnetization ( $M_r/M_s$ ) were relatively low, between 0.04 and 0.12, and ratios of remanent coercivity to



coercivity ( $H_{cr}/H_c$ ) were moderate to high, having values ranging from 2.8 - 4.94. These parameters suggest the carrier of magnetization to be a mixture of pseudo-single domain (a term given to a mixture of multidomain and single domain material) and multi domain grains (PSD/MD). This infers that the material was not compositionally unmixed small single domain exsolved material, as was the intention of annealing. ARM demagnetization spectra agree with mentioned hysteresis parameters, displaying spectra with low medium destructive fields of less than 15 mT for most samples, confirming the carriers of magnetic remanance to be of PSD/MD particles.

When imaged using SEM and reflecting light microscopy oxide grains were found to be homogeneous with compositions distinctive of the respective starting material. Samples modeled off the SNC meteorite chemistry (M-type) created two populations of equant titanomagnetite grains approximately ~30-80  $\mu\text{m}$  in diameter, and a subordinate population of clustered grains ~5-15  $\mu\text{m}$  in diameter. Those modeled from TES satellite data (T-type) created two phases of Fe-oxide minerals of titanomagnetite and ilmenite composition. The titanomagnetite grains found within T-type samples differ from that of M-type in that they are ~5-10  $\mu\text{m}$  in diameter and contain roughly 5% chromite, while M-type samples had no notable Cr impurities. Ilmenite grains are euhedral and elongated ~5-30  $\mu\text{m}$  in diameter.

Both M-type and T-type material displayed high magnetic susceptibility and saturation magnetization values suggesting that, although not quantified, there is a large abundance of Fe-oxide minerals present in these rocks. M-type samples displayed higher magnetic susceptibility, saturation magnetization, and were better recorders of magnetic fields, acquiring a higher TRM and ARM. We believe this is to be a product of the

abundance of magnetic material present in the sample. Oxide abundances were not quantified, however, assuming iron was conserved during synthesis one can make an assumption without quantification that more Fe-oxide minerals would crystallize in M-type samples as it is a product of a Fe-rich starting reagent. Iron within M-type samples is distributed into three phases, titanomagnetite, and to a lesser extent clinopyroxene and glass. T-type samples possessed a lesser Fe/Al ratio, contained the iron bearing minerals of titanomagnetite, ilmenite, olivine, clinopyroxene, and glass (Tatsumi-Petrochilos 2010).

Experimental studies of grain size dependence on titanomagnetite domain state show grain sizes  $\sim 30\text{-}80\ \mu\text{m}$  in diameter are multi-domain magnetic material and  $\sim 5\text{-}10\ \mu\text{m}$  titanomagnetite grains are pseudo-single domain (Day et al. 1977, Dunlop and Özdemir, 1997). In these respects, we infer the hysteresis measured of M-type samples to be controlled by the more abundant multi-domain grains. Similarly, we can conclude that the loops displayed in T-type samples are carried by  $\sim 5\text{-}10\ \mu\text{m}$  titanomagnetite. The contribution by the much weaker ilmenite is likely masked.

The differences in grain size between the two materials, M-type and T-type, are seen in hysteresis parameter ratios ( $H_{cr}/H_c$ ) and ( $M_r/M_s$ ) and shown to plot in two distinct regions in a 'Day Plot' (Figure 9). These ratios agree with the grain size observations that show M-type grains to behave more multidomain than T-type. ARM demagnetization spectrum of both sample compositions displayed low MDF ( $<15\text{mT}$ ) provide further evidence that these are PSD/MD grains.

An apparent change in the ARM AF demagnetization spectrum was observed with increasing time annealed. Some samples that were annealed for periods greater than

48 days displayed high median destructive fields, with one sample greater than 50 mT. It is possible that the degree to which glass is devitrified is responsible. During the devitification process, where glass is becoming more ordered in a crystalline structure it is possible for small single domain particles of magnetite to form. These particles would be too small to be imaged using scanning electron microscopy techniques and overpowered by the paramagnetic and multidomain signal measured during hysteresis. However, these particles would be observed using remanence measuring techniques, as the SQUID magnetometer is several orders of magnitude more sensitive than any other instrument used, and paramagnetic minerals make no contribution to remanent magnetizations. Therefore we believe it is possible that these small magnetic inclusions in glass carry the anomalous high coercivities present in the ARM demagnetization spectra. Bowels, et al., 2010, observed quenched starting material, lacking observable crystallized oxides, to have single domain characteristics, which was interpreted to be magnetic inclusions found within glass.

Moment as a function of temperature curves measured Curie points of 350 °C and 180 °C for M-type and T-type samples respectively. Both temperatures are interpreted to be carried by titanium-rich titanomagnetite with the concentration of ulvöspinel and chromite impurities and the presence of ilmenite in T-type samples accounting for the differences in Curie temperatures. The curves appeared to be reversible in the sense the Curie points displayed are seen in both the heating and cooling curves, however cooling curves display a higher magnetic moment than their respective heating curves. This is more apparent in T-type samples. It is possible that this type of nonreversibility is a product of cation reordering at high temperature, as seen in synthetic samples rich in

ulvöspinel by Lattard et al., 2006, or alteration creating new magnetic material at high temperatures. There is a subtle increase in Curie points found in both samples with increasing anneal time. This agrees with the microprobe observation that titanomagnetite is progressively approaching end-member magnetite.

Curie temperatures suggest these materials would be magnetic at depths up to 300 °C, equating to 5-30 km for T-type samples and 10-40 km for M-type samples. This simple calculation displays the depth below which there is no magnetic signal. Experiments in this study are approaching magnetite composition with increasing time annealed. A realistic shallow igneous intrusion is held at temperatures significantly longer than 158 days, the longest duration in this study. Therefore one can speculate that true intrusions will produce higher Curie temperatures and deeper Curie isotherms.

The remanence carried by the material decreases with increasing temperatures, therefore is lost with increasing depth. The amount of remanence lost is a function of the materials' blocking temperature spectrum, with single domains being more stable than multi domain grains. Bowles et al. 2009, measured thermal demagnetization on synthetic samples of this composition and found that increasing grain sizes have lower blocking temperatures, hence would produce a less intense anomaly.

Rapidly cooled samples of similar composition and oxygen fugacity conditions were performed by Brachfeld and Hammer, 2006 and Bowles et al. 2009. These two studies focused on the effects of oxygen fugacity and cooling rate on the magnetic properties of basalt. Brachfeld and Hammer, 2006 produced one set of six samples under QFM buffer conditions with similar composition to that of M-type samples produced in this study, but without Cr and Mn in their starting reagents. These samples were cooled at

rapid rates, the slowest being 3° C /hr, a rate significantly faster than the smallest anneal time in this study of 21 days. Bowles et al., 2009 synthesized nine samples under QFM  $fO_2$  conditions. These samples were very similar to those created in this experiment, in the sense that two compositions were created had identical chemistry to this study, but were also cooled much more rapidly.

When comparing these studies we find that by annealing the material we create larger magnetic grains that are found in much greater abundances. M-type starting materials in this study acquired TRM and ARM amplitudes up to 2 orders of magnitude higher than quickly cooled basalts (figure 13). All samples that were created in this set of experiments recorded remanences that are capable of accounting for the anomalies found on Mars. Samples created in this experiment possess remanences of 0.11 to 948 A/m for M-type samples and 0.01 to 141 A/m for T-type samples. These values are several orders of magnitude higher than the suggested 10 A/m needed to produce the Martian crustal anomalies at satellite altitude (Nimmo, 2000).

The high remanences produced in this study possess low coercivities, therefore the remanences are unstable and prone to lose its magnetization with environmental variables likely to be present in the 4 Ga Martian history. Variables that may affect the long-term stability of an anomaly carried by shallow igneous intrusions are shock pressure demagnetization by meteorite impactors or subsequent volcanism. Dense cratering indicates that the crust of the Southern hemisphere of Mars experienced a period of heavy bombardment, which likely continued sometime after the dynamo was turned off. Craters in the southern hemisphere such as Hellas and Argyre impact basins do not carry magnetic anomalies (Acuña et al., 1999; Connerney et al., 2001). These

large impact basins likely experienced pressures exceeding 1-2 GPa (Hood and Richmond et al., 2003). Regions surrounding these impact basins display significantly weaker anomalies, showing the effect of the impact event.

A titanomagnetite carrier is likely to lose magnetization in the upper 5-10 km of the crust due to shock demagnetization during meteorite impacts (Bezaeva et al., 2010, Louzada et al., 2010a,b). Given the Curie Isotherm limits of the magnetized layer and the soft coercivity spectra, the thickness of the magnetized layer would be reduced by one half (Figure 13). For these reasons, for the material created to be a candidate for the magnetic anomalies on Mars they must carry a stronger remanence and a hard coercivity that is more resistive to impact events.

## **CONCLUSIONS**

This study examines the magnetic susceptibility, natural remanent magnetization (NRM), ARM demagnetization, magnetic hysteresis, and temperature dependence of magnetic moment of two probable Martian chemistries annealed for durations of 21, 32, 48, 111, and 158 days. The magnetic mineral assemblages created were reliable recorders of magnetic remanence. All samples acquired an intense remanence during synthesis, which is assumed to be a thermoremanent magnetization (TRM) acquired in the ambient laboratory field of 35  $\mu$ T. The samples were also capable of recording an imparted anhysteretic magnetization (ARM), which was intense relative to the imparting bias field. The NRM values measured are capable of accounting for the magnetic anomalies found on Mars. However the minerals displayed low coercivities implying that the remanence recorded was magnetically soft and easily demagnetized.

Curie temperatures in the range of 180 to 350 °C suggest a magnetized layer of 5-40 km. Due to the low coercivities of the material created it is probable that 5-10 km of this crust would be demagnetized if exposed to shock demagnetization and thermally demagnetized by a subsequent intrusion. Therefore for these reasons we conclude that although the material created reordered a strong remanence capable of accounting for the anomalies on Mars they are most likely not probable candidates for carriers of the Mars crustal anomalies given their soft coercivities.

## References

- Acuña, M., Connerney, J., Wasilewski, P., P., Lin, R., Anderson, K., Carlson, C., McFadden, J., Curtis, D., Mitchell, D., Reme, H., Mazelle, C., Sauvaud, J., d'Uston, C., Cros, A., Medale, J., Bauer, S., Cloutier, P., Mayhew, M., Winterhalter, D., Ness, N., (1998), *Science*, **279**, 1676-1680
- Acuña, M., Connerney, J., Ness, N., Lin, R., Mitchell, D., Carlson, C., McFadden, J., Anderson, K., Réme, H., Mazelle, C., Vignes, D., Wasilewski, P., Cloutier, (1999) Global Distribution of Crustal Magnetization Discovered by the Mars Global Surveyor MAG/ER Experiment, *Science*, **284**, pp 790-793
- Antretter, M., M. Fuller, E. Scott, M. Jackson, B. Moskowitz, and P. Solheid, (2003) Paleomagnetic record of Martian meteorite ALH84001, *J. Geophys. Res.*, **108**(E6), 5049, doi:10.1029/2002JE001979
- Bezaeva, N., Gattacceca, J., Rochette, P., Sadykov, R., Trukhin, V., (2010), Demagnetization of terrestrial and extraterrestrial rocks under hydrostatic pressure up to 1.2 GPa, *Phys. of Earth and Planet. Interiors*, **179**, 7-20
- Bowles, J., Hammer, J., Brachfeld, S., (2009) Magnetic and petrologic characterization of synthetic Martian basalts and implications for the surface magnetization of Mars, *J. of Geophys. Res.*, E10003, doi:10.1029/2009JE003378
- Bowles, J.A., L. Tatsumi, and J.E. Hammer, (2010) Spinel unmixing in synthetic Martian analog crustal rocks: implications for the magnetization of Mars, *manuscript in preparation*
- Brachfeld, S., Hammer, J., (2006) Rock-magnetic and remanence properties of synthetic Fe-rich basalts: Implications for Mars crustal anomalies, *Earth and Planet. Sci. Lett.*, **248**, pp. 599-617, doi:10.1016/j.epsl.2006.04.015
- Connerney, J., Acuna, M., Wasllewski, P., Kletetschka, G., Ness, N., Reme, H., Lin, R., Mitchell, D., (2001), The global magnetic field of Mars and implications for crustal evolution, *Geophys. Res. Lett.*, **28**, 4015-4018, doi:10.1029/2001GL013619
- Droop, G.T.R., (1987) A general equation for estimating Fe<sup>3+</sup> concentrations in ferromagnesian silicates and oxides from microprobe analyses, using stoichiometric criteria, *Mineralogical Mag*, **51**, 3, p 431 ISSN: 0026-461X.
- Dunlop, D., Kleteschka, G., (2001) Multidomain hematite: a source of planetary magnetic anomalies? *Geophys. Res. Lett.*, **28**, 3345-3349, doi: 0094-8276/01/2001GL013125
- Evans, M. E., and Wayman, M. L. (1974) An investigation of the role of ultra-fine



titanomagnetite intergrowths in paleomagnetism. *Geophysical Journal of the Royal Astronomical Society*, **36**, 1–10.

Grommé, C., T. Wright, and D. Peck (1969) Magnetic Properties and Oxidation of Iron-Titanium Oxide Minerals in Alae and Makaopuhi Lava Lakes, Hawaii, *J. Geophys. Res.*, **74**(22), 5277-5293.

Hamilton, V.E., M.B. Wyatt, H.Y. McSween, and P.R. Christensen, (2001) Analysis of terrestrial and Martian volcanic compositions using thermal emission spectroscopy 2. Application to Martian surface spectra from the Mars Global Surveyor Thermal Emission 894 Spectrometer, *J. Geophys. Res.*, **106**, 14,733-14,746

Hammer, J., (2006) Dynamic crystallization of Fe-rich basalt:  $fO_2$  and cooling rate controls on the kinetics and energetics of solidification, *Earth and Planet. Sci. Lett.*, **248**, pp. 618-637 doi: 10.1016/j.epsl.2006.04.022

Hood, L., Richmond, N., Pierazzo, E., Rochetter, P., (2003), Distribution of crustal magnetic fields on Mars: Shock effects of basin-forming impacts, *Geophys. Res., Lett.*, **30**(6), 1281, doi:10.1029/2002GL016657

Lattard, D., R. Engelmann, A. Kontny, and U. Sauerzapf (2006), Curie temperatures of synthetic titanomagnetites in the Fe-Ti-O system: Effects of composition, crystal chemistry, and thermomagnetic methods, *J. Geophys. Res.*, **111**, B12S28, doi:10.1029/2006JB004591.

Louzada, K., Stewart, S., Weiss, B., Gattacceca, J., Bezaeva, N., (2010), Shock and static pressure demagnetization of pyrrhotite and implications for the Martian Crust, *Earth and Planet. Sci. Lett.*, **290**, 90-101

Louzada, K., Stewart, S., Weiss, B., Gattacceca, J., Lillis, R., Halekas, J, (2010), Impact Demagnetization of the Martian Crust: Current Knowledge and Future Directions, *EPSL Frontiers* (submitted)

McEnroe, S.A., Brown, L.L., Robinson, P., (2004) Earth analog for Martian magnetic anomalies; remanence properties of hemo-imenite norites in the Bjerkreim-Sokndal intrusion, Rogaland, Norway, *J. of App. Geophys.*, **56**, 195-212 doi:10.1016/j.jappgeo.2004.07.002

Nimmo, F., (2000) Dike intrusion as a possible cause of linear Martian magnetic anomalies, *Geology*, **28**, 391-394

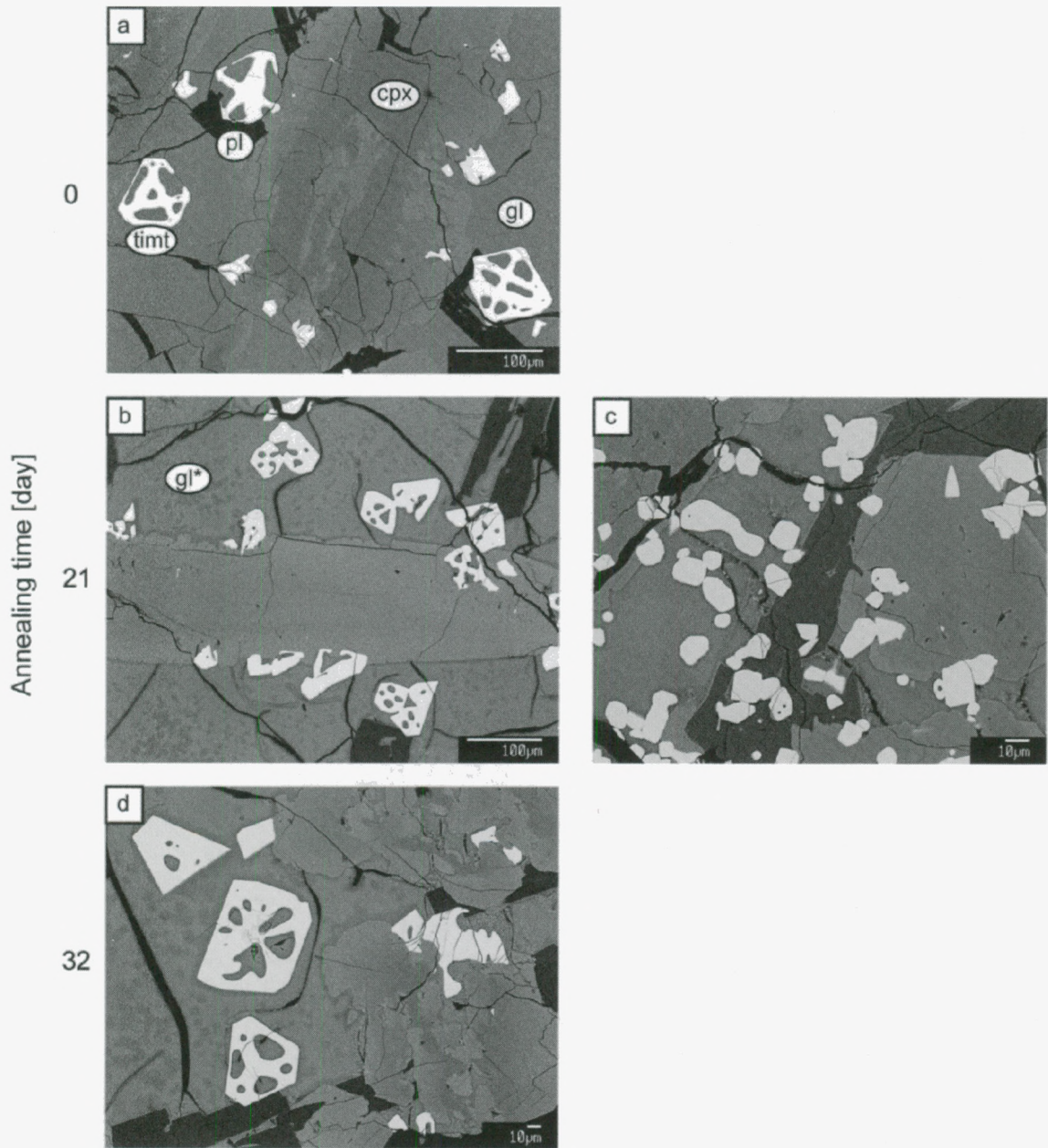
Scott, E., Fuller, M., (2004) A possible source for the Martian crustal magnetic field, *Earth and Planet.Sci. Lett.*, **220**, pp. 83-90 doi:10.1016/S0012-821X(04)00032-9

Tatsumi-Petrochilos, L., (2010) Experimental and analytical studies of titanomagnetite in synthetic and natural samples, Masters Thesis University of Hawaii, 147 pp.

Treiman, A. H., (1993) The parent magma of the Nakhla (SNC) meteorite, inferred from magmatic inclusions, *Geochim. Cosmochim. Acta*, **57**, 4753-4767

Weiss B., Vali, H., Baudenbacher, F., Kirschvink, J., Stewart, S., Shuster, D., (2002) Records of an ancient Martian magnetic field in ALH84001, *Earth Planet. Sci. Lett.* **201**, 449–463, PII: S001 2 - 821X(02)00728-8

Figure 1: Backscatter electron images of M-type samples



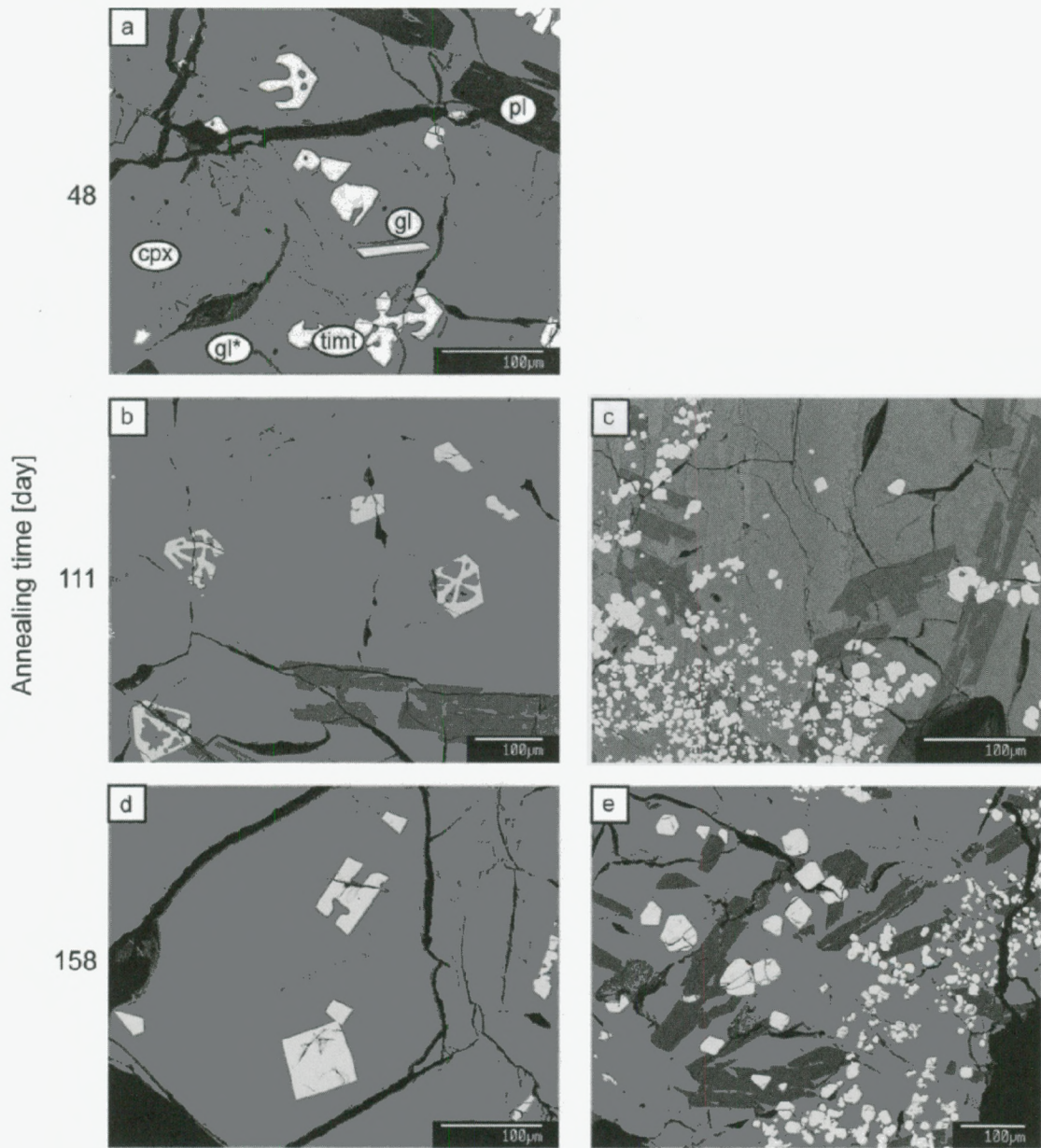


**Figure 1. Fe-oxides of M-type starting composition.** The first image on each page displays a key labeling each phase present within a sample. cpx: clinopyroxene, pl: plagioclase, timt: titanomagnetite, gl: glass. The time annealed is displayed as days on the left hand column of the figures. Images are divided into left and right columns to display the two different populations of oxides. The left column displays titanomagnetite grains that are euhedral, and equant  $\sim 30\text{--}80\ \mu\text{m}$  in diameter. The right column displays the subordinate clustered population of grains that are  $\sim 5\text{--}15\ \mu\text{m}$  in diameter. Devitrified glass is labeled as gl\* and normal glass as gl. (images from Tatsumi-Petrochilos, 2010).

Figure 2: Fe-Oxides of T-type Composition

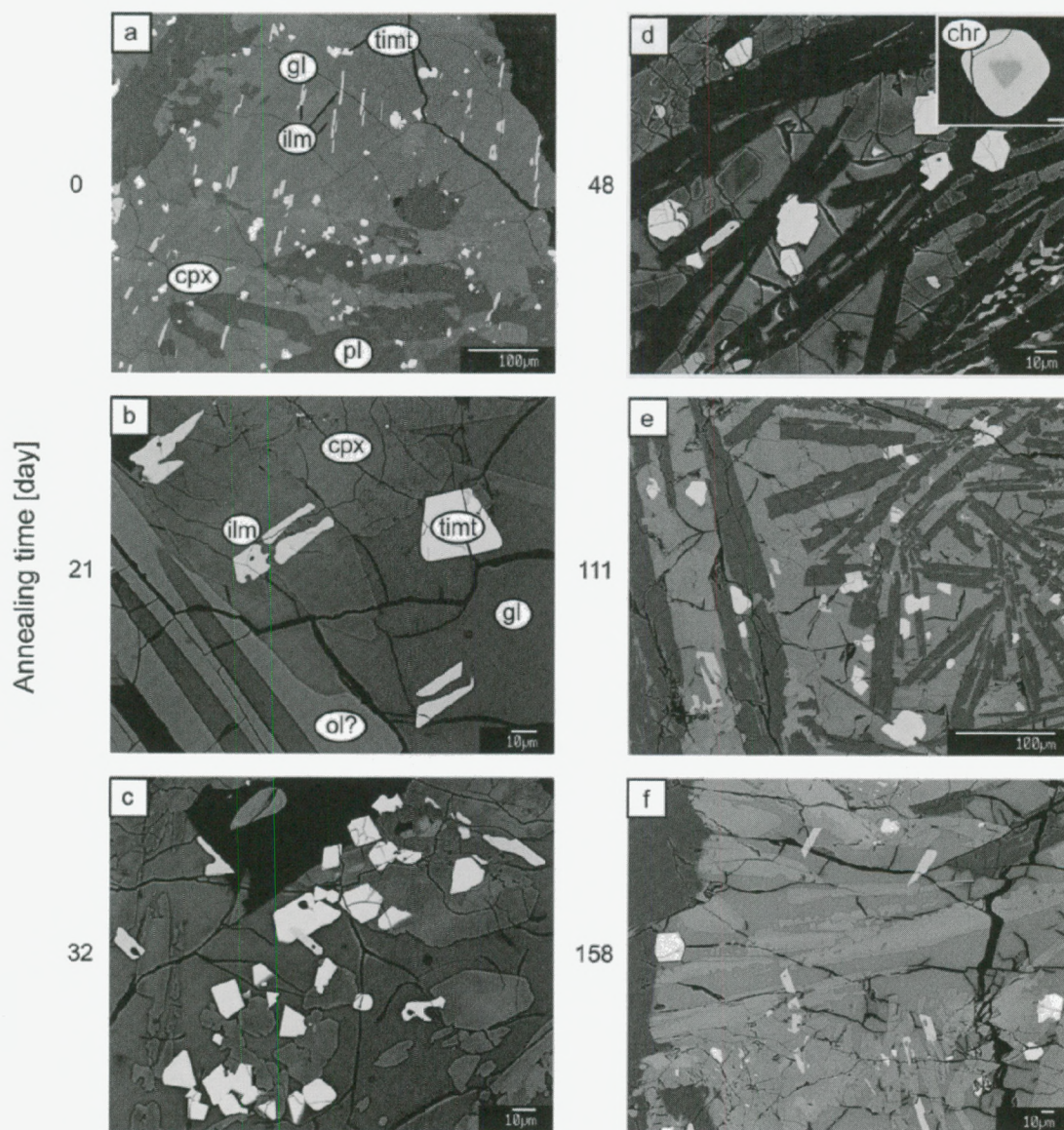


**Figure 2. Fe-oxides of T-type composition.** Two phases of oxides can easily be distinguished by their shapes. Illmenite grains are elongated (~5-30  $\mu\text{m}$ ) while the titanomagnetite grains are more equant (~5-10  $\mu\text{m}$ ). Image d displays an example of the oxide grains that contain Cr-rich cores and titanomagnetite rims, a feature only seen in samples annealed for 48 days (images from Tatsumi-Petrochilos, 2010).

Figure 3: Magnetic Susceptibility

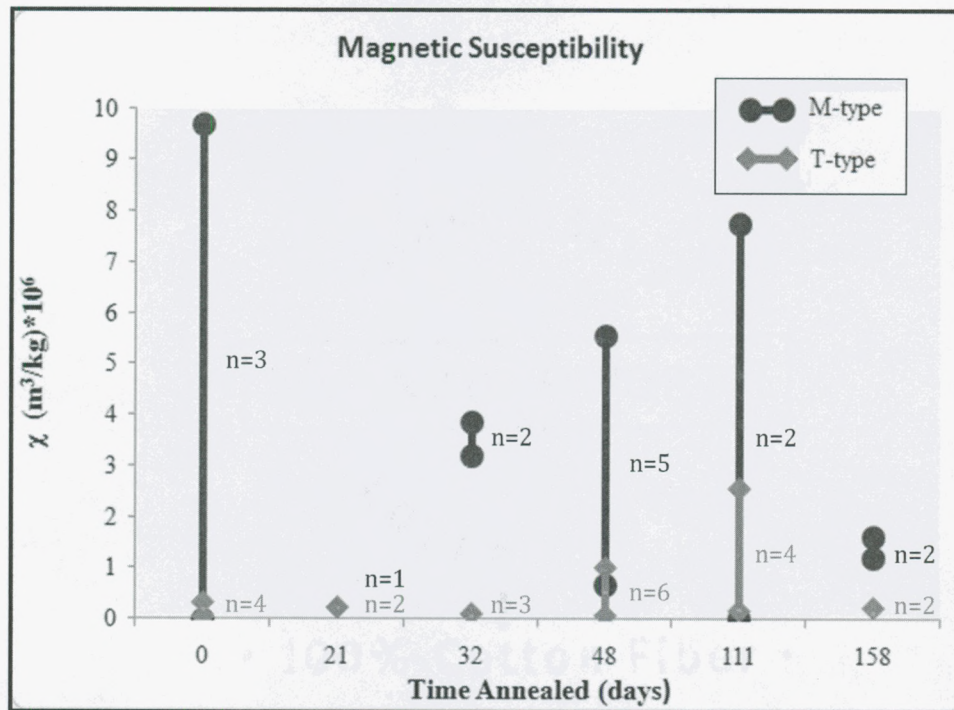
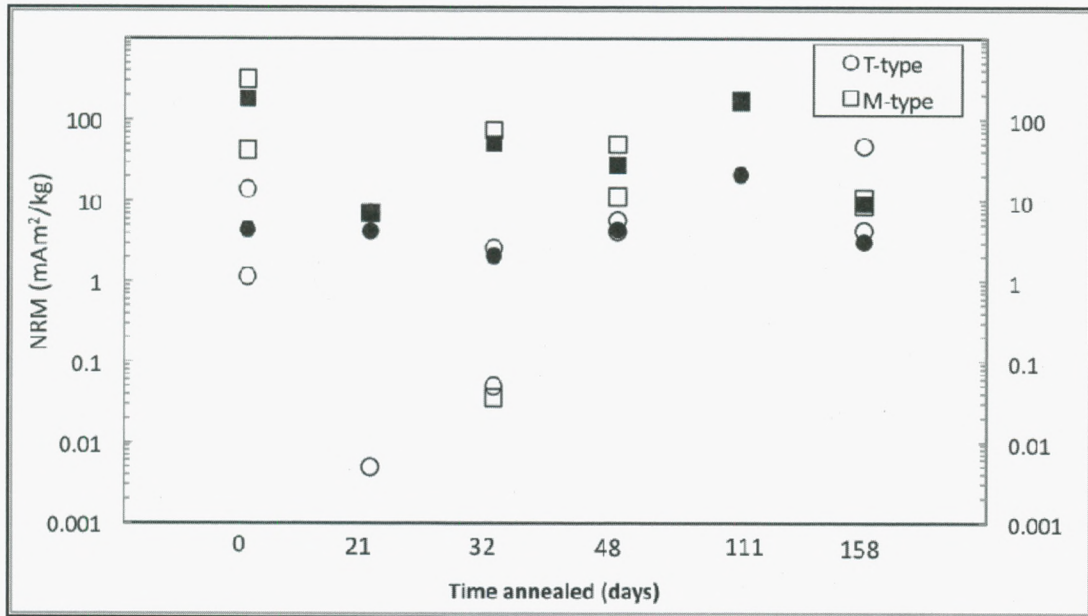


Figure 3. Range of magnetic susceptibility values as a function of anneal time. The black lines with rounded caps represent M-type samples. The grey lines with diamond heads represent T-type samples. M-type samples possess a higher magnetic susceptibility, thought to be a product of more magnetic material present in the samples

**Figure 4: Natural Remanent Magnetization**



**Figure 4. Range of natural remanent magnetization measured in M-type and T-type samples.** M-type samples are represented by squares and T-type samples by circles. Filled in data points are weighted averages by mass of the material. Natural remanent magnetization was measured on the two heaviest sample chips per annealing period.

Figure 5: Remanence Measurements

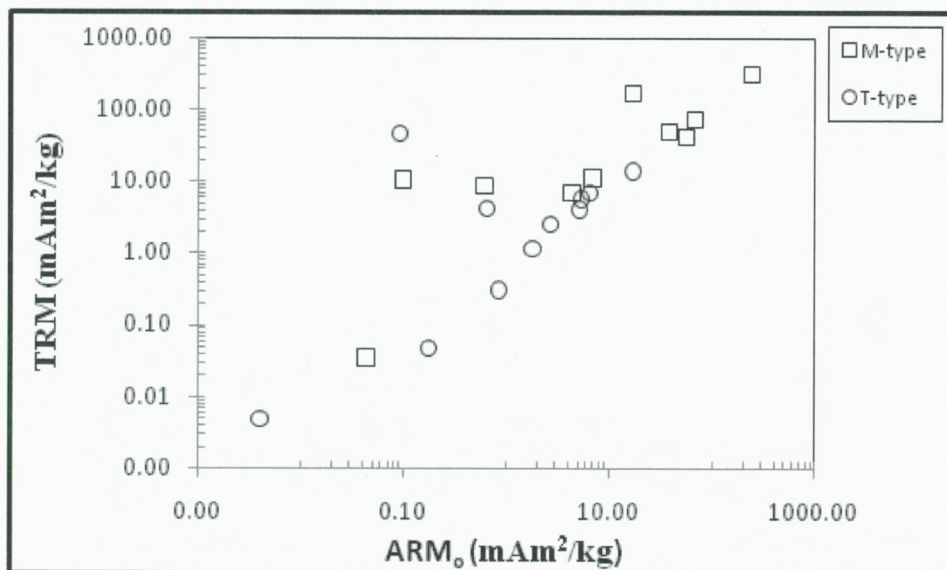
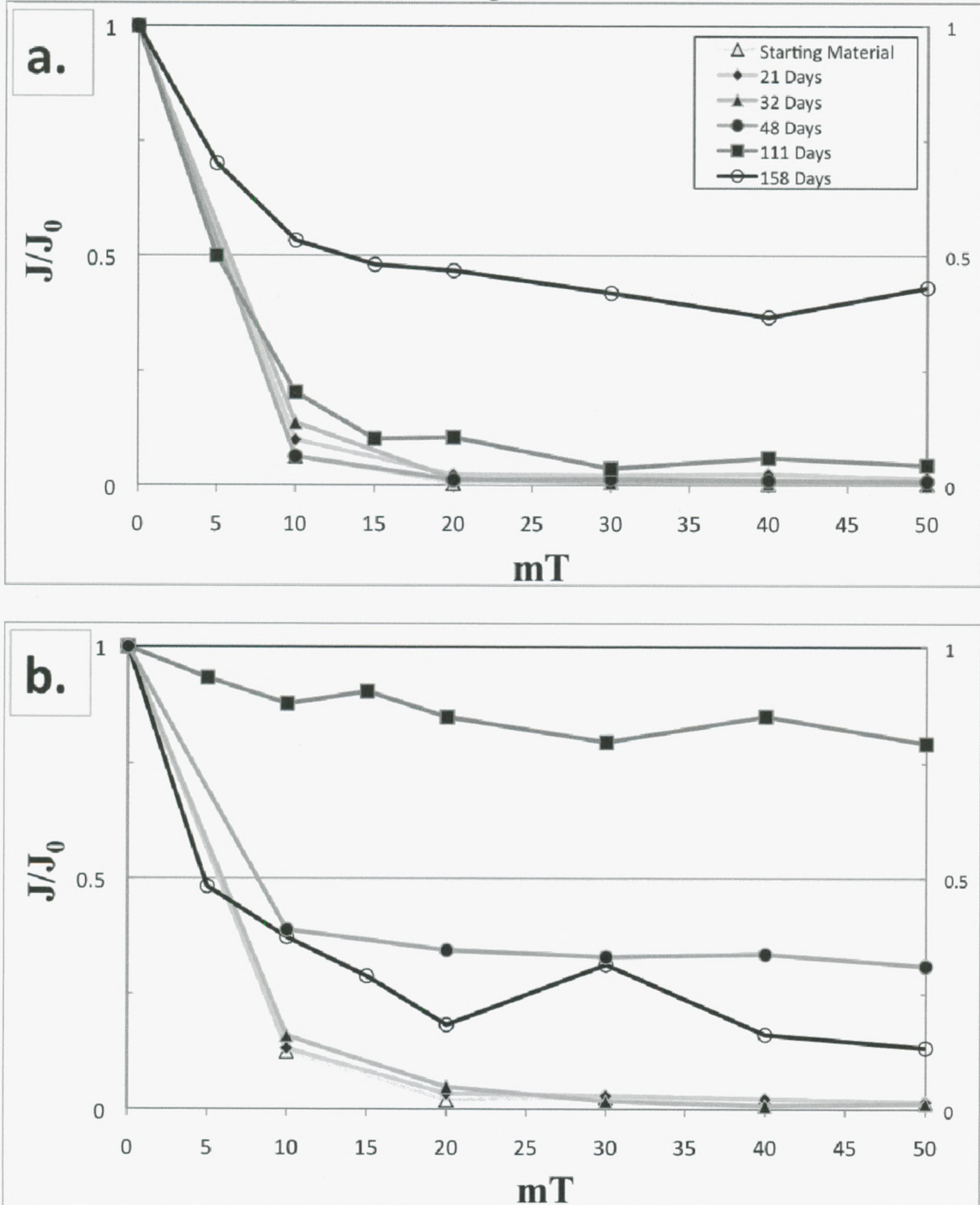


**Figure 5. Remanence acquired during synthesis (inferred to be a TRM) and ARM.** This figure displays the recording abilities of M-type samples relative to T-type. M-type samples plot higher and to the right in this plot, showing their ability to record a higher NRM and ARM, relative to T-type.



Figure 6: AF Demagnetization of ARM



Figures 6: Step-wise AF demagnetization of ARM for M-type (a) and T-type (b) samples. The values displayed in this graph are mass weighted averages of the largest two chips within each annealing period. The y-axis, labeled  $J/J_0$ , is the ARM measured at a particular demagnetization step divided by the ARM measured prior to any demagnetization.

Figure 7: Magnetic Hysteresis Loops (M-type)

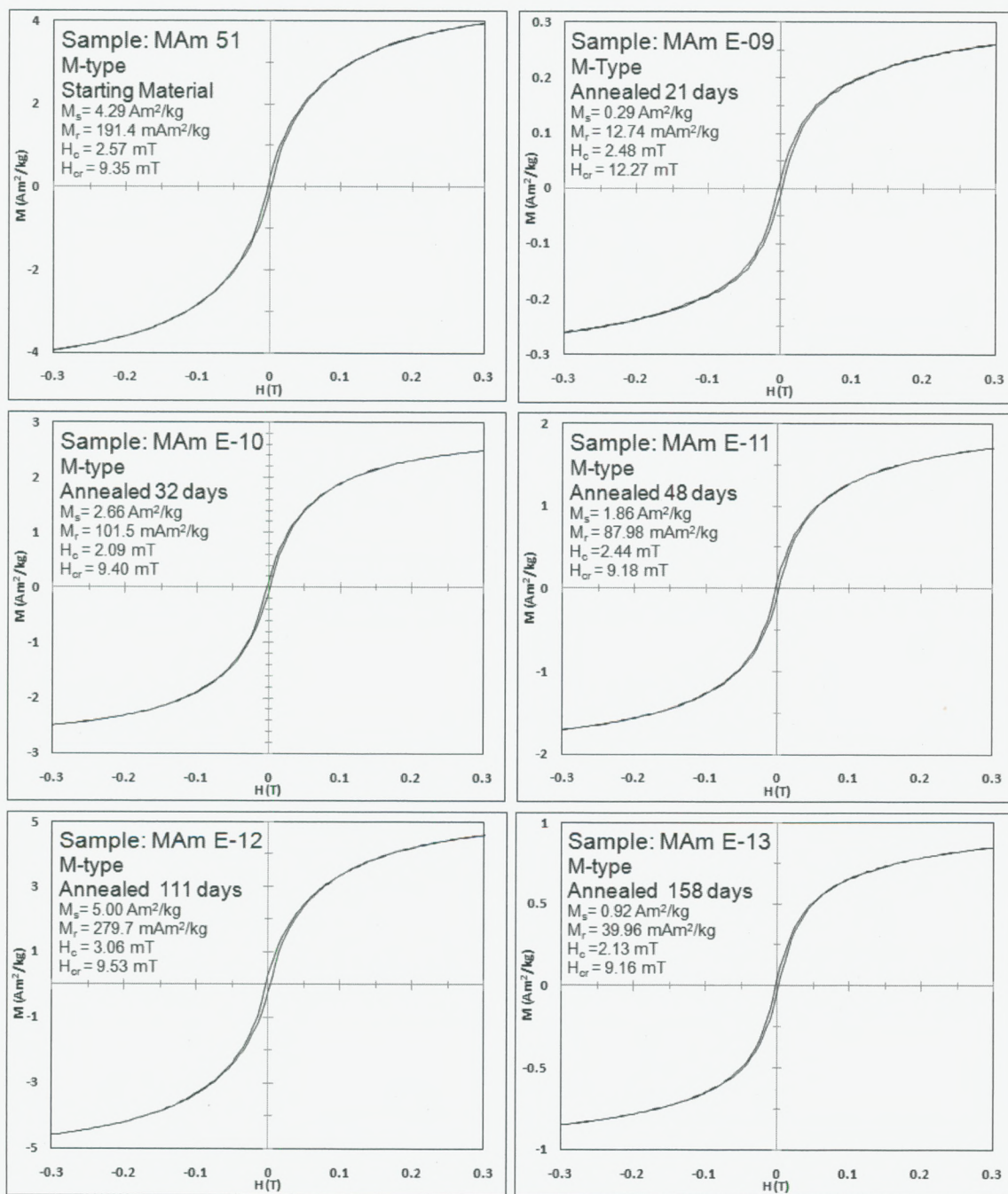


Figure 7. Hysteresis loops for M-type samples are multidomain.

Figure 8: Magnetic Hysteresis Loops (T-type)

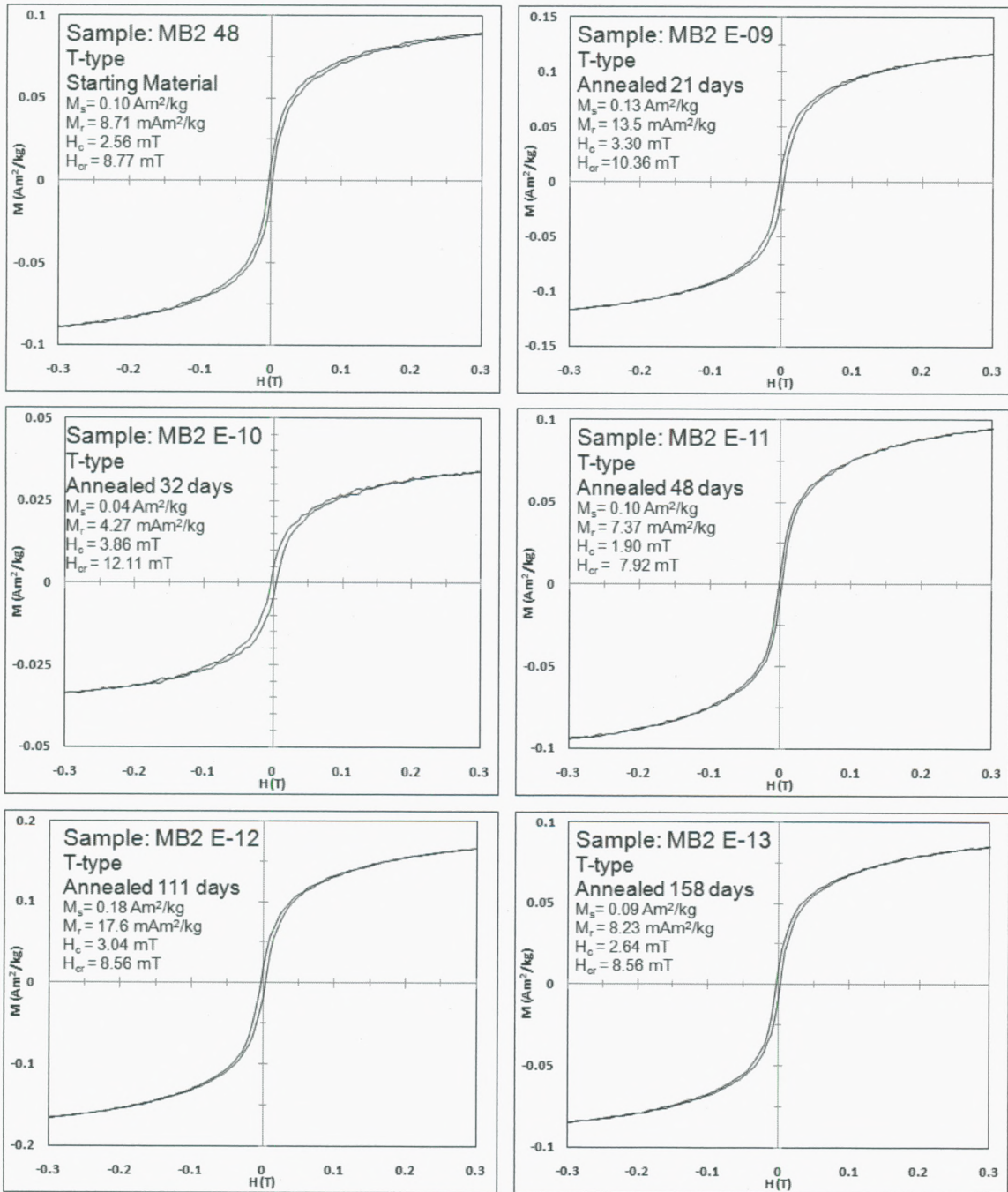
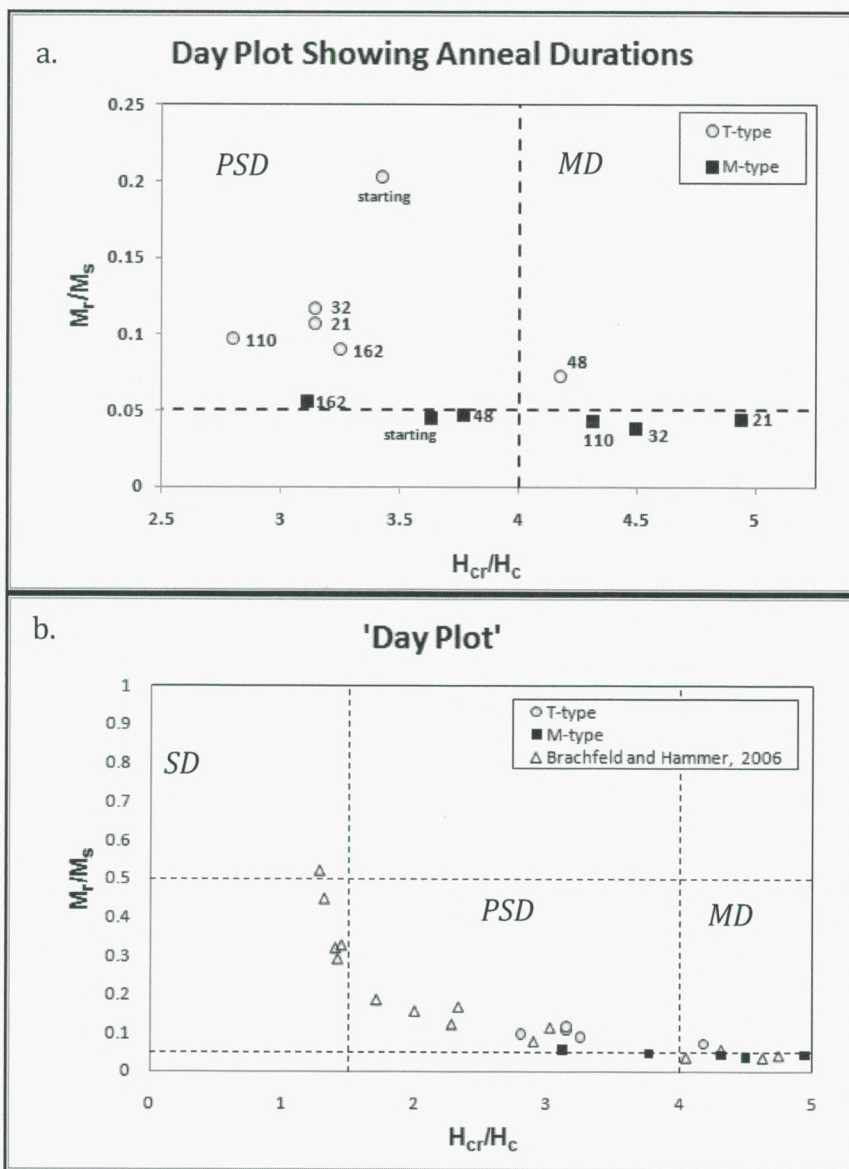


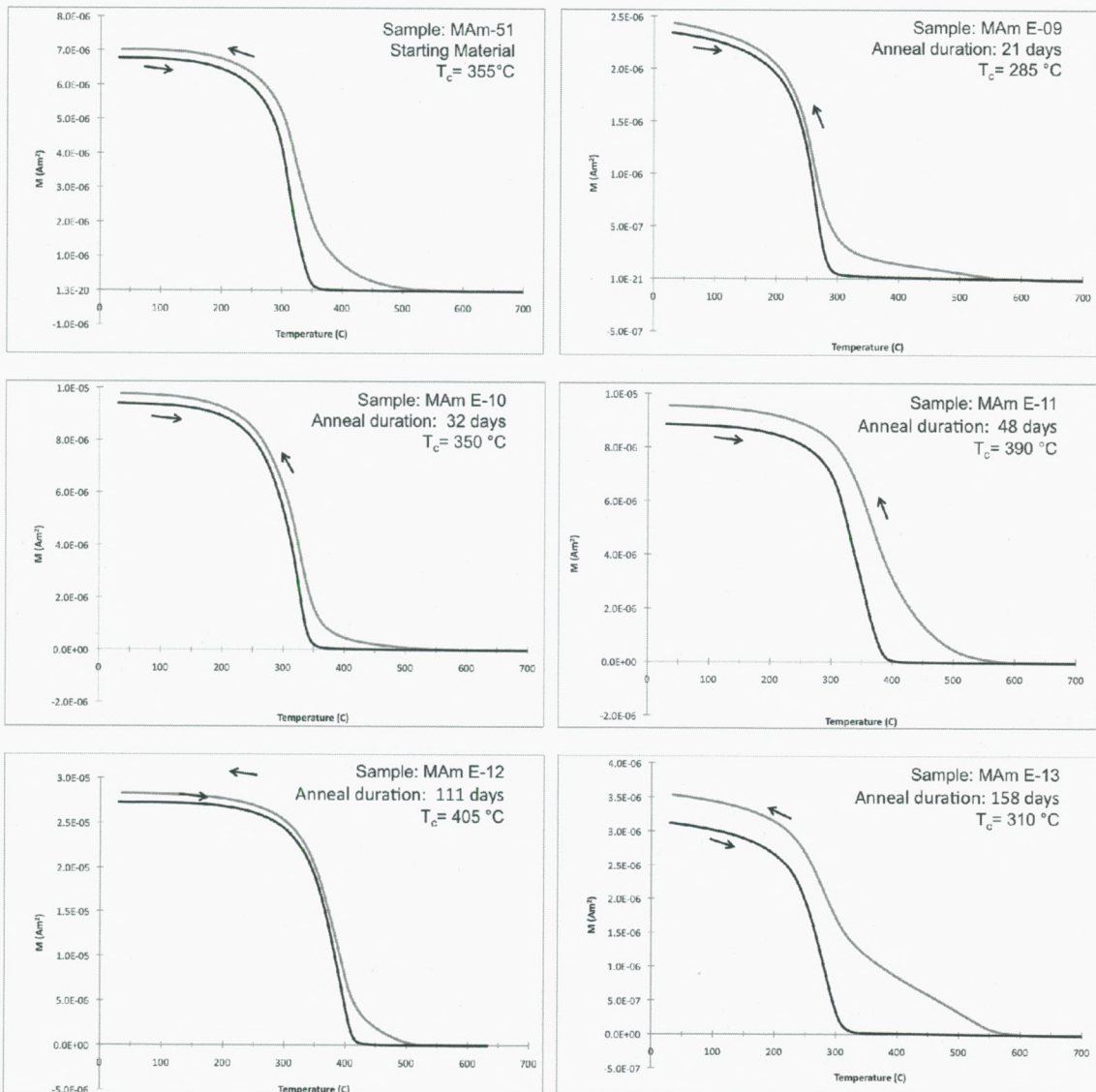
Figure 8. Hysteresis loops for T-type samples are pseudo single domain and multidomain.

Figure 9: 'Day Plots'



**Figure 9. 'Day Plots' displaying the hysteresis parameters found in M and T-type samples.** Dashed lines show experimental regions of magnetic domain state of titanomagnetite grains determined by Day et al., 1977. The numbers next to the symbols in figure 9a show the anneal duration of the adjacent datapoint in days. Figure 9b is a 'zoomed' out version of 9a showing QFM  $fO_2$  synthesized rapidly cooled samples from Brachfeld and Hammer, 2006.

**Figure 10: Moment as a function of temperature curves (M-type)**



**Figure 10. Magnetic moment as a function of temperature for M-type samples.** Curves were measured in a 50 mT applied field. Solid lines represent heating curves and dashed lines represent cooling curves.

Figure 11: Moment as a function of temperature (T-type)

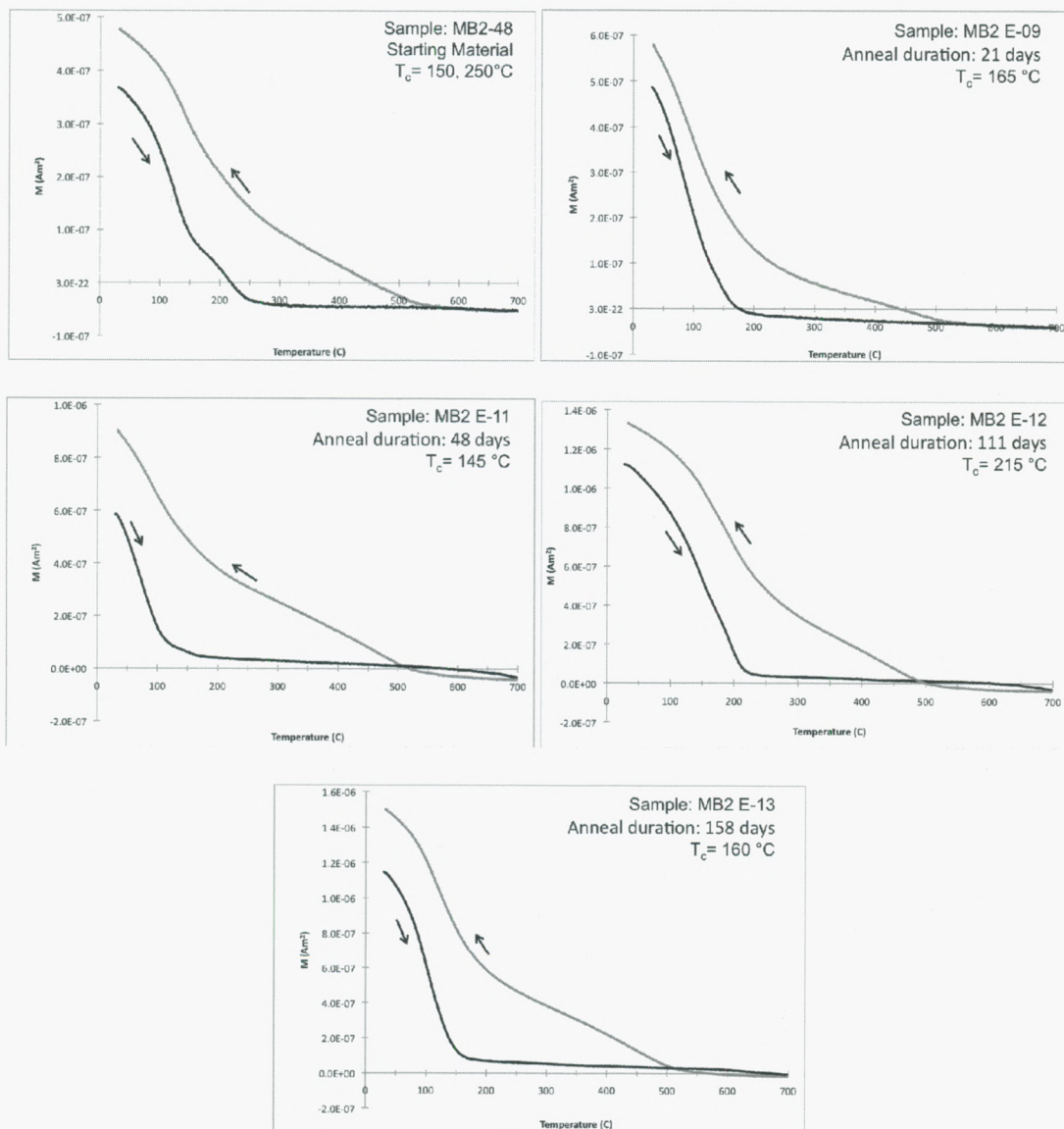


Figure 11. Magnetic moment as a function of temperature for T-type samples. Curves were measured in a 50 mT applied field. Solid lines represent heating curves and dashed lines represent cooling curves.  $M(T)$  curve for sample annealed for 32 days could not be obtained.

Figure 12. Depths to the Curie Isotherm

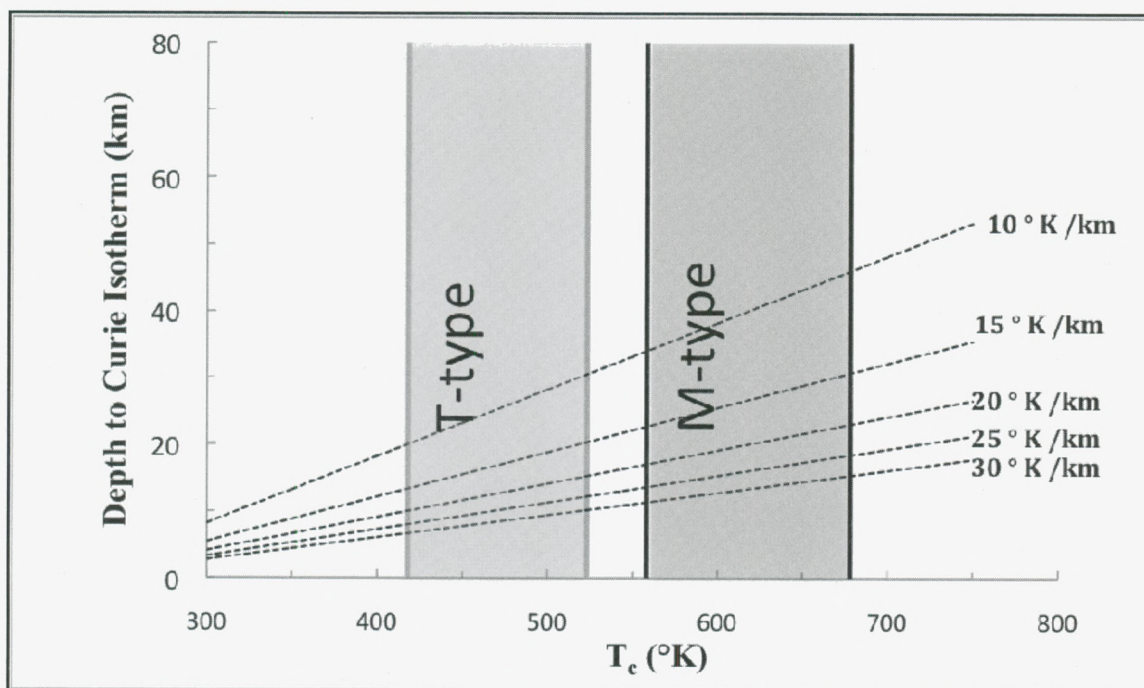


Figure 12. Depth to the Curie Isotherm given ranges of Curie temperatures within T-type and M-type samples. The dashed lines on the graph display possible geothermal gradients of 5-25 K/km using a surface temperature of 220 K. Curie points of T-type and M-type samples suggests the magnetized layer is roughly 5-30 km thick for T-type samples and 10-40 km thick for M-type samples.

Figure 13. Thermal and anhysteretic remanence

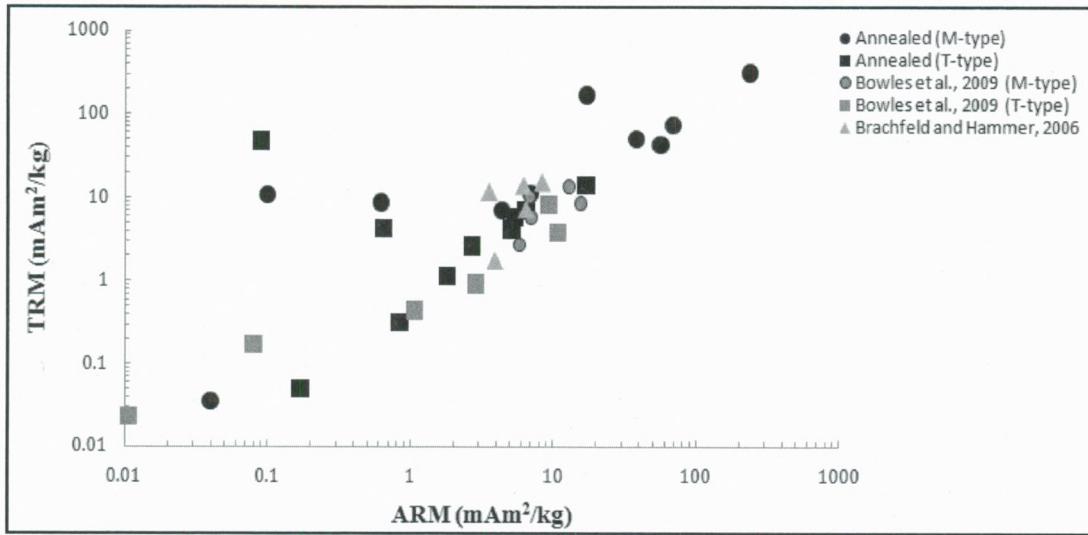


Figure 13. Thermal and anhysteretic remanences acquired by synthetic basalts of proposed Martian composition under QFM  $fO_2$  (Bowles et al., 2009, Brachfeld and Hammer, 2006). TRM in Brachfeld and Hammer, 2006 samples was acquired in an applied field of 50  $\mu$ T. M-type samples in this study acquired higher remanences than previous experimental runs.



**Table 1: Sample Nomenclature**

<b>Sample</b>	<b>Composition</b>	<b>Anneal Time (days)</b>
Mam 51	M -type	0
Mam E-09	M -type	21
Mam E-10	M -type	32
Mam E-11	M -type	48
Mam E-12	M -type	111
Mam E-13	M -type	158
MB2 48	T- type	0
MB2 E-09	T- type	21
MB2 E-10	T- type	32
MB2 E-11	T- type	48
MB2 E-12	T- type	111
MB2 E-13	T- type	158

**Table 2: Summary of Magnetic Properties of Martian Analogs**

Sample		Anneal Time (days)	Susceptibility (m <sup>3</sup> /kg)	TRM (mAm <sup>2</sup> /kg)	ARM (mAm <sup>2</sup> /kg)	MDF (mT)	T <sub>c</sub> (°C)
Mam 51 a	M -type	0	3.48E-05	42.62	56.27	3.7	
Mam 51 b	M -type	0	9.69E-05	316.14	238.85	3.9	
MAM 51 weighted average by mass			6.64E-05	181.68	149.1		350
Mam E-09 a	M -type	21	4.29E-06	7	4.38	3.5	
MAM E-09 weighted average by mass			4.29E-06	7	4.38	3.5	285
Mam E-10 a	M -type	32	3.86E-05	74.33	68.38	3.1	
Mam E-10 b	M -type	32	3.20E-05	0.0357	0.04	3.9	
MAM E-10 weighted average by mass			3.65E-05	51.02	46.94		345
Mam E-11 a	M -type	48	6.71E-06	11.28	6.94	4.1	
Mam E-11 b	M -type	48	3.12E-05	49.91	38.04	3.8	
MAM E-11 weighted average by mass			1.71E-05	27.69	20.15		385
Mam E-12 a	M -type	111	7.78E-05	169.72	17.22	6.3	
Mam E-12 b	M -type	111	2.59E-05		3.06	1.4	
MAM E-12 weighted average by mass			5.45E-05	169.72	10.86		410
Mam E-13 a	M -type	158	1.23E-05	8.67	0.62	1.1	
Mam E-13 b	M -type	158	1.62E-05	10.74	0.1	40	
MAM E-13 weighted average by mass			1.34E-05	9.25	0.47		310
MB2 48 a	T- type	0	7.19E-07	1.15	1.8	10.4	
MB2 48 b	T- type	0	3.47E-06	14.03	16.96	6.4	
MB2-48 weighted average by mass			1.41E-06	4.39	5.61		155, 255
MB2 E-09 a	T- type	21	1.93E-06	7.04	6.46	6.4	
MB2 E-09 b	T- type	21	2.42E-06	0.0049	0	5.6	
MB2 E-09 weighted average by mass			2.13E-06	4.2	3.86		175
MB2 E-10 a	T- type	32	8.31E-07	2.61	2.69	6.5	
MB2 E-10 b	T- type	32	3.21E-07	0.05	0.17	30.7	
MB2 E-10 weighted average by mass			7.25E-07	2.08	2.17		
MB2 E-11 a	T- type	48	2.54E-06	4.15	5.13	5.7	
MB2 E-11 b	T- type	48	2.82E-06	5.72	5.43	>50	
MB2 E-11 weighted average by mass			2.57E-06	4.35	5.17		130
MB2 E-12 a	T- type	111	6.76E-06				
MB2 E-12 b	T- type	111	4.17E-07	47.13	0.09	>50	
MB2 E-12 weighted average by mass			3.91E-06	21.18	0.04		220
MB2 E-13 a	T- type	158	2.41E-06	4.24	0.65	10.2	
MB2 E-13 b	T- type	158	3.93E-07	0.32	0.84	50	
MB2 E-13 weighted average by mass			1.94E-06	3.07	3.92		155

**Table 3: Hysteresis Parameters of Martian Analogs**

<b>Sample ID</b>	<b><math>M_s</math> (<math>\text{Am}^2/\text{kg}</math>)</b>	<b><math>M_r</math> (<math>\text{Am}^2/\text{kg}</math>)</b>	<b><math>H_c</math> (mT)</b>	<b><math>H_{cr}</math> (mT)</b>
MB2 48	0.095	0.009	2.56	8.77
MB2 E-09	0.126	0.014	3.30	10.36
MB2 E-10	0.036	0.004	3.86	12.11
MB2 E-11	0.101	0.007	1.90	7.92
MB2 E-12	0.180	0.018	3.04	8.50
MB2 E-13	0.091	0.008	2.64	8.56
MAm 51	4.295	0.191	2.56	9.35
Mam E-09	0.291	0.013	2.48	12.27
Mam E-10	2.664	0.102	2.09	9.40
Mam E-11	1.857	0.088	2.44	9.18
Mam E-12	4.998	0.280	3.06	9.53
Mam E-13	0.924	0.040	2.13	9.16

**Rock Magnetic and Remanence Properties of East Antarctic Dropstones:  
to aid the interpretation of Antarctic magnetic studies**

**INTRODUCTION**

This study presents a data set containing the magnetic properties of dropstones collected by Antarctic research vessel *Nathaniel B. Palmer*, cruise 01-01 (NBP01-01); an expedition that traversed across the East Antarctic Margin (Leventer et al., 2006). The intent of creating a magnetic dataset using sub-glacial crustal material is to aid the interpretation of magnetic anomaly maps of east Antarctica and provide characterization of the carriers of magnetization in east Antarctic rocks, which can be used as tracers in various magnetic studies performed along the East Antarctic Margin. The dropstones displayed are considered sub-glacial crustal material and contain carriers of magnetization within their original crystalline matrix unaltered from the sedimentation process, as well as bulk rock magnetic properties that contribute to the magnetic moment measured in an airborne and satellite magnetic survey.

Ninety-eight % of the Antarctic continent is covered by ice, therefore magnetic surveying of the Antarctic crust has become the most effective method used to interpret the geology of the subglacial landscape. These surveys include information on the composition of the Antarctic cratonic nuclei that encompasses the majority of east Antarctica and holds important information on the reconstruction of Precambrian geology, including the assemblage of Rodinia and break up of Gondwana. At a given location, altitude, and time a magnetic survey measures the total magnetic field present. This is described as the sum of three components; the ambient geomagnetic field (which is a function of the magnetic field of the core), the magnetization within the crust induced

by the ambient geomagnetic field (which is a function of the crusts' magnetic susceptibility), and the magnetic remanence found within rocks in the crust (i.e. the anomalies). To calculate the anomaly field from the total field measured one must first subtract the other contributors. The field of the core (subsequently filtered by the mantle) is distinguished due to its large intensity and low harmonic order (Aldredge et al., 1963). The fields produced by induction of the crust and the fields carried by magnetic remanence are unique to the magnetic material measured, thus some knowledge is needed about the material when making an interpretation of a magnetic survey. It is common for magnetic surveys to subtract the induced component of the crustal field using susceptibility measurements of the nearest exposure available for all measurements taken within ones survey line. However, areas far away from the Antarctic coast are of very complex geology and are overlain by several kilometers of ice where outcrops are limited or absent. The dataset provided in this study consists of direct observations of bedrock samples, which will provide a realistic range of susceptibility values for Antarctic rock types. This can lead to more accurate calculations of inducing components, therefore better determination of magnetic remanence values. Direct observations in this study also provide guidelines for the stability of the material in the deeper crustal regions, yielding information for the volume of the crust that may be measured in a survey. Factors affecting the rocks' remanent magnetization (NRM), susceptibility ( $k$ ), and stability, include the abundance of magnetic material in the rock, the magnetic mineralogy, magnetic domain state, and the materials' thermomagnetic properties. In this study we display these properties for each sample found and relate them to a possible anomaly they would produce.

## **Sample Location and Description**

U.S. Antarctic Program cruise 01-01 of the *Nathaniel B. Palmer* (NBP01-01) visited the East Antarctic Margin in 2001 with the primary goal of developing climate and oceanographic change during the Quaternary (Leventer et al., 2006). The expedition collected core, dredge, and grab samples in three main areas along the East Antarctic Margin. These regions include the George V Coast, Prydz Bay, and MacRobertson Land (Table 4, Figure 14). The dataset is composed of several 'lone-stones' inferred to be eroded from crustal material, transported and deposited as ice rafted debris or "dropstones" dropped from melting ice. The dropstones recovered are roughly 3 cm in diameter. In hand sample they can be generally described as igneous, metaigneous, or metapelitic origin. Based on the known geology of local outcrops it is probable that these samples are Archean to Proterozoic in age (Liu et al., 2009, Goodge and Fanning, 2010).

## **METHODS**

### **Sample Nomenclature**

Sample names described in this thesis are based on the following labeling scheme: cruise name, type of core, station from which the core was taken, and the core depth at which the dropstone was collected, i.e. sample NBP01-01 JPC34 59-62 cm is a dropstone taken by NBP01-01, extracted from a jumbo piston core at station 34, and the dropstone was taken from interval 59-62 cm. Samples collected from dredge stations were recovered from several hundred pounds of material and sorted into sample bags based on a rough estimate of the sample's lithology, i.e. the rocks were washed off then placed in the granitoid bag, or the fine-grained black rock bag, etc. Following a similar scheme but

adjusting for different collection device, dredge samples are labeled by the cruise number, the station at which the dredging was performed, the dredge number, and then the sample bag number into which the sample was sorted. For example, dropstone NBP01-01 S5-D3-B7 was collected by cruise NBP01-01, dredge number 3 at station five, and taken from sample bag number 7.

### **Optical Microscopy**

Transmitted light microscopy was used to classify rocks based on mineralogy and reflected light microscopy was used to obtain a rough estimate of the iron oxides' size, shape and quantification of their abundance. Thin sections were analyzed on a Zeiss Aksioskop. Percent abundance of iron oxide and iron sulfide minerals was quantified using approximately 12-20 random fields of view in polished section. These fields of view were loaded as .jpeg images into Zeiss Axiovision software and a routine was created to distinguish the bright iron oxide or sulfide minerals from the rest of the matrix. The total area the oxides occupied was calculated using the software and from that a two-dimensional areal percentage of the total field of view was calculated.

### **Electron Microscopy**

Thin sections were analyzed on a Hitachi S-3400N variable pressure scanning electron microscope (SEM) equipped with a Bruker X-flash x-ray microanalysis system. Measurements were taken under an accelerating voltage of 15 kV. Both uncoated polished sections and carbon-coated sections were used for analysis. The benefit of using uncoated samples was the ability to use the same thin sections for SEM analysis and reflected light microscopy. The disadvantage was analysis was done in a variable

pressure environment of ~20-60 Pa to prevent sample charging. This commonly caused beam skirting where oxygen and nitrogen gas molecules within the sample chamber deflect the electron beam away from the analysis spot, resulting in x-rays generated within neighboring minerals and appearing as artifacts within the spectrum. For these reasons selected samples were chosen to be carbon coated. Carbon coating was done on a Denton Desk IV TSC sample coater.

For coated samples, analysis of x-ray spectra was performed using Bruker Esprit 1.9 software to identify peaks and perform standardless quantitative analysis. Analysis was done three different ways, with iron assigned to the compounds FeO, Fe<sub>2</sub>O<sub>3</sub>, or Fe<sub>3</sub>O<sub>4</sub>. The compound that produced the total cumulative oxide percentage closest to 100% was determined to be the correct oxidation state of iron. For uncoated samples, likely artifacts within the spectrum produced by beam skirting, typically Si, Al, and Mg, were discarded and values were renormalized to 100%. Ratios of iron to titanium were compared to idealized Fe / Ti atomic ratios of common iron oxide minerals and used to classify iron oxide mineralogy. Any uncertainties with this method are stated in the results section.

### **Magnetic Susceptibility**

Magnetic susceptibility was measured on an AGICO KLY4 Kappabridge under an applied field of 300 A/m and a frequency of 920 Hz. Three measurements of each sample were taken, averaged together, and average values were normalized by mass. For Königsberger Ratio calculations ( $Q=NRM/kH$ ) the absolute value of volume-normalized units are reported for susceptibility and NRM values. Susceptibility and NRM values



were converted from mass-normalized to volume-normalized units using the sample's density. Density was measured using a buoyancy method by immersing the material in water and the volume of this displaced water was used to calculate density.

### **Magnetic Remanence Measurements**

Natural remanent magnetization (NRM) measurements were carried out on a 2G cryogenic magnetometer at the Paleomagnetism Laboratory at Lamont-Doherty Earth Observatory, Palisades NY. Unoriented samples were measured to obtain a bulk intensity of remanence and normalized by mass.

### **Magnetic Hysteresis**

Magnetic hysteresis loops were measured on a Princeton Measurement Corp. 3900-04C vibrating sample magnetometer (VSM). Small chips of each dropstone were attached to a plastic sample mount with silicon grease. Measurements were made in a 1 T peak applied field. Measurements were normalized by mass and the paramagnetic and diamagnetic contributions were subtracted using the high field slope above 0.7 T. Coercivity of remanence ( $H_{cr}$ ) was measured by inducing an isothermal remanent magnetization in a 1-T field and then demagnetizing the remanence in DC field increments of 10 mT up to 100 mT. Hysteresis parameters discussed in this study are saturation remanence ( $M_r$ ), saturation magnetization ( $M_s$ ), coercivity ( $H_c$ ), and coercivity of remanence ( $H_{cr}$ ).

## **Magnetic Susceptibility as a Function of Temperature**

Magnetic susceptibility as a function of temperature, referred to in the following sections as  $\chi(T)$  curves, were measured on a KLY-4 Kappabridge under a 300 A/m applied field. A 'partial magnetic extract' was used for analysis. Extracts were made by breaking chips with a mortar and pestle and then using a magnet to pick up magnetic particles within the crushed sample. We call this extract a partial extract because the material picked up by the magnet commonly clumped with other material, providing a mixture of magnetic and non-magnetic grains. Before measurement, the samples were combined with aluminum oxide powder to provide thermal connectivity between the sample and the temperature sensor, mixed, and evenly surrounded around the platinum resistance temperature sensor. Magnetic susceptibility was measured from 30-700°C in an argon atmosphere. A blank measurement of only aluminum oxide was used to subtract the furnace contribution from all curves. Curie temperatures were calculated by taking the first derivative of the curve and plotting it as a function of applied temperature. The maximum value of  $d\chi/dT$  in this plot was considered to be the Curie temperature. For weakly magnetic material a 4 to 10 point smoothing was performed to reduce noise from the paramagnetic and diamagnetic contributions before attempting to calculate the Curie temperature. Curie calculations using smoothed curves are stated in the results section.

## **RESULTS**

### **Meta Granitoids from Mac Robertson Land.**

*NBP01-01 JPC40 2302-2305 cm*

*NBP01-01 JPC40 2272-2275 cm*

Two dropstones were recovered from a jumbo piston core collected off the coast of MacRobertson Land, the western most sampling location in this study. Samples NBP01-01-JPC40 2302-2305 cm and NBP01-01-JPC40 2272-2275 cm are garnet bearing granitic gneisses. The gneissic fabric in both samples is faint due to the small size of the hand sample. Sample NBP01-01 JPC40 2302-2305 cm contains plagioclase, microcline, biotite and large garnet crystals that are typically found with ilmenite inclusions. Sample NBP01-01 JPC40 2272-2275 cm is an orthopyroxene-bearing meta-granite. The sample contains orthopyroxene, plagioclase, biotite, and garnet.

Susceptibility values for these samples were moderate to low with values within the range of  $10^{-4}$  SI. NRM values for sample NBP01-01 JPC40 2272-2275 cm are high, within the order of  $10^{-2}$  A/m, and much lower for sample NBP01-01 JPC40 2302-2305 cm, within the order of  $10^{-4}$  A/m.

Both samples displayed opaque oxide abundances within the range of 0.60 – 0.75%. Both samples displays Fe/Ti atomic ratios similar to ilmenite, however, they differ in their textures. Sample NBP01-01-JPC40 2272-2275 cm displays fractured ilmenites that commonly contain rutile intergrowths, inclusions, or what appears to be an alteration texture of rutile composition (Figure 15). Grains that contain rutile intergrowths typically have higher Fe/Ti ratios, suggesting the rutile is a product of exsolution or alteration. Sample NBP01-01 JPC40 2302-2305 cm contains equant ilmenite grains that are homogeneous in composition. Also present within both samples is an iron sulfide mineral with Fe/S ratios of roughly 1. Sample NBP01-01 JPC40 2302-2305 cm displays these grains with shapes determined by grain boundaries of other minerals (Figure 16).

Magnetic hysteresis data could not be obtained for either sample due to either the low abundance of oxides and high abundance of para- and diamagnetic silicates with the sample chip. Further, ilmenite is weakly magnetic and can be antiferromagnetic (appearing 'non magnetic' at room temperature) or canted antiferromagnetic depending on precise composition (Dunlop and Özdemir, 1997). Sample JPC40 2302-2305 cm displays an inverted hysteresis loop with a negative saturation magnetization. Hysteresis data for sample NBP01-01 JPC40 2272-2275 cm is extremely noisy and behaves as diamagnetic material in fields >100 mT.

$\chi(T)$  curves were noisy and a required 5-point smoothing of the curve to determine a Curie temperature in sample NBP01-01 JPC40 2272-2275 cm and a 10 point smoothing was needed to uncover a Curie temperature in sample NBP01-01 JPC40 2302-2305 cm. Sample NBP01-01 JPC40 2272-2275 cm displays a Curie temperature of 170°C seen only in the heating curve and a Curie temperature of 600°C seen in both the heating and cooling curves. This is interpreted as an ilmenite, and possibly a titanomagnetite carrier that has been maghemitized at higher temperatures. Sample NBP01-01 JPC40 2302-2305 cm displays a subtle change in susceptibility at a temperature of 575°C, however the curve appears to be linear and the observed Curie point is very subtle even after a 10-pt smoothing.

### **Prydz Bay Amphibolite**

*NBP01-01 JPC34 72 cm*

One amphibolite sample was found in the Prydz Bay area, sample NBP01-01

JPC34 72 cm. The dominant mineralogy in this rock is green amphiboles that possess a preferred orientation seen in thin section. Also present within this rock is quartz, biotite, and plagioclase.

This sample displayed a relatively low susceptibility and high NRM values of on the order of  $10^{-4}$  SI and  $10^{-2}$  A/m respectively. Oxide phases found within this rock are composed of irregularly shaped titanomagnetite grains or pure magnetite found commonly enclosed within micas, elongated and parallel to cleavage plains. Titanomagnetite grains (Fe/Ti ~15) are ~16  $\mu\text{m}$  in diameter and have aspect ratios of ~4 (Figure 17). Magnetite grains come in two varieties; acicular grains that appear to be reaction textures within micas, up to 75  $\mu\text{m}$  in length, or as inclusions within amphiboles, with the largest analyzed being 3  $\mu\text{m}$  in size.

$\chi(T)$  curves of sample NBP01-01 JPC34 72 cm display a Curie temperature of 570 °C, (obtained after 4-pt smoothing), seen in both the heating and cooling curves. We interpret this signal measured to be that of the ~16 $\mu\text{m}$  titanomagnetite seen using SEM techniques. Magnetic hysteresis could not be obtained in this sample, due to a negative measured saturation magnetization.

### **Prydz Bay Quartz Alkali feldspar Syenite**

*NBP01-01 JPC36 424-427 cm*

Sample NBP01-01 JPC36 424-427 cm recovered from Prydz Bay is a microcline-dominated metaigneous rock. For this reason we refer to it as alkali feldspar syenite, however this name is loosely given because modal mineral compositions and chemistry

are not known. Also present within the sample is quartz and biotite. Feldspars commonly display quartz grains enclosed within them.

The oxide phases present in this sample are composed of ~30  $\mu\text{m}$  grains and are of magnetite and ilmenite composition. Ilmenite grains contain high concentrations of manganese impurities up to ~ 3 wt%. Both oxide phases are irregularly shaped and display alteration textures, seen as dark regions in back scatter electron images (Figure 18). The composition of the alteration could not be achieved. The area of the altered regions are small and close to that of the interaction volume of the electron beam. In addition, this uncoated sample is affected by beam skirting.

This sample displayed low susceptibility and moderate remanence values of  $7.32 * 10^{-4}$  SI and  $4.05 * 10^{-2}$  A/m respectively. Hysteresis was not observed in this sample due to the low abundance of oxide grains as well as the dominance of paramagnetic feldspar found in this sample.

$\chi(T)$  curves for sample NBP01-01 JPC36 424-427 cm appear very noisy due to the lack of oxides. A 10-pt smoothing was applied to uncover a Curie temperature of 575°C, which is extremely subdued in the heating curve. This is interpreted to be the Curie temperature of the magnetite seen in SEM analysis.

### **Prydz Bay Meta-Granitoids**

*NBP01-01 JPC24 1611-1612 cm*

*NBP01-01 JPC34 75-78 cm*

*NBP01-01 JPC34 75-83 cm*

Three metamorphosed granitoids were recovered from the Prydz Bay area; samples NBP01-01 JPC24 1611-1612 cm, NBP01-01 JPC34 75-78 cm, and NBP01-01 JPC34 75-83 cm. Sample NBP01-01 JPC24 1611-1612 cm is a meta-granitoid that contains plagioclase and a potassium feldspar commonly found in exsolved perthitic textures. This rock also contains quartz with recrystallized textures, strained garnet that has recrystallized within its cracks, and an amphibole of unknown composition that displays high-order interference colors. Sample NBP01-01 JPC34 75-78 cm contains a similar amphibole as well as quartz, plagioclase, and minor amounts of microcline. Also present within this rock are regions, which contain fine-grained quartz, likely to be a microvein or a product of mylonitization. Sample NBP01-01 JPC34 75-83 cm is more tonalitic in composition, in the sense that the sample contains little microcline. The rock displays plagioclase, biotite, and hornblende. The biotite is commonly found to have reacted to chlorite mineral, as the two phases are seen together with interlocking textures.

Sample NBP01-01 JPC34 75-78 cm displays a moderate susceptibility and relatively high remanence values of  $8.97 \cdot 10^{-3}$  SI and  $2.03 \cdot 10^{-2}$  A/m. Iron oxides found within this sample are of magnetite composition, are equant in shape, and  $\sim 25$ - $100 \mu\text{m}$  in diameter. Magnetite grains commonly occur in clusters around areas that display similar spectrum to that of biotite (Figure 19). It is also common for these grains to contain inclusions that display similar spectra to the mineral outside the oxide, believed to be biotite.

Hysteresis plots display a thin multidomain loop with  $M_r/M_s$  values of 0.013 and  $H_c/H_{cr}$  values of 1.39. In fields of  $\sim 25$  mT the loop appears to be slightly 'pot bellied', displaying a second mineral with a slightly higher coercivity.

Curie temperatures of 450°C and 562°C are found for this sample. It is reasonable for the 562°C Curie temperature to be that of the magnetite seen in SEM analysis. It is unclear what the carrier of the 450°C Curie temperature is, as magnetite is the only oxide found using SEM techniques. It is possible that this is the same mineral that displays the 450°C Curie temperature however was not observed in SEM analysis.

Sample NBP01-01 JPC24 1611-1612 cm displays moderate susceptibility and high remanence values of  $4.82 * 10^{-4}$  SI and  $2.56 * 10^{-2}$  A/m. This sample contains an abundance of iron sulfide minerals. Sulfides within this sample come in two varieties, either as recrystallized minerals within cracks in mica (Fe/S = 1) or with textures that display iron rich regions, either as rims or as reaction textures (Fe/S = 1.5) (Figure 20).

Hysteresis loops for samples NBP01-01 JPC24 1611-1612 cm could not be obtained, most likely due to the lack of oxides present within the sample. The  $\chi(T)$  curves display a disturbance at ~ 400°C that shows a large peak in magnetization. This is most likely an artifact produced by clumped material, stuck high within the quartz measuring tube moving to the bottom closer to the sensor during measurement.

### **Prydz Bay Orthopyroxene-bearing Granites**

*NBP01-01 JPC34 59-62 cm*

*NBP01-01 JPC36 100-103 cm*

Two orthopyroxene bearing granitoids, similar to rocks of charnokitic-type composition, are found in the Prydz Bay area and include sample NBP01-01 JPC34 59-62 cm and sample NBP01-01 JPC36 100-103 cm. These rocks contain plagioclase,



orthopyroxene, clinopyroxene, quartz, biotite, and minor amounts of potassium feldspar.

Both samples display moderate susceptibility values and high remanence. Sample NBP01-01 JPC34 59-62 cm displays a susceptibility of  $3.74 * 10^{-3}$  SI and NRM of  $2.01 * 10^{-1}$  A/m. Sample NBP01-01 JPC36 100-103 cm displays a susceptibility value of  $9.25 * 10^{-4}$  SI and a NRM value of  $1.2 * 10^{-2}$  A/m.

Sample NBP01-01 JPC34 59-62 cm contains three oxides phases, the most dominant being an iron-rich ilmenite (Fe/Ti ratios  $\sim 1.4$ ). Also present is a subordinate population of magnetite and titanomagnetite (Fe/Ti ratios  $\sim 28$ ). Ilmenite grains are most commonly found on grain boundaries of micas, however, they are also seen as isolated equant grains. Magnetite grains are found within cleavage planes in mica or as irregularly shaped grains that display a myrmekitic type texture. A sole titanomagnetite grain was found in this sample. The grain is equant and contains chromite. Sulfide grains found within this sample are blocky and contain dark regions within the grain that display higher Fe/S ratios (Figure 20). Sample NBP01-01 JPC36 100-103 cm contains magnetite grains that have sulfur-rich regions or cores (Fe/S  $\sim 1.77$ ), and ilmenite grains that are equant and fractured (Figure 21).

Sample NBP01-01 JPC34 59-62 cm possesses a multidomain hysteresis loop with  $M_r/M_s$  and  $H_{cr}/H_c$  ratios of 0.054 and 5.05, respectively. Hysteresis loops for sample NBP01-01 JPC36 100-103 cm could not be observed because the measurement was too noisy.

Sample NBP01-01 JPC34 59-62 cm displays Curie temperatures of  $540^{\circ}\text{C}$ , seen in both the heating and cooling curves, and  $400^{\circ}\text{C}$  seen in just the heating curve. Due to the

general oxide abundances seen in SEM analysis we infer the 540°C Curie point to be that of titanomagnetite and the 400°C to be that of the iron sulfide.  $\chi(T)$  for sample NBP01-01 JPC36 100-103 cm displays a Curie point of 560°C, seen in both the curves but more pronounced in the cooling curve, and 312°C seen in only the heating curve. These values are inferred to be the Curie points of the Cr-titanomagnetite and the iron sulfide both seen in SEM analysis. In both samples, the iron sulfide likely alters during the experiment.

### **Prydz Bay Quartzite**

*NBP01-01 JPC34 345-350 cm*

One quartzite sample was recovered from the Prydz Bay, sample JPC34 345-350 cm. The sample is dominated by quartz that commonly display recrystallized textures. An amphibole mineral is also present that defines a faint fabric present within the rock, believed to be a product of grain flattening.

This sample possesses moderate susceptibility and NRM values of  $1.94 * 10^{-4}$  SI and  $6.36 * 10^{-3}$  A/m respectively. The carrier of magnetization in this sample is an Mn-bearing ilmenite. Ilmenite grains commonly contain Ti-rich alteration regions, displayed as rims or as alteration within cracks on the grain or are fractured and recrystallized with apatite. The grains are commonly  $\sim 200 \mu\text{m}$  in diameter and elongated (Figure 22).

The sample contains 0.04% oxides. Susceptibility values are low, displaying values of  $1.94 * 10^{-4}$  SI. NRM values were also low, displaying values of  $6.36 * 10^{-3}$  A/m. Hysteresis loops were noisy and parameters could not be determined for this

sample.  $\chi(T)$  could also not be obtained due to insufficient magnetic material.

## **Metapelitic Rocks of the George V Coast**

### **Biotite Hornfels**

*NBP01-01 S4-D2-B10*

*NBP01-01 S3-D1-B7*

Two quartz and mica dominated meta-sedimentary rocks were collected in the dredges on the George V Coast. We interpret these rocks to be hornfels due to the subtleness of their fabric and obvious sedimentary origin. Sample NBP01-01 S4-D2-B10 is a biotite hornfels dominated by coarse grains of quartz. The matrix of the rock is composed of biotite and iron oxide minerals. Sample NBP01-01 S3-D1-B7 displays a similar texture, however, quartz grains are smaller and the matrix of the rock contains chlorite and amphibole. These samples display relatively moderate susceptibilities within the range of  $10^{-3}$  to  $10^{-4}$  SI. Sample NBP01-01 S4 D2 B10 carries an intense remanence of  $1.59 * 10^{-1}$  A/m. Sample NBP01-01 S3 D1 B7 A carries a weaker remanence of  $1.44 * 10^{-4}$  A/m.

SEM analysis was performed on sample NBP01-01 S4-D2-B10. The iron oxides found within this sample are elongated Ti-rich ilmenite grains (Fe/Ti ~1.1). Ti-rich ilmenite grains commonly contain regions that display myrmekitic textures that are rich in titanium or regions within the grain that are of rutile composition. A lesser population of Mn-bearing ilmenite grains and magnetite are also present. Magnetite grains commonly contain inclusions of quartz (Figure 23).

Hysteresis measurements for sample NBP01-01 S4-D2-B10 display a narrow multi-domain type loop, with  $M_r/M_s$  and  $H_c/H_{cr}$  values of 0.006 and 1.73 respectively. NBP01-01 S3-D1-B7 displays a wider hysteresis loop that appears to be slightly wasp-waisted (i.e. constricted in its center), suggesting there are two magnetic minerals present with different coercivities (Figure 24). Parameters show that magnetic minerals in this rock have relatively higher coercivities with  $M_r/M_s$  ratios of 0.03. Remanent coercivity ( $H_{cr}$ ) could not be measured due to the magnetization increasing with increased demagnetizing field. It is possible that the isothermal remanent magnetization was never acquired in the original 1 T applied field.

Sample NBP01-01 S4-D2-B10 displays a  $\chi(T)$  curve with a Curie temperature of 568°C, seen in both the heating and cooling curve. Sample NBP01-01 S3-D1-B7 displays Curie temperatures of 562°C and 465°C also seen in both the heating and cooling curves. The 568°C Curie temperature mentioned for sample NBP01-01 S4-D2-B10 is high for the Fe-rich ilmenite seen in SEM analysis. It is possible for oxides present in the extract possess an oxide phase not seen in thin section, as the extract contains a larger abundance of oxides. The two Curie points for sample NBP01-01 S3-D1-B7 are likely carried by a similar ilmenite seen in sample NBP01-01 S4-D2-B10 and the lower  $T_c$  of 465°C carried by the second magnetic phase seen in hysteresis measurements. However it is still unclear as to which mineral is carrying the magnetic signal because all three oxide phases observed could produce a Curie temperature of 568°C and SEM analysis was not performed for sample NBP01-01 S4-D2-B10.

### **Mica Schists**

*NBP01-01 S3 D1 B4 C*

*NBP01-01 JPC11 2305 cm*

*NBP01-01 S4-D2-B7*

Samples NBP01-01 S3-D1-B4 C and NBP01-01 JPC11 2305 cm are interpreted to be two mica schists, displaying either biotite or muscovite as a dominant mica. The fabric in these samples is defined by elongated biotite or muscovite grains within a matrix of quartz and minor amounts of plagioclase. Sample NBP01-01 JPC11 2305 cm is a muscovite schist with a dominant mineralogy of muscovite, quartz, and plagioclase. Sample NBP01-01 S3-D1-B4 C is a higher grade schist containing biotite as its dominant mica and also containing an abundance of quartz. Sample NBP01-01 S4-D2-B7 is a biotite schist that contains a dominant mineralogy of biotite and quartz. This sample displays two phases of biotite, those that are euhedral and have a preferred orientation, and those that are subhedral and are randomly oriented in the sample. The matrix of the rock is composed of fine-grained material, possibly altered clays.

These samples all display moderate susceptibility values on the order of  $10^{-4}$  SI. NRM values were not obtained for these samples. Iron oxides within sample NBP01-01 S3-D1-B4 C are Mn-bearing ilmenite composition ( $Fe/Ti = 1.1$ ). These oxides are commonly elongated and situated within the fabric of the rock (Figure 25). The oxide phase within sample NBP01-01 JPC11 2305 cm is also ilmenite, however these minerals commonly contain intergrowths of rutile composition (Figure 26).

Hysteresis measurements for sample NBP01-01 JPC11 2305 cm display a distorted loop where magnetization increases at fields lower than saturation. Parameters for this loop therefore display  $M_r/M_s$  values are greater than 1 and this data is considered

invalid. Sample NBP01-01 S3-D1-B4 C displays an inverted hysteresis loop with a negative saturation magnetization. The inability to acquire reliable data for mica schists of the George V Coast is due to the lack of magnetic material within the samples. For this same reason magnetic extracts could also not be obtained for  $\chi(T)$  curves.

### **Biotite-Magnetite Schist**

*NBP01-01 S3 D1 B4 A*

*NBP01-01 S3-D1-B4 B*

Samples NBP01-01 S3-D1-B4 A and NBP01-01 S3-D1-B4 B are both schists that contain a fine-grained matrix and porphyroblasts of biotite and iron oxide. The biotite grains appear to have a preferred orientation in line with the fabric displayed in the matrix of the rock. The iron oxides do not appear to have the same orientation suggesting they are post-tectonic, however most grains are equi-dimensional. This type of fabric is more apparent in sample NBP01-01 S3-D1-B4 B than NBP01-01 S3-D1-B4 A.

Sample NBP01-01 S3-D1-B4 A displays a susceptibility of  $3.61 * 10^{-4}$  SI and a low NRM value of  $4.26 * 10^{-5}$  A/m. Sample NBP01-01 S3-D1-B4 B displays a higher susceptibility within the order of  $10^{-2}$  SI, however NRM values were not obtained for sample NBP01-01 S3-D1-B4 B.

Both biotite-magnetite schist samples display two oxide phases, one of ilmenite composition situated within the matrix of the rock and are elongated. The other is of magnetite composition, which is believed to be the porphyroblasts, observed as opaque minerals in transmitted light. Ilmenite grains commonly contain inclusions. The

magnetite grains are roughly 100  $\mu\text{m}$  in diameter and rectangular in shape (Figures 27 and 28).

Hysteresis loops for sample NBP01-01 S3-D1-B4 B are narrow, appearing multidomain. Hysteresis parameters  $M_r/M_s$  and  $H_{cr}/H_c$  display ratios of 0.004 and 3.38 respectively. Hysteresis loops could not be obtained for sample NBP01-01 S3-D1-B4 A due to negative saturation magnetization values.

Curie temperature data was obtained for both samples. Sample NBP01-01 S3-D1-B4 A displays a Curie temperature of 560°C seen in both the heating and cooling curves and 463°C seen in only the cooling curve (7-pt smooth). Sample NBP01-01 S3 D1 B4 B displays Curie temperatures of 565 and 600°C seen in both the heating and cooling curves.

### **Meta-sandstone**

#### *NBP01-01 S5-D3-B7*

One meta-sandstone sample was found in the dredges collected off the George V Coast. The sandstone contains sub-rounded quartz grains and minor amounts of biotite. Several of the quartz grains contain inclusions of unknown composition. The extent of metamorphism is seen in the recrystallized texture of quartz.

This sample possesses a low susceptibility of  $2 * 10^{-5}$  SI and moderate NRM value of  $2.7 * 10^{-3}$  A/m. Two oxides phases are found within this rock and are of titanomagnetite and magnetite composition. Fe/Ti ratios for titanomagnetite are roughly 10. Magnetite grains are found to have blocky structures while titanomagnetite grains

appear to be more equant. These grains are commonly found scattered within a grain of quartz or within cracks, appearing to be either a product of alteration of the quartz grains where iron oxides would crystallize as inclusions or as relict textures from the source material of this rock (Figure 29).

Magnetite hysteresis for this sample is inverted, displaying a negative saturation magnetization. A  $\chi(T)$  curve could not be obtained, as enough extract for measurement was not available.

### **Meta-granites of the George V Coast**

*NBP01-01 S5-D3-B5*

*NBP01-01 S5-B2*

*NBP01-01 S3-D1-B1 A*

Three metamorphosed granitoids were found in the dredges taken at the George V Coast. One is a granitic gneiss, containing an abundance of two feldspars, and two are more plagioclase rich rocks, considered to be tonalitic in composition. Sample NBP01-01 S5-D3-B5 is a granitic gneiss that contains quartz, plagioclase, microcline, and biotite, as well as minor amounts of iron rich chlorite. Samples NBP01-01 S5-B2 and NBP01-01 S3-D1-B1 A are plagioclase rich metamorphic rocks. The rocks contain quartz, plagioclase, biotite, and muscovite and accessory amounts of rutile and chlorite. Sample NBP01-01 S5-B2 contains minor amounts of microcline, however, it is highly fractured and has begun to recrystallize within its cracks.

These samples have roughly 0.08% oxides and display relatively moderate to low



susceptibility values within the order of  $10^{-3}$  SI. NRM values for this sample are within the order of  $10^{-4}$  A/m for sample NBP01-01 S3-D1-B1 A,  $10^{-3}$  A/m for sample NBP01-01 S5-D3-B5, and  $10^{-2}$  A/m for sample NBP01-01 S5-B2. Sample NBP01-01 S5-D2-B5 contains titanomagnetite (Fe/Ti = 44). These grains are equant, roughly 40  $\mu\text{m}$  in diameter, are commonly enclosed within a cluster of micas, and contain rims of unknown composition (Figure 30). Sample NBP01-01 S3-D1-B1 A contains two oxide phases. One is a magnetite phase that contains blocky grains and commonly appears to have cracks in their centers or sulfur-rich cores. The second is an ilmenite phase that is commonly associated with potassium micas appearing on their grain boundaries (Figure 31). Sample NBP01-01 S5-B2 was not analyzed using SEM techniques.

Sample NBP01-01 S5-D3 B5 displays a 'pot-bellied' hysteresis loop suggesting two magnetic phases with different coercivities.  $M_r/M_s$  and  $H_{cr}/H_c$  ratios for this sample are 0.02 and 7.6 suggesting multidomain type magnetic grains. Both samples NBP01-01 S3-D1-B1A and NBP01-01 S5-B2 display negative saturation magnetization.

$\chi(T)$  curves were able to be measured for samples NBP01-01 S5-B2 and NBP01-01 S3-D1-B1A. Both samples display Curie temperatures of 580°C seen in both the heating and cooling curves. Sample NBP01-01 S3-D1-B1 A displays a Curie temperature of 330°C seen only in the heating curve. The 580°C Curie is most likely that of the magnetite observed in SEM analysis and the 330°C Curie point most likely that of the sulfide.

## **George V Coast Mafic Igneous Rocks**

### *NBP01-01 S-II Volcanics*

*NBP01-01 S4-D2-V 4-2-2*

*NBP01-01 S3-D1-B10*

Three samples considered mafic igneous rocks were recovered from the George V Coast. Two samples, NBP01-01 S3-D1-B10 and NBP01-01 S4-D2-V 4-2-2, are fine-grained igneous rocks of dolerite/gabbro-type composition and sample NBP01-01 S-II Volcanics is a vesicular basalt. Doleritic samples contain clinopyroxene, orthopyroxene, and plagioclase. Clinopyroxene and plagioclase grains are commonly twinned. The vesicular basalt sample contains phenocrysts of pyroxene situated within a matrix most likely composed of plagioclase, apatite, and/or pyroxene, however, it is too fine grained to be identified.

Oxide phases found within dolerite samples NBP01-01 S3-D1-B10 and NBP01-01 S4-D2-V 4-2-2 are ilmenite grains that contain laths of titanomagnetite ( $\text{Fe/Ti} \sim 7$ ) displayed as sets running parallel to each other and meeting at angles of roughly 120 degrees (Figure 32). This type of texture is observed in grains 5 - 600  $\mu\text{m}$  in diameter. However, it is more developed in larger grains. It is also common for the grains to display highly fractured sections that have branch-like patterns where rutile has crystallized. Oxide grains within the vesicular basalt sample, NBP01-01 S-II Volcanics, are of titanomagnetite composition ( $\text{Fe/Ti} \sim 4.56$ ). These grains are found in cruciform type structure and are found within size ranges of 1-10  $\mu\text{m}$  (Figure 33).

All mafic igneous rocks display single domain hysteresis loops. Hysteresis parameters are roughly 0.3 for  $\text{Mr/Ms}$  and 2.1 for  $\text{Hcr/Hc}$ . The basalt sample has a slightly higher coercivity than the doleritic samples with  $\text{Mr/Ms} = 0.5$  and  $\text{Hcr/Hc} = 1.3$

and appears to be wasp waisted, suggesting the presence of another magnetic mineral not seen in SEM analysis.

Sample NBP01-01 S4-D2-V 4-2-2 displays a Curie temperature of 568°C seen in both the heating and cooling curves. Sample NBP01-01 S3-D1-B10 displays Curie temperatures of 538°C and 465°C in the heating curve, and 503°C seen only in the cooling curve. Sample NBP01-01 S-II volcanics displays a Curie temperature of 485°C seen in both the heating and cooling curves. For the doleritic type samples it is likely that the two Curie temperatures represent titanomagnetite and for the volcanic samples it is likely the 485°C Curie temperature is that of titanomagnetite. Volcanic samples, NBP01-01 S-II volcanics  $\chi(T)$  curves show Curie points of roughly 540°C and 515°C.

## DISCUSSION

This study consists of a dataset displaying the magnetic properties of 27 dropstones collected off the coast of east Antarctica. The dataset is compiled to aid the interpretation of magnetic anomaly maps along the East Antarctic Margin.

In the following section samples are distinguished based upon the ratio of their induced and remanent magnetization. We calculate this from the samples' natural remanent magnetization (NRM) and magnetic susceptibility ( $\chi$ ). The Königsberger Ratio (Q) is defined as the ratio of natural remanent magnetization (NRM) over the induced magnetization  $[k*H]$ , where k is magnetic susceptibility and H is the amplitude of the inducing field ( $Q = NRM/kH$ ). We use a value of 50  $\mu T$  for the inducing field.

Displaying the data in this fashion allows comparison to a hypothetical magnetic anomaly these rocks would produce if they were a homogeneous body of crust. Samples that display Q values greater than 1 can be considered remanent dominated anomalies and those Q values less than 1 can be considered induced dominated anomalies.

Three main areas were sampled along the East Antarctic Margin (EAM), these include MacRobertson Land, Prydz Bay and the George V Coast. The majority of samples recovered along the EAM are composed of metamorphosed plutonic rocks, metapelitic hornfels and schists, and mafic igneous bodies. Plutonics are found throughout the East Antarctica Margin, while metapelitic rocks and mafic rocks are concentrated in areas around the George V Coast. The majority of the samples display NRM and k values that generate Q values  $< 1$ , displaying high susceptibilities relative to remanence (Table 5). The majority of the rocks recovered are of deep crustal origin where rocks are mostly felsic in composition, lack iron, and the iron present is commonly found in paramagnetic mineral phases such as biotite and amphibole.

The majority of the samples displayed  $< 1\%$  oxides with the majority of remanence carriers consisting of multidomain magnetite, titanomagnetite, ilmenite, or iron-sulfide. For most samples, magnetic hysteresis could not be obtained due to the large paramagnetic and diamagnetic contribution present and lack of iron oxides. Figure 34 displays the range of domain state of the magnetic mineral found in the dataset. When hysteresis could be obtained, most samples were observed to have low coercivities believed to be multidomain. The distributions of Q values, magnetic susceptibility, and natural remanent magnetization are displayed in figure 35.

The carriers of magnetization found within this dataset are ilmenite, magnetite, titanomagnetite, and iron sulfides. A large range of Curie temperatures was observed, having Curie points ranging from 170 to 580°C. Curie temperatures below 200 °C are likely ilmenite. Curie points between 400 and 580°C are interpreted to be titanium-rich to titanium poor titanomagnetite and stoichiometric magnetite. Curie temperatures between 300-400 °C are likely sulfide minerals. Given geothermal gradients of 5-30°C/km we suspect these minerals to be magnetic between 5-110 km. Figure 36 plots temperature vs depth for several geothermal gradients and displays the range of depths to the Curie isotherm for each magnetic mineral.

The most abundant rock type found along the East Antarctic Margin is what is labeled in this study as meta-granites. We use this label as a general term for all rocks composed of what appears to be a plutonic igneous composition and show some sign of metamorphism. These rock types were found at all three sampling locations and display a wide range in composition from quartz alkaline syenite to tonalite. Most of the granitoids possess Q values < 1 or slightly above 1. These rocks display a wide range of iron oxide types. The majority of the rocks contain a low abundance of iron oxides, and are of magnetite, titanomagnetite, or ilmenite composition. These rocks also displayed iron sulfide minerals with variable Fe:S ratios, that may be paramagnetic or ferromagnetic depending on composition. These grains were commonly found within iron oxide grains or as isolated minerals.

Two meta-granites of similar composition were recovered from MacRobertson Land. Both rocks possess Q values > 1, have roughly the same percentage of iron oxides, and similar moderate susceptibility values (within the order of  $10^{-4}$  SI), but with orders of

magnitude different remanence values. The differences in remanence account for the different Q values of 0.06 and 0.69 and can be attributed to the differences in the magnetic mineralogy of the rocks. Remanence within the Q = 0.69 sample is carried by equant ilmenite grains that are homogeneous in composition. Remanence in the Q = 0.06 sample possesses ilmenite grains with rutile inclusions.

Meta granites found in the Prydz Bay area display Q values of 0.05, 0.23, and 1.06. These samples possess susceptibilities on the order of  $10^{-4}$  -  $10^{-3}$  SI and display relatively high NRM values on the order of  $10^{-2}$  -  $10^{-3}$  A/m. The samples with the 0.23 and 1.06 Q values contain iron sulfide minerals that possess rim type reaction textures of magnetite. These rocks possess similar susceptibility values, however differ in NRM values. The higher Q value sample (Q=1.06) contains 0.95% oxides, whereas the iron oxide abundance for samples with lower Q values contain is 0.05 % or less.

The sample with the lowest Q value within the Prydz Bay meta-granites (Q = 0.05) contains ~25-100  $\mu\text{m}$  equant, multi-domain, magnetite as well as an oxide phase with an unknown mineralogy. This sample displayed a Curie temperature of 450°C and a relatively high coercivity. These NRM is within an order of magnitude of other meta granitoids within Prydz Bay, however due to a different carrier of remanence, have much higher susceptibility, thus leading to a lower value for Q.

Three meta granite samples were found along the George V Coast. These samples possess low to moderate susceptibility values on the order of  $10^{-4}$  SI, and a range of NRM values of  $10^{-4}$  to  $10^{-2}$  A/m. The difference in remanence recorded has led to Q values of 0.09, 0.11, and 4.02. The three samples each possess a unique magnetic mineral

assemblage. The carriers of magnetization in the low Q values samples are either multidomain titanomagnetite,  $\sim 40 \mu\text{m}$ , commonly associated with micas, or blocky magnetite grains that commonly are seen with sulfur-rich cores or pitted centers. SEM analysis was not performed on the high Q value sample, however Curie temperature analysis suggests the carrier of remanence to be magnetite.

Two orthopyroxene bearing granitoids were found in the Prydz Bay area. These samples possess Q values of 1.07 and 0.26. The differences in remanence recorded can be attributed mostly to the percentage of iron oxides. These samples possess moderate to high susceptibilities and NRM,  $10^{-4}$  to  $10^{-3}$  SI and  $10^{-2}$  to  $10^{-1}$  A/m. The sample with the higher NRM possesses the higher Q value. The Q = 1.07 sample contains magnetite with sulfur rich regions. Magnetite comprises 3.43% of the rock. The Q = 0.26 sample possesses a lower percentage of iron oxides, roughly 0.40 %, in which occurs in three varieties; an Fe-rich ilmenite, magnetite, and titanomagnetite. The sample displays pseudo-single domain hysteresis parameters.

One quartz alkaline-feldspar syenite sample was found along the Prydz Bay area. The syenite sample displayed a high Q value of 2.41. It is inferred to that this value is due to the material's low susceptibility, not due to an exceptional NRM recorder. The syenite sample possesses a susceptibility on the order of  $10^{-5}$  SI and NRM on the order of  $10^{-3}$  A/m. This low value can be attributed to the abundance of diamagnetic potassium feldspar in the sample. The carrier of magnetization in this sample is magnetite  $> 30 \mu\text{m}$ , commonly displayed with alteration textures.

One amphibolite sample was recovered from the Prydz Bay region. This sample

possesses a Q value of 1.11, moderate susceptibility on the order of  $10^{-4}$  SI but carries a high remanence on the order of  $10^{-2}$  A/m. Two carriers of remanence are found in this sample, titanomagnetite,  $\sim 15 \mu\text{m}$  in length, and the other a subordinate population of magnetite inclusions found in amphiboles. It is probable that the inclusions found carry this remanence as smaller grains are generally capable of recording higher NRM's (Dunlop and Özdemir, 1997).

An array of metapelitic rocks were found along the George V Coast. The rock types include quartzite, metasandstone, hornfels, and schist. Many of the samples possess Q values  $> 1$  due to their low susceptibility values. There are several metamorphic facies present within this dataset including hornfels, muscovite schist, muscovite-biotite schist, biotite schist, and biotite magnetite schist. It cannot be determined from a dredge if these rocks are part of the same sequence, or if their source locations are in proximity, however an apparent change in magnetic properties should be mentioned. The low grade hornfels samples possess an abundance of iron oxides. As schistosity develops, these iron oxides are not seen in thin section until the higher grade schists where large magnetite grains begin to crystallize as metamorphic minerals.

Two samples within the George V Coast are interpreted to be hornfels. These rocks display Q values of 0.8 and 0.01. Both samples possess oxides that occupy 0.26% of the rock. The Q = 0.01 sample possesses susceptibility and NRM values within the range of  $10^{-4}$  SI and  $10^{-4}$  A/m respectively. SEM analysis was not performed on this sample. However, two Curie points of 465°C and 562°C and a multidomain slightly wasp-waisted hysteresis loop suggest two carriers of remanence, possibly titanomagnetite and ilmenite or an iron-sulfide. The higher Q value sample possesses a higher



susceptibility and NRM values within the range of  $10^{-3}$  SI and  $10^{-3}$  A/m respectively. The carrier of remanence within this rock is multidomain grains of Mn-bearing Ti-rich ilmenite, as well as a subordinate population of magnetite.

Three mica schists were recovered from the George V Coast. These rocks have susceptibilities in the range of  $10^{-4}$  SI and possess 0.06, 0.81, 0.22 % oxides. NRM values were not obtained for these samples. The carriers of magnetization within these samples are ilmenite grains that are elongated and situated within the fabric of the rock. These rocks are commonly found with Mn impurities or with rutile intergrowths.

Two biotite-magnetite schists were found in the George V Coast dredges. These rocks have large porphyroblasts of magnetite and biotite situated within a fine grained matrix that contains ilmenite grains with a preferred orientation in line with the fabric of the rock. The differences in these samples is clearly seen in how defined this texture is. The sample which displays a less defined texture displays low susceptibility and NRM values of  $10^{-4}$  SI and  $10^{-5}$  A/m respectively, leading to a Q value of 0.002. NRM was not measured for the sample with a more defined texture, however this sample possesses a much high susceptibility within an order of  $10^{-2}$  SI.

One meta-sandstone sample was found in the dredges off the George V Coast. This sample possesses a very low susceptibility of  $10^{-5}$  SI and moderate remanence of  $10^{-3}$  A/m, leading to a Q value of 2.69. The low can be attributed to the diamagnetic properties of quartz. The remanence here is carried by small equant titanomagnetite grains found within cracks between quartz grains, and small magnetite grains found as inclusions in quartz.

One quartzite sample was found in the Prydz Bay area. This sample displays a Q value of 0.65. This sample possesses a relatively low susceptibility of  $10^{-4}$  SI thought to be a function of the large abundance of diamagnetic quartz in this sample. The NRM value is within the range of  $10^{-3}$  A/m. The remanence is carried by elongated, fractured, ilmenite grains that occupy 0.04 % of the rock.

The highest Q value samples are mafic igneous rocks that were all found along the George V Coast. These rocks came in two varieties, vesicular basalt and dolerite. The Q values range from 1-9 for dolerite samples and 54-84 for basalts. Susceptibility values are on the order of  $10^{-3}$  SI for basalts and  $10^{-2}$  SI for the dolerites. NRM values of 12 to 22 A/m were observed for basalt samples and 1.5 - 4 A/m for dolerites. This suggests that both rock types possess an excellent magnetic recording assemblage. The carrier of remanence in volcanic samples were small single domain titanomagnetite grains that displayed a cruciform type growth morphology. Dolerite samples displayed grains with exsolution textures of ilmenite, titanomagnetite, and rutile. Both rock types displayed single domain hysteresis parameters attesting to the recording abilities of these samples.

## CONCLUSIONS

The dataset displayed in this study is composed of the magnetic properties of dropstones found along the East Antarctic Margin. We display these properties in the context of the type of magnetic anomaly they would produce. The majority of magnetic minerals are found in low abundances (<1%) in granitic and metamorphic rocks. The magnetic mineralogy is composed of (titano)magnetite, ilmenite, and iron sulfides. The

majority of these samples did not produce magnetic hysteresis due to an abundance of paramagnetic and diamagnetic silicates and low abundance of iron oxides. Samples that did produce hysteresis loops yielded multidomain hysteresis parameters. This suggests rocks found along the East Antarctic Margin consist of poor remanence recorders found in low abundances. Similarly, the majority of samples displayed Q values less than 1 suggesting they would produce induced dominated anomalies. The exception to this are two mafic igneous rocks, vesicular basalt and dolerite, that possess single domain magnetic minerals and recorded remanences several orders of magnitude higher than other east Antarctic rock types. The majority of samples displayed Q values less than 1 suggesting they would produce induced dominated anomalies. The exception to this are two mafic igneous rocks, vesicular basalt and dolerite, that possess single domain magnetic minerals and recorded remanences several orders of magnitude higher than other east Antarctic rock types.

Within these weakly magnetic rocks we find a wide range of magnetic properties that have a strong influence on the materials' Q value. These characteristics include the composition and texture of the magnetic mineralogy, the abundance of magnetic material, and the abundance and type of silicates. The most influential factor in east Antarctic rocks is the magnetic mineralogy and to a lesser extent abundance of magnetic material and type of silicates present. We find that rocks of similar bulk composition may possess very different magnetic mineral assemblages and therefore possess different magnetic properties and Q values. Most rocks are carried by one to several magnetic minerals that possess interesting textures and composition that contribute to the magnetic properties of the rock. The oxides and sulfides present, along with the silicates in the rock contribute to

the rocks unique remanence and susceptibility that may be seen in a magnetic survey.

## REFERENCES

Allredge, L., Van Voorhis, G., Davis, T., (1963) A magnetic profile around the world, *J. Geophys. Res.*, **68** (12) pp 3679-3692

Dunlop, D., Özdemir Ö., (1997), *Rock Magnetism Fundamentals and frontiers*, Cambridge Studies in Magnetism, Cambridge University Press, 573 pp., ISBN 0 521 32514 5

Goode, J., Fanning, M., (2010) Composition and age of east Antarctic shield in eastern Wilkes Land determined by proxy from Oligocene-pleistocene glaciomarine sediment and beacon supergroup sandstones, Antarctica, *Geological Society of America Bulletin* July 2010, **122**, p. 1135-1159, first published on March 29, 2010, doi:10.1130/B30079.1

Leventer, A., Domack, E., Dunbar, R., Pike, J., Stickely, C., Maddison, E., Brachfeld, S., Manley, P., McClennen, C., (2006), Marine sediment record from the East Antarctic margin reveals dynamics of ice sheet recession, *GSA Today*, **16**, 4-10

Liu X., Zhao, Y., Song, B., Liu, J., Cui, J., (2009), SHRIM U-Pb zircon geochronology of high-grade rocks and charnockites from the eastern Amery Ice Shelf and southwestern Prydz Bay, East Antarctica: Constraints on Late Mesoproterozoic to Cambrian tectonothermal events related to supercontinent assembly, *Gondwana Research*, **16**, 342-361

Figure 14. Ice Drainage Basin Map and Sample Locations

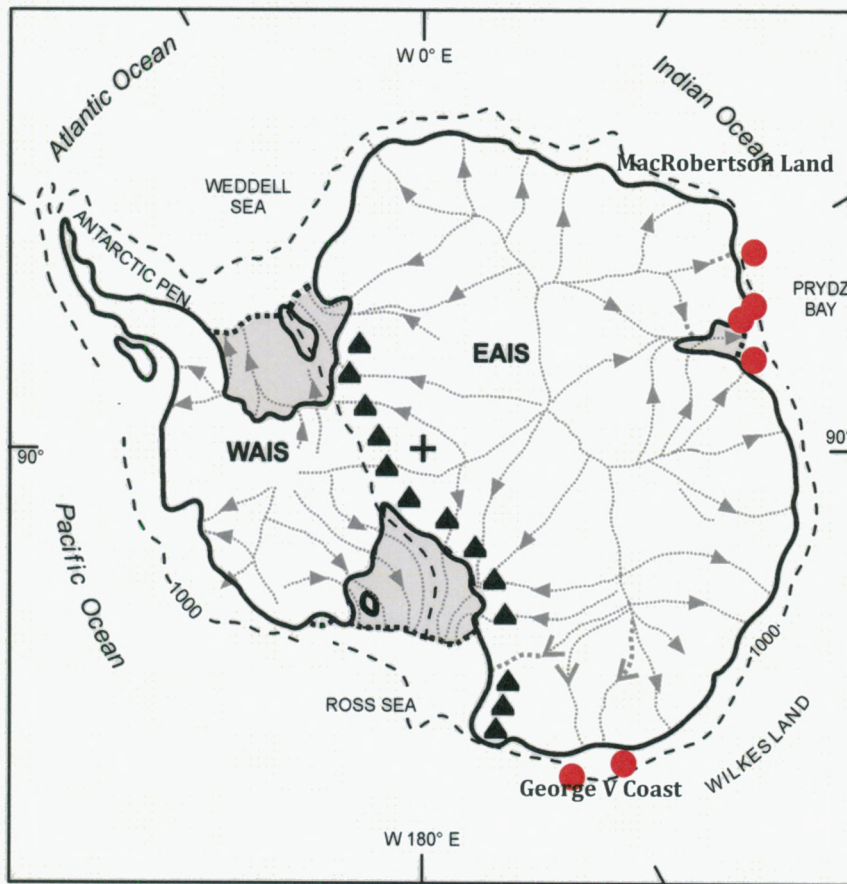


Figure 14. Ice drainage basin map of Antarctica. The circles represent approximate core and dredge locations where samples were collected. Ice drainage basin map taken from Naish et. al, 2009.

Figure 15: Sample NBP01-01 JPC40 2272-2275 cm

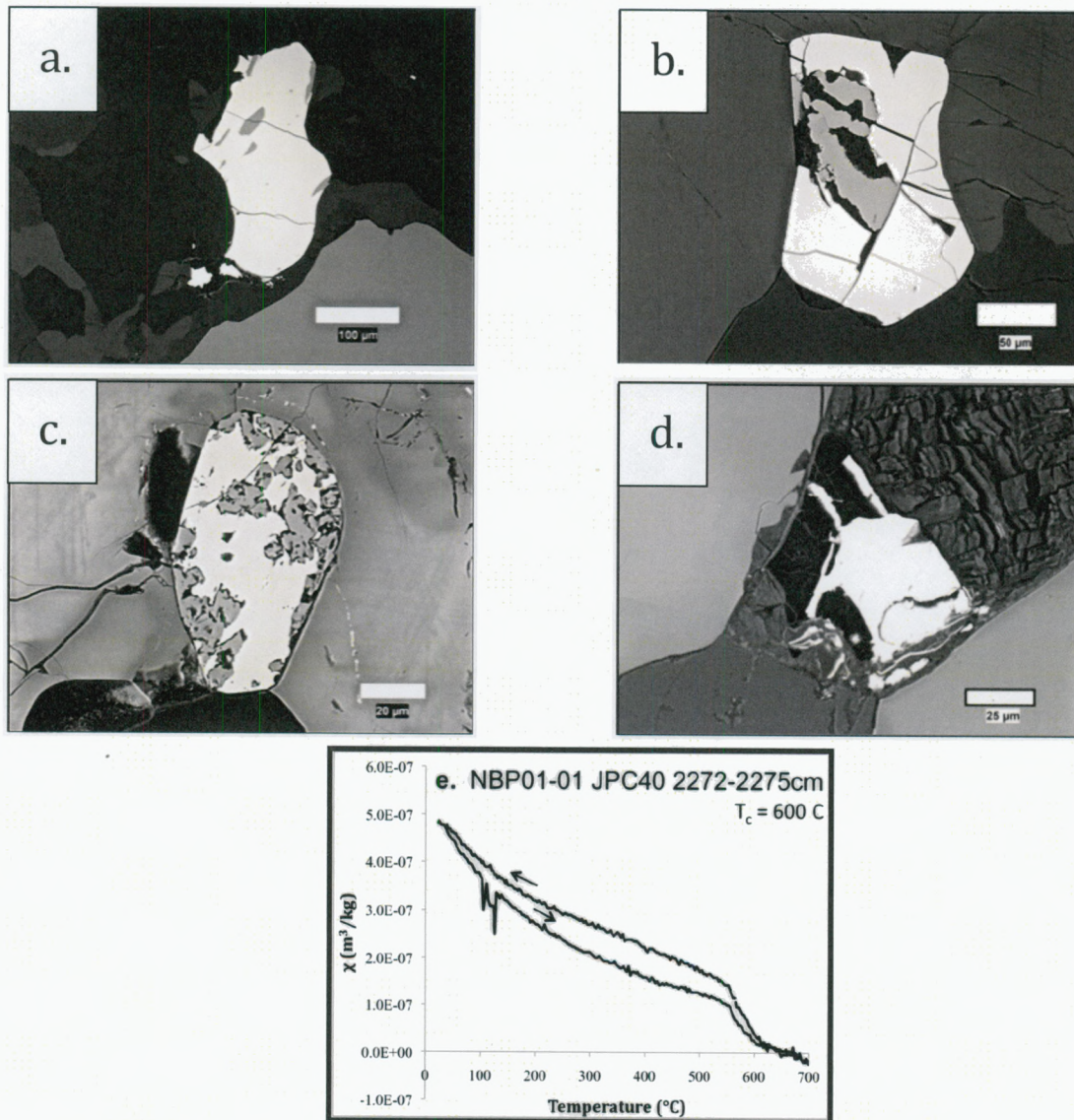


Figure 15. Sample NBP01-01 JPC40 2272-2275 cm

**a.** The large grain in the center of the image is an ilmenite ( $Fe/Ti = 1.2$ ). The darker regions within the grain are of rutile composition. The bright mineral on the tail of the grain is an iron sulfide ( $Fe/S$  ratio of 1.72). **b.** The mineral centered in figure b is an ilmenite grain. The dark center of the grain is of rutile composition. **c.** The mineral in the center of the image is a Fe-rich ilmenite ( $Fe/Ti = 1.32$ ). The darker sections near the grain boundary and approaching the center of grain are Ti-rich - Fe-poor regions interpreted to be a product of oxidation. **d.** Iron sulfide ( $Fe/S = 1$ ) located between the grain boundaries of two quartz grains. **e.** The  $\chi(T)$  curve displays a Curie temperature of 600 °C, most apparent in the cooling curve.

Figure 16: Sample NBP01-01 JPC40 2302-2305 cm

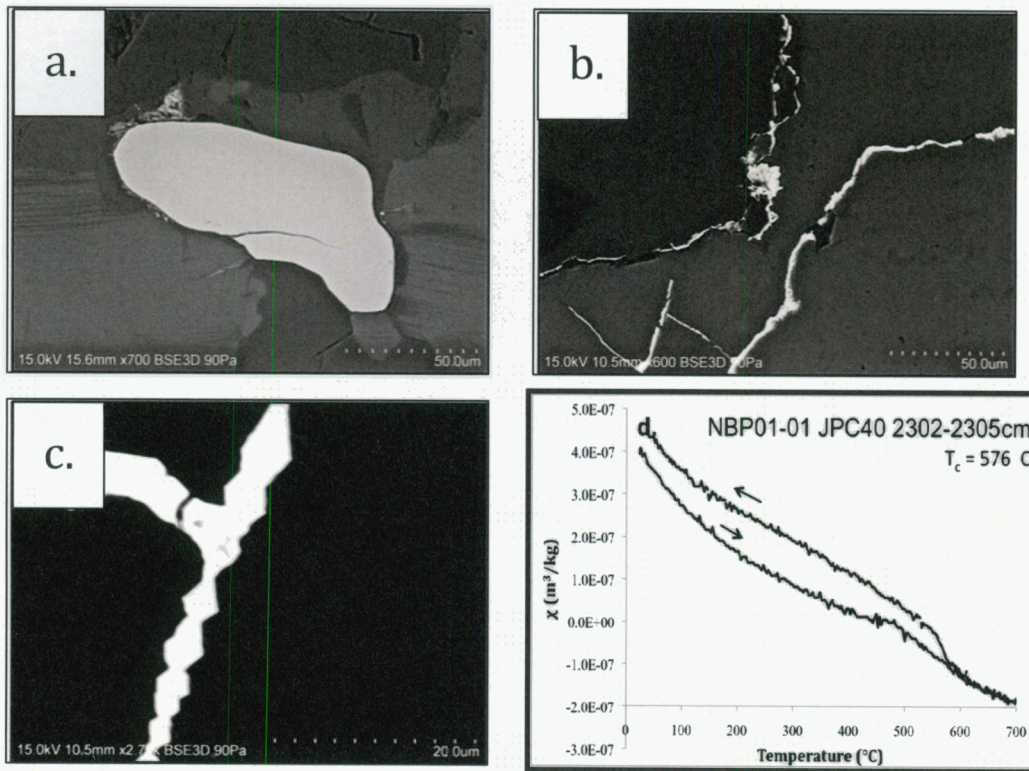


Figure 16. Sample NBP01-01 JPC40 2302-2305 cm

a. Equant ilmenite grain ( $\text{Fe}/\text{Ti} = 1.1$ ). b. and c. are iron sulfides ( $\text{Fe}/\text{S} \sim 1$ ). These sulfides appear to be secondary minerals forming in the cracks within what appears to be a mica, however, spectra were not taken. d.  $\chi$  (T) plot displays a weak Curie point of 576 °C after a 10 pt smoothing of  $d\chi/dT$  data. However, both the heating and cooling curve appear to be linear.

Figure 17: NBP01-01 JPC34 72 cm

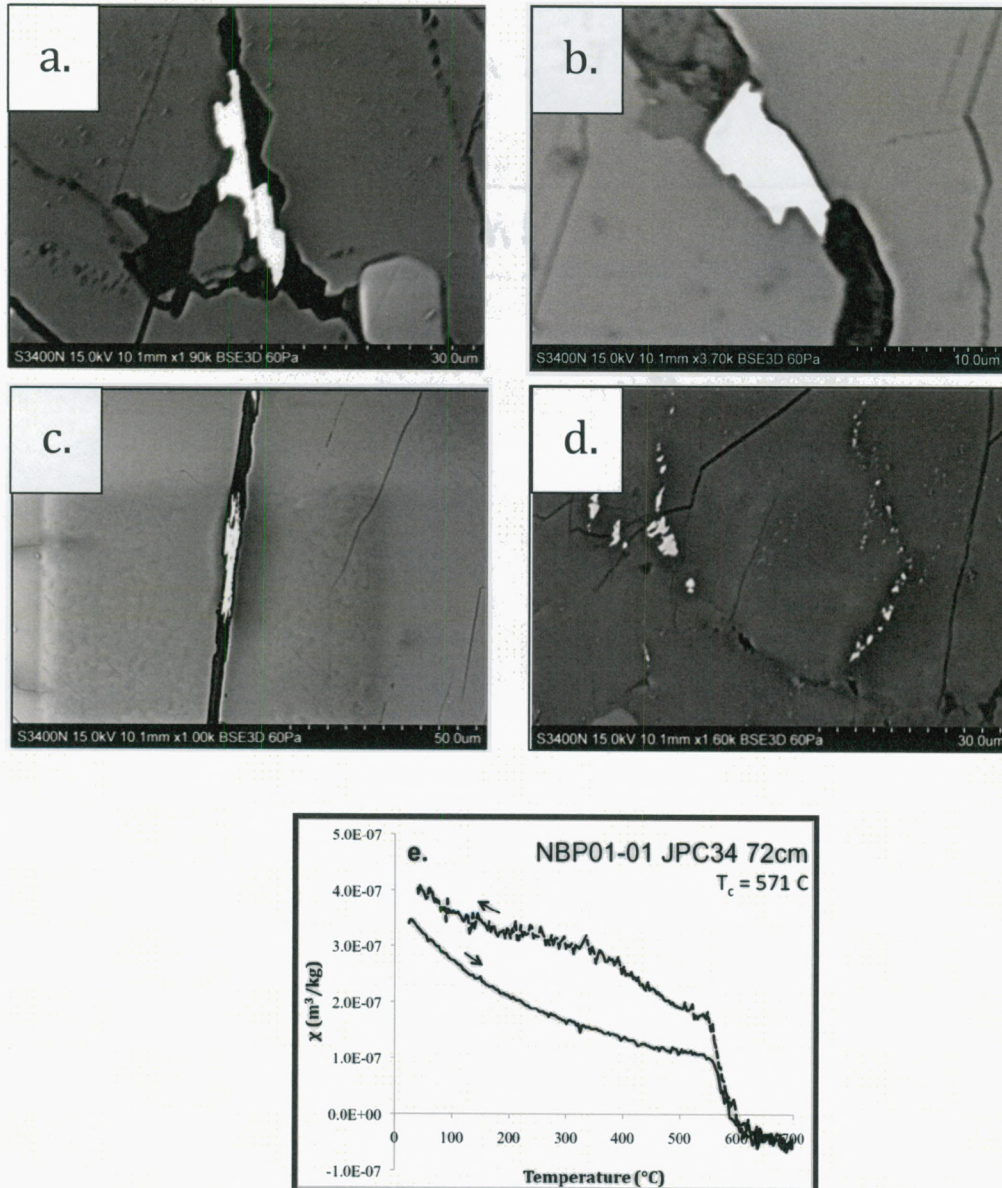


Figure 17. Sample NBP01-01 JPC34 72 cm.

**a.** and **b.** display irregularly shaped titanomagnetite grains ( $\text{Fe}/\text{Ti} \sim 15$ ). **c.** and **d.** display magnetite grains. Image **c** is a magnetite grain within a crack between two micas. **d.** displays a cluster of inclusions within an amphibole. **e.** A Curie temperature of 571  $^{\circ}\text{C}$  is observed in the  $\chi$  (T) plot, interpreted to be that of titanomagnetite.



Figure 18: NBP01-01 JPC36 424-427 cm

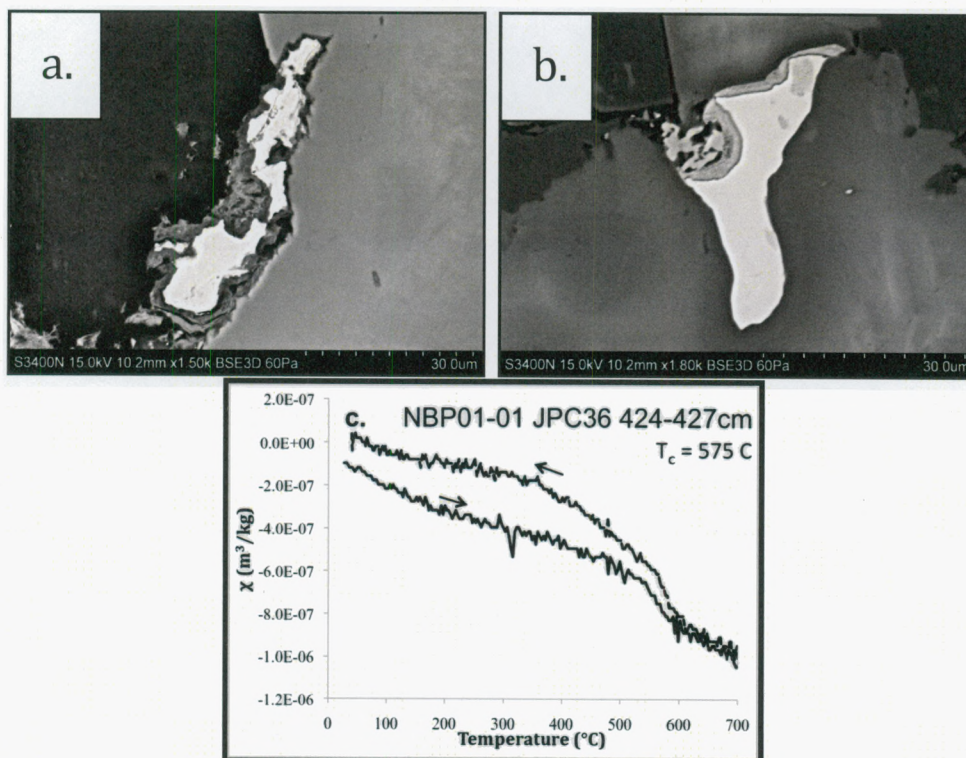


Figure 18. Sample NBP01-01 JPC36 424-427 cm

**a.** Magnetite partially enclosed within a bitotite grain. To the right of the oxide is a k-feldspar. **b.** is a Mn bearing ilmenite grain. The mineral is found on the boundary of two feldspars, microcline (bottom) and a perthitic feldspar (top). Alteration regions in grains a and b are thinner than the interaction volume of the beam, therefore a valid composition could not be obtained. **e.**  $\chi$  (T) plot. Displays a Curie temperature of 575  $^{\circ}\text{C}$  believed to be that of magnetite.

Figure 19: Sample NBP01-01 JPC34 75-78 cm

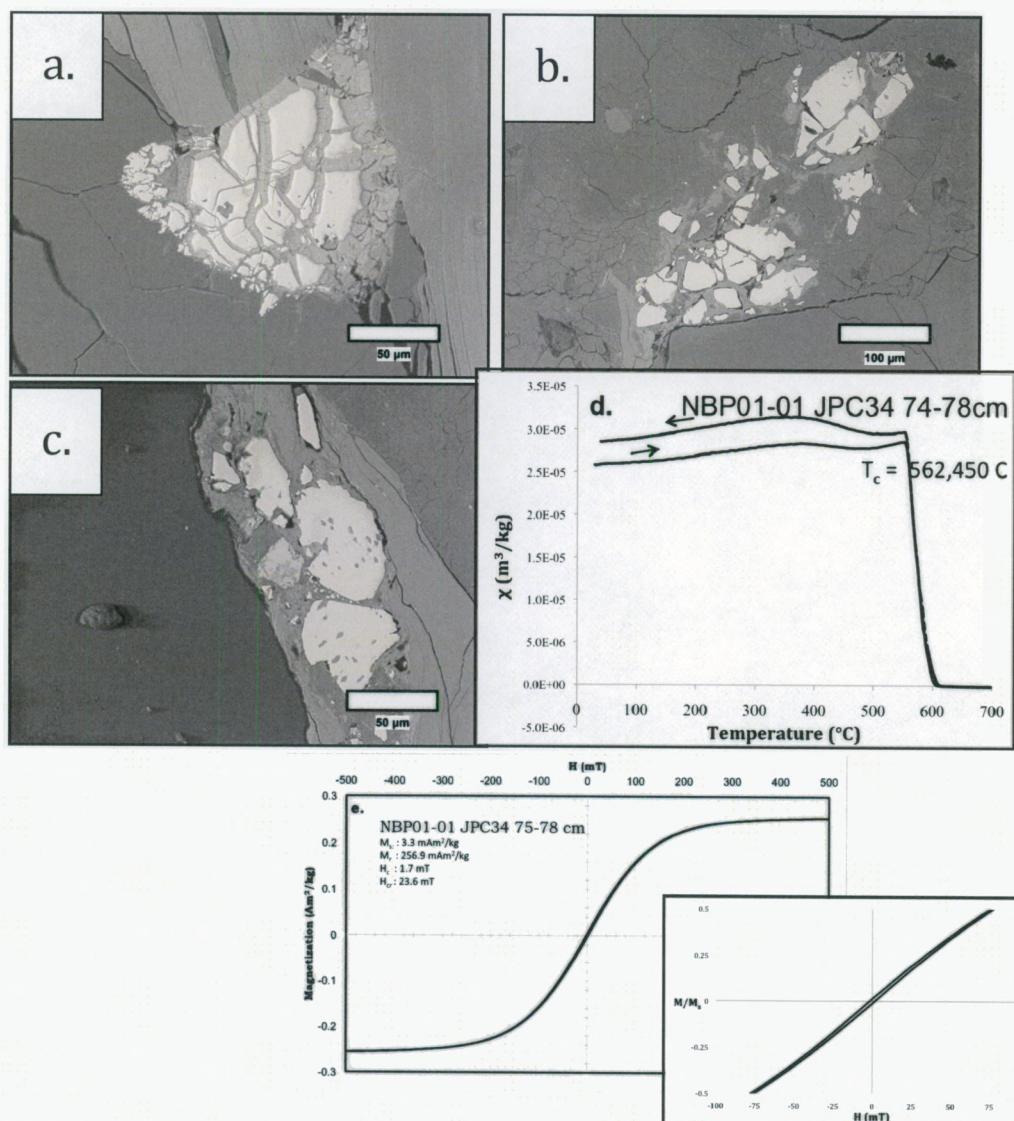


Figure 19: Sample NBP01-01 JPC34 75-78 cm.

Backscatter electron images **a.** **b.** and **c.** display three clusters of grains of magnetite composition. The light areas around the grains display similar EDS spectra to that of biotite. **d.** Curie temperatures of  $450^{\circ}$  and  $562^{\circ}\text{C}$  are that of an unknown mineral and magnetite. Magnetite was the only mineral observed in SEM analysis. **e.** Magnetic hysteresis for this sample displays a thin multidomain loop. (inset) The y-axis is magnetization normalized by saturation magnetization and displays a close up near the origin  $\pm 100$  mT to show a slightly pot-bellied loop.

Figure 20. Samples NBP01-01 JPC24 1611-1612 cm

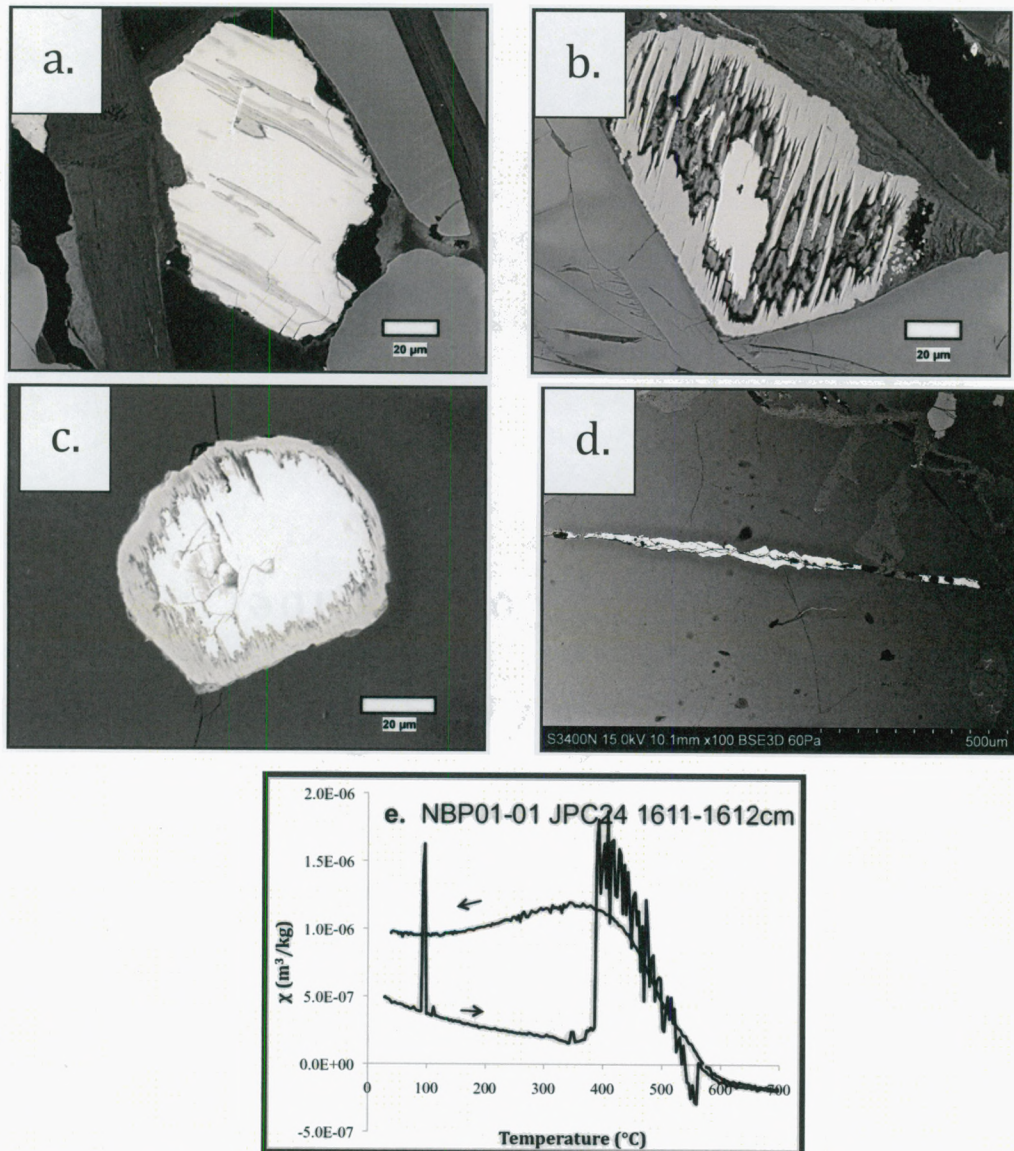


Figure 20: Sample NBP01-01 JPC24 1611-1612 cm.

**a. b. and c.** Backscatter electron images. The lighter regions within these grains are sulfides ( $\text{Fe/S} \sim 1.5$ ). The darker regions around these grains are more iron rich. **d.** A sulfide grain enclosed within a potassium mica. **e.** The  $\chi$  (T) plot displayed appears to be disturbed at roughly 400  $^{\circ}\text{C}$ . This is most likely sample moving in the quartz tube during the experiment.

Figure 21. Samples NBP01-01 JPC34 59-62 cm

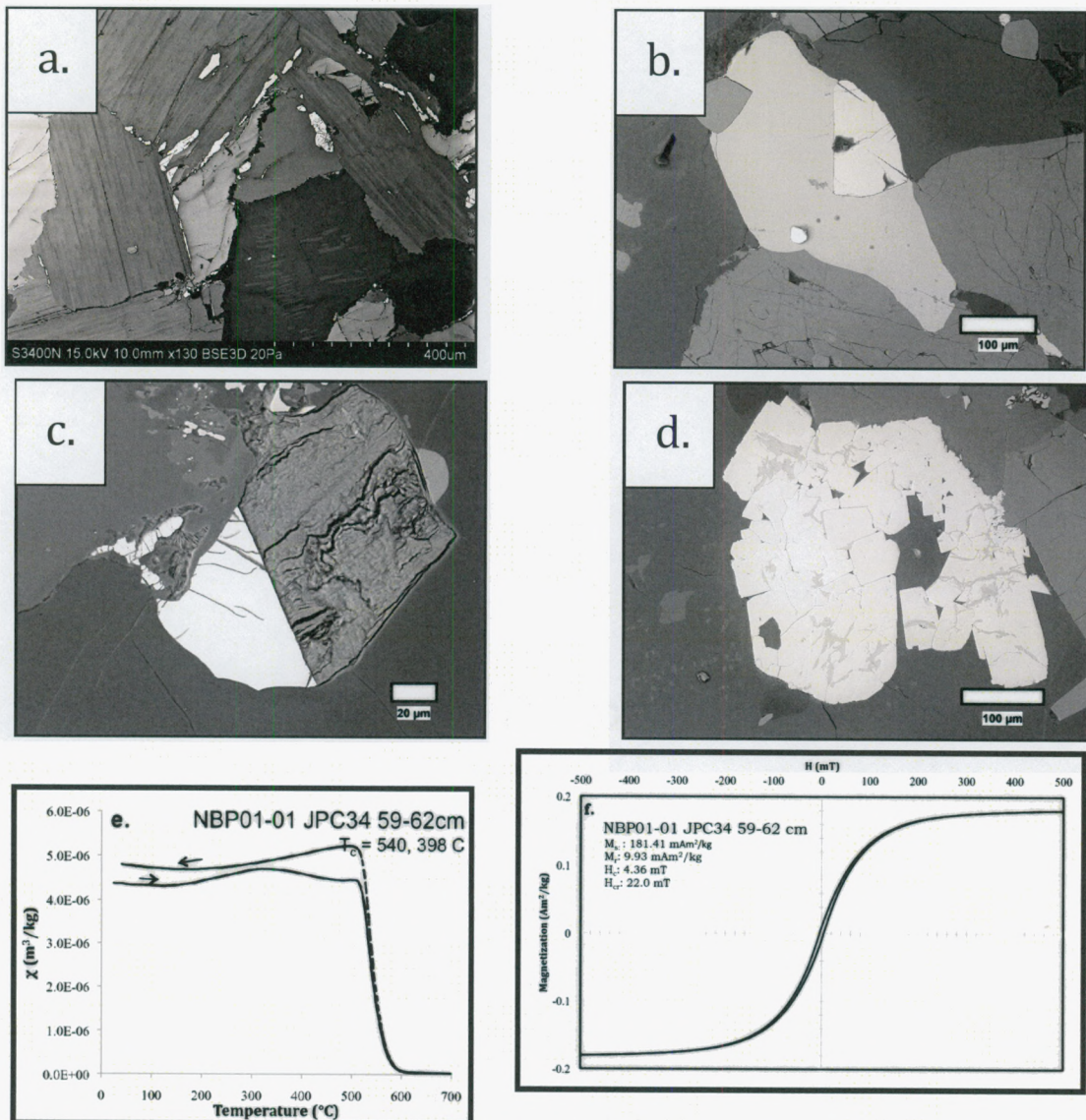


Figure 21. Sample NBP01-01 JPC34 59-62 cm

**a.** Ilmenite grain found on grain boundaries of a mica. **B.** ilmenite grain (Fe/Ti = 1.5). The dark regions around the ilmenite are of K-feldspar composition. Lighter regions outside the grain are a white mica. **b.** Titanomagnetite (Fe/Ti = 20) grain that contains chromium impurities. Surrounding the grain is an ilmenite. **c.** Magnetite grain with a myrmekitic texture that displays a similar spectrum to that of a Ca-pyroxene or amphibole. **d.** Iron sulfide (Fe/S = 1.3) with darker, altered areas that are more iron rich (Fe/S = 6.17).

**e.** Curie temperatures of 540 °C and 398 °C. The 540 °C point is believed to be that of titanomagnetite and the 398 °C point is believed to be that of the iron sulfide.

Figure 22. Sample NBP01-01 JPC36 100-103 cm

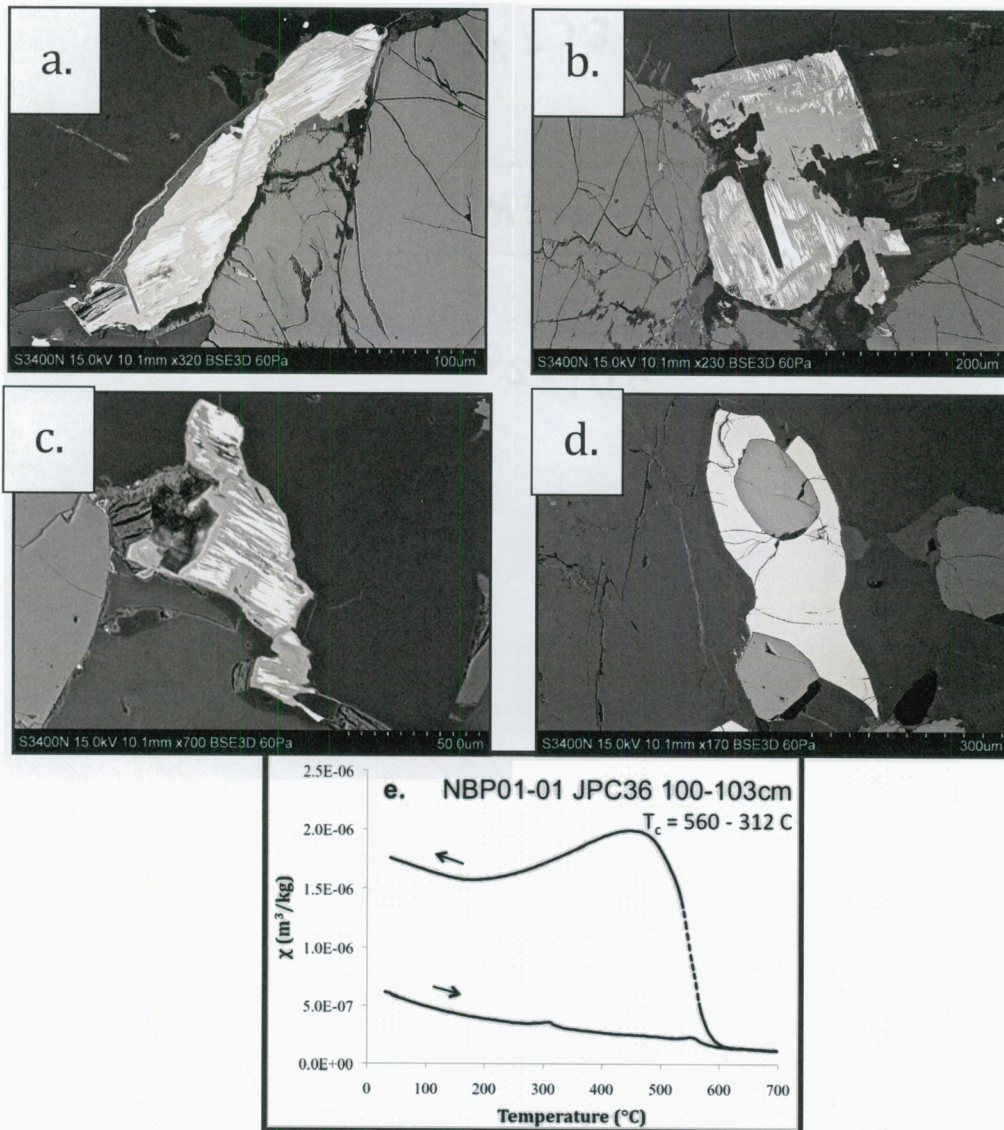


Figure 22. JPC36 100-103 cm

Sample NBP01-01

**a. b. and c.** Backscatter electron images of magnetite grains found in sample NBP01-01 JPC36 100-103 cm. The dark areas within the magnetite grain may be intergrowths or alteration. **d.** Ilmenite grain found in sample NBP01-01 JPC36 100-103 cm. Enclosed within the grain is an apatite. **e.** Curie temperatures of 312  $^{\circ}\text{C}$  and 560  $^{\circ}\text{C}$  are believed to be that of the ilmenite and magnetite respectively.

Figure 23. Sample NBP01-01 JPC34 345-350 cm

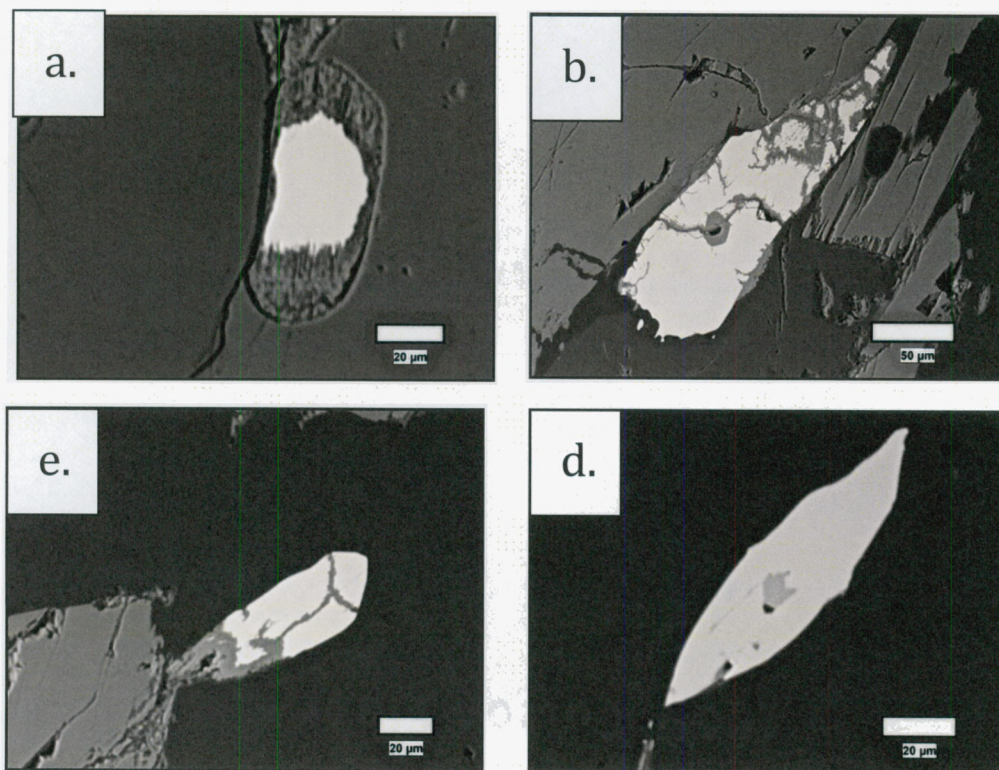


Figure 23. Sample NBP01-01 JPC34 345-350 cm.

**a.** Mn bearing Ilmenite ( $\text{Fe}/\text{Ti} = 1.11$ ). The reaction rim around the ilmenite has a similar spectrum to a biotite. The mineral around the grain is quartz. **b.** Mn bearing ilmenite. The alteration areas inside the grain display similar spectra to that of apatite. **c.** Mn bearing ilmenite ( $\text{Fe}/\text{Ti} = 1.18$ ). **d.** Mn-bearing ilmenite grain with a Ti-rich core in the center of the grain. Around the grain is quartz.

Figure 24. Sample NBP01-01 S4-D2-B10

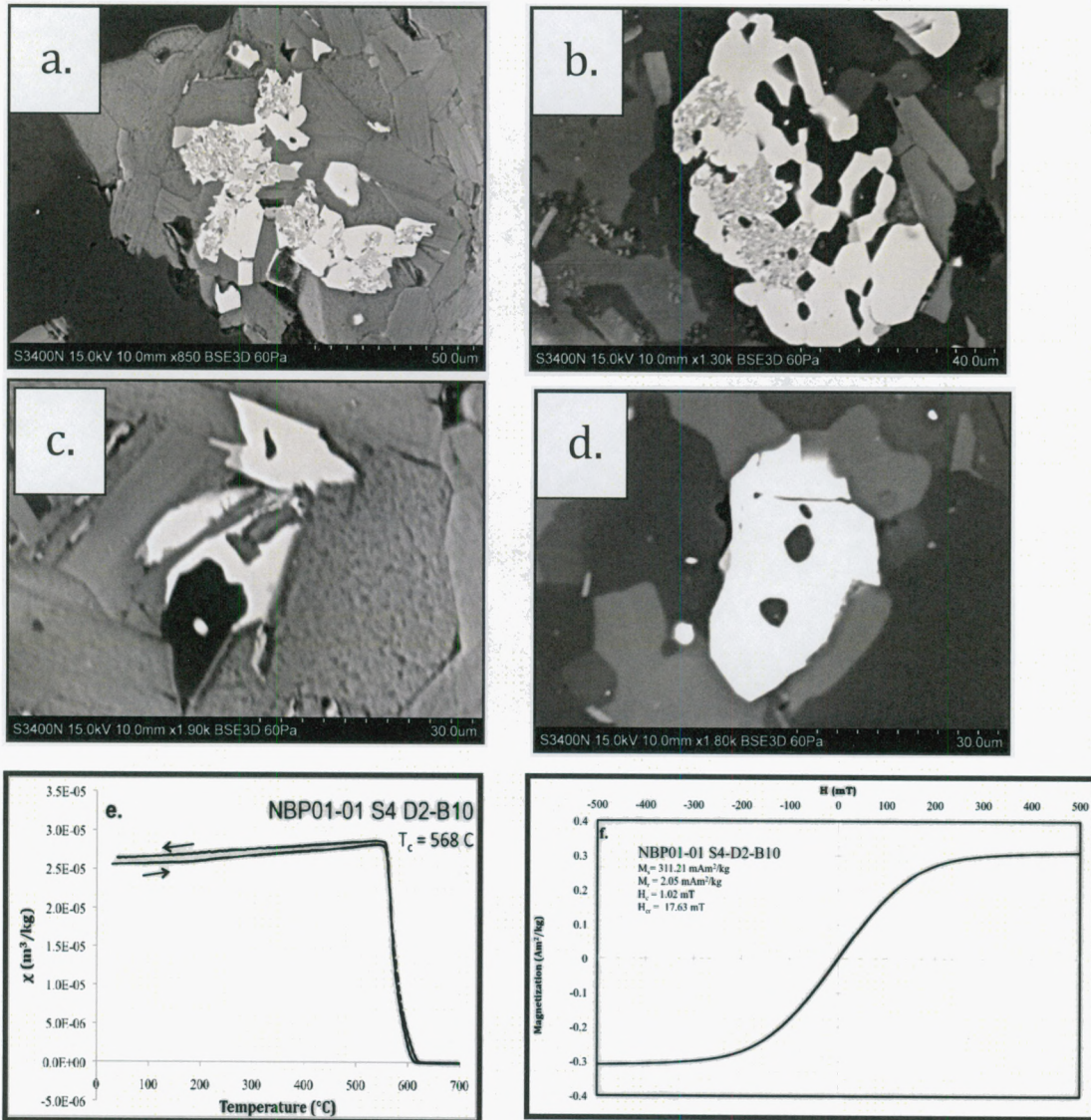


Figure 24. Sample NBP01-01 S4-D2-B10.

**a.** and **b.** ilmenite grains with myrmekitic type textures. **c.** Mn –bearing ilmenite grain without grungy texture **d.** Magnetite grain with inclusion of quartz. **e.**  $\chi(T)$  plot displaying a magnetite Curie temperature. **f.** The magnetic hysteresis loop is very narrow and multidomain.

Figure 25. Sample S3-D1-B7

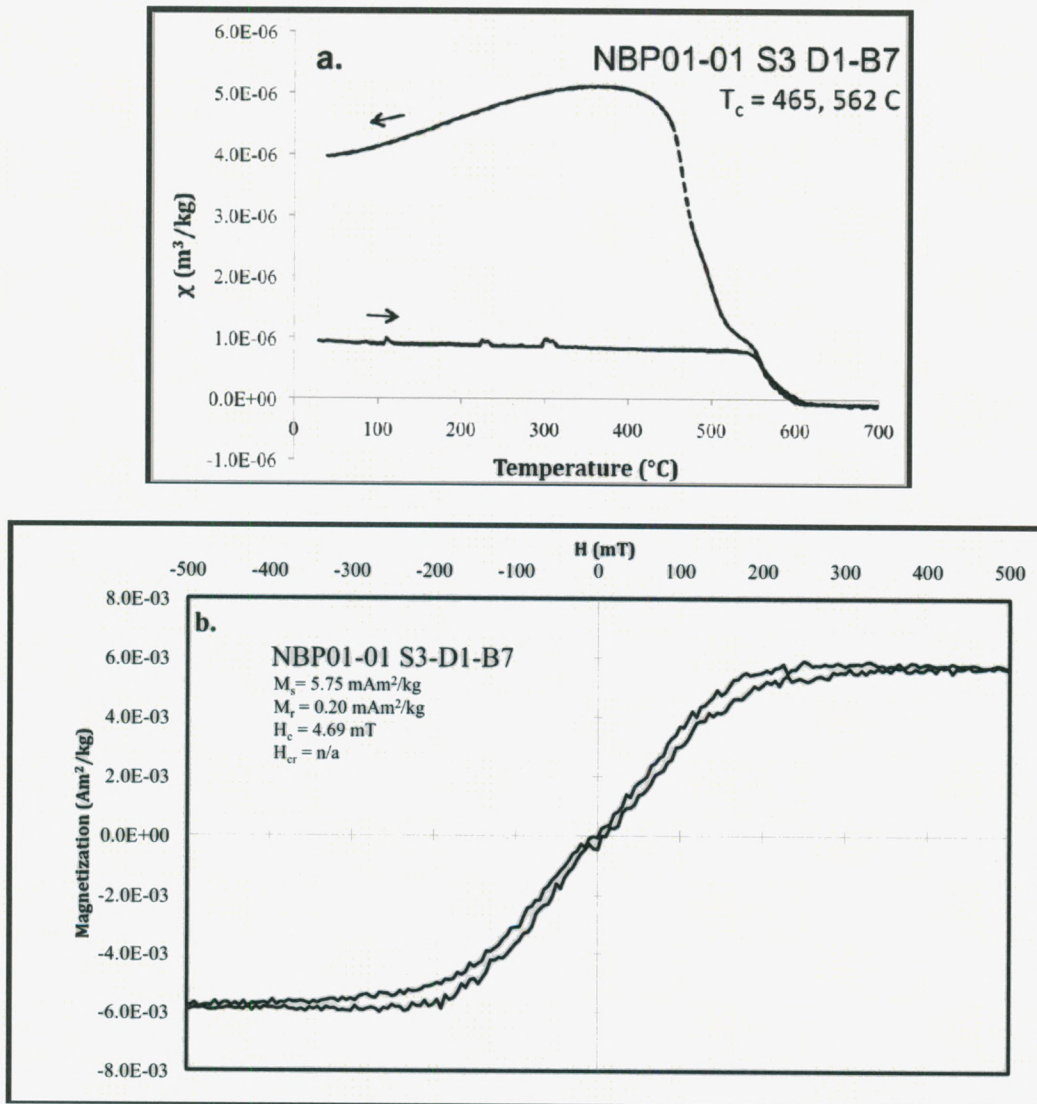
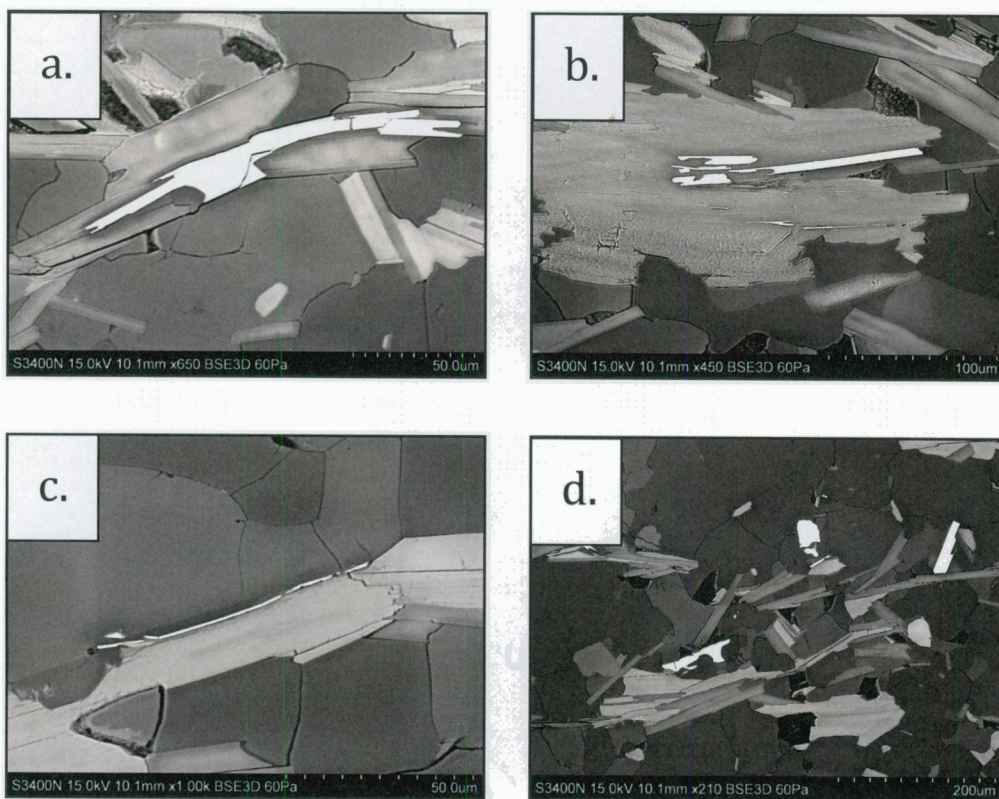


Figure 25. Sample NBP01-01 S3-D1-B7

**a.**  $\chi(T)$  plot. The curve displays Curie temperatures of 562 °C seen in the heating curve and 465 °C seen in the cooling curve. The cooling curve displays higher susceptibility values than the heating curve, suggesting magnetic material was created during the experiment. **b.** Magnetic hysteresis loop displaying what appears to multidomain slightly wasp-waisted loop.



**Figure 26. Sample NBP01-01 S3-D1-B4 C**



**Figure 26. Sample NBP01-01 S3-D1-B4 C.**

The above are Mn-bearing ilmenite grains. **a.** Elongated ilmenite cutting through an amphibole. **b.** Elongated ilmenite grain between a sodic feldspar and a muscovite. **c.** Elongated grain found on the boundary of a mica. **d.** Group of ilmenite grains displaying more equant shapes.

Figure 27. Sample NBP01-01 JPC11 2305 cm

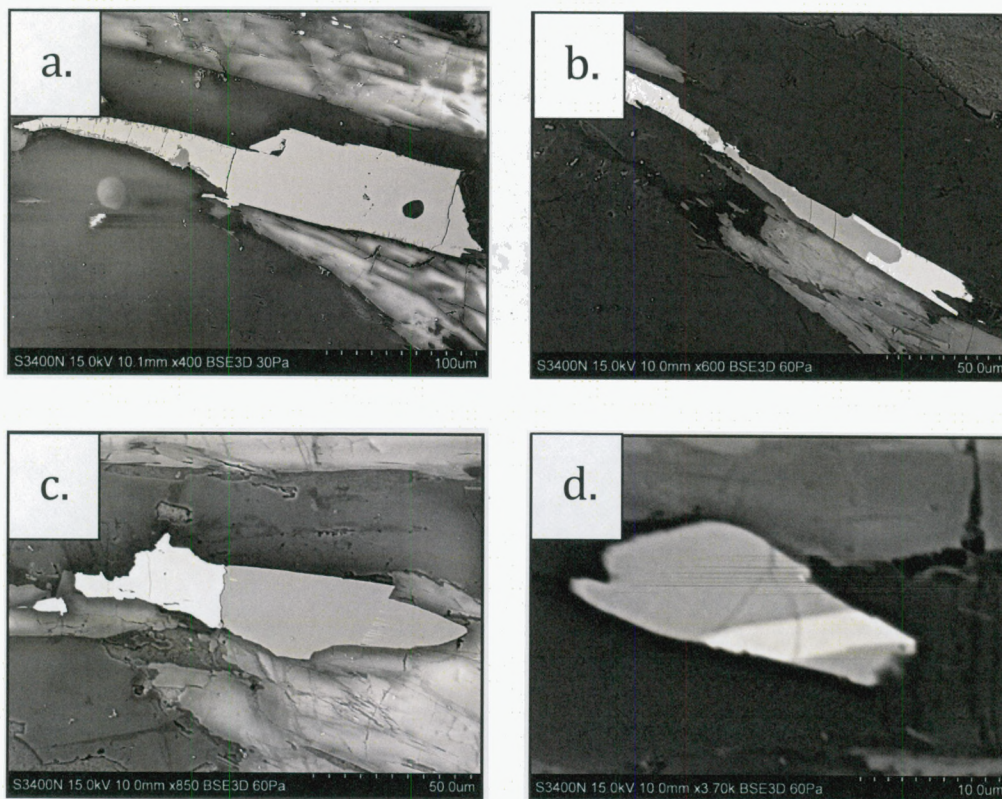


Figure 27. Sample NBP01-01 JPC11 2305 cm.

**a. b. c. and d.** Ilmenite grains showing exsolution or intergrowths of rutile. Rutile is the darker regions within the grain. **a.** Irregularly shaped ilmenite grain. The dark areas on the thin area of the grain that appear to be pointing inward toward the grain are of rutile composition. **b. c.** Rutile occupies the majority of the grains and is seen as the darker regions. **d.** A magnetite strip dividing an ilmenite grain.

Figure 28. Sample NBP01-01 S3 D1 B4 A

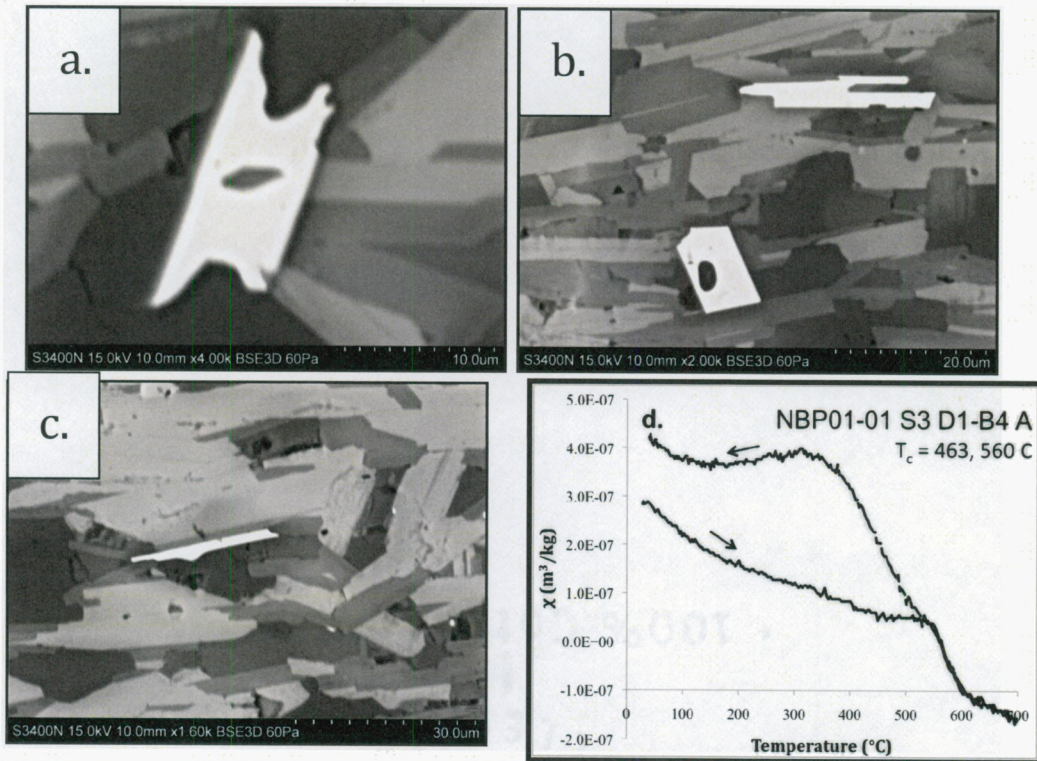


Figure 28. Sample NBP01-01 S3 D1 B4 A.

**a.** Ilmenite grain with k-feldspar inclusion. Grain is bounded by K-feldspar (bottom + top) and K-mica (right). **b.** Two ilmenite grains, one with an inclusion of quartz. **c.** Elongated ilmenite grain aligned with fabric of rock. **d.**  $\chi(T)$  curve displays a Curie temperature of 463  $^{\circ}\text{C}$  and 560  $^{\circ}\text{C}$ . The 560  $^{\circ}\text{C}$  Curie point is seen in the heating curve while the 463  $^{\circ}\text{C}$  Curie point is seen in only the cooling.

Figure 29. Sample NBP01-01 S3-D1-B4 B

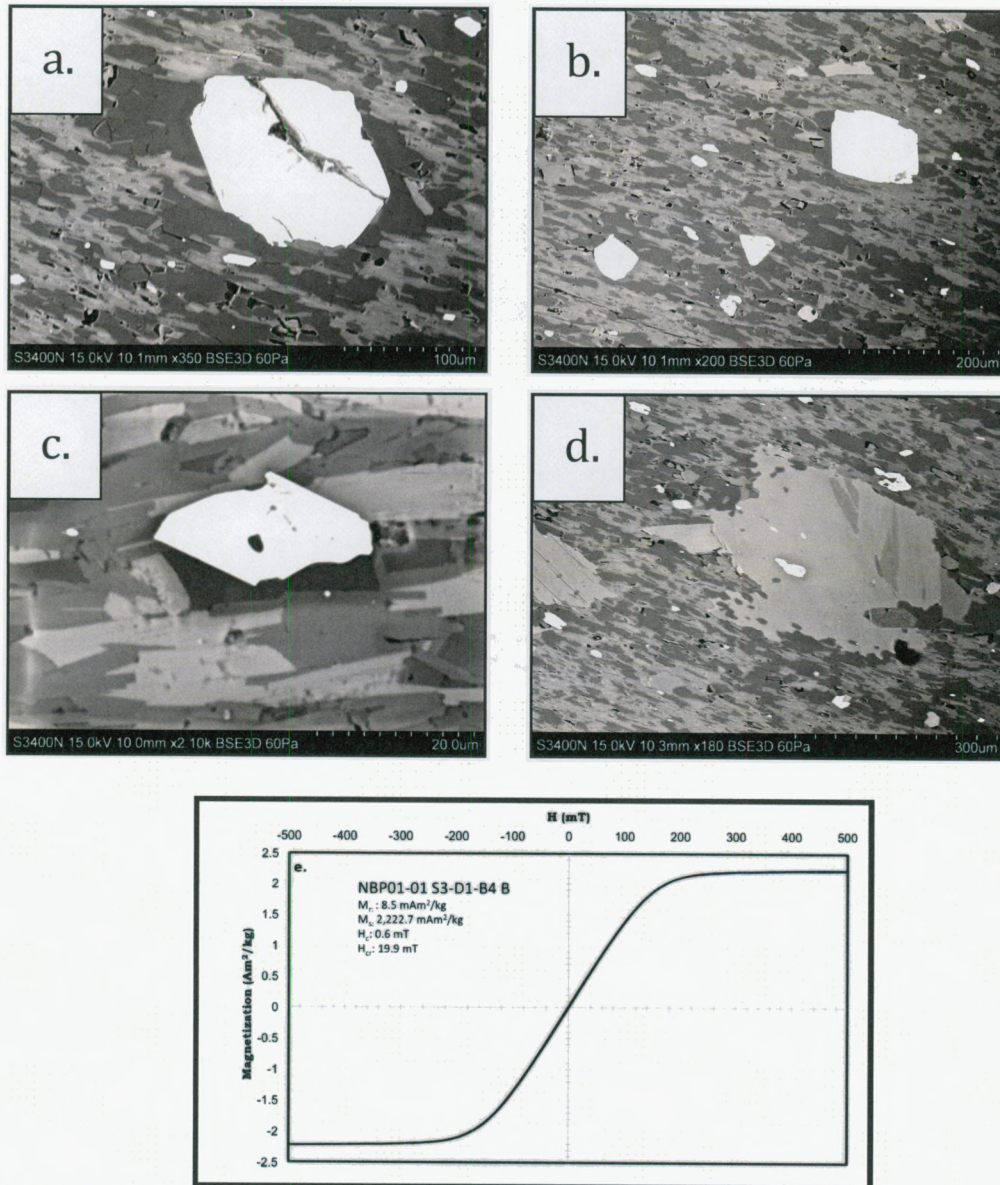


Figure 29. Sample NBP01-01 S3-D1-B4 B.

**a.** and **b.** Two oxide phases are present in this sample. The larger equant grains are magnetite and smaller grains situated within the fabric of the rock are ilmenite. **c.** Ilmenite grain that contains an inclusion of unknown composition. **d.** Ilmenite grain as an inclusion within biotite. **e.** Hysteresis loop displaying multidomain behavior.

Figure 30. Sample S5-D3-B7

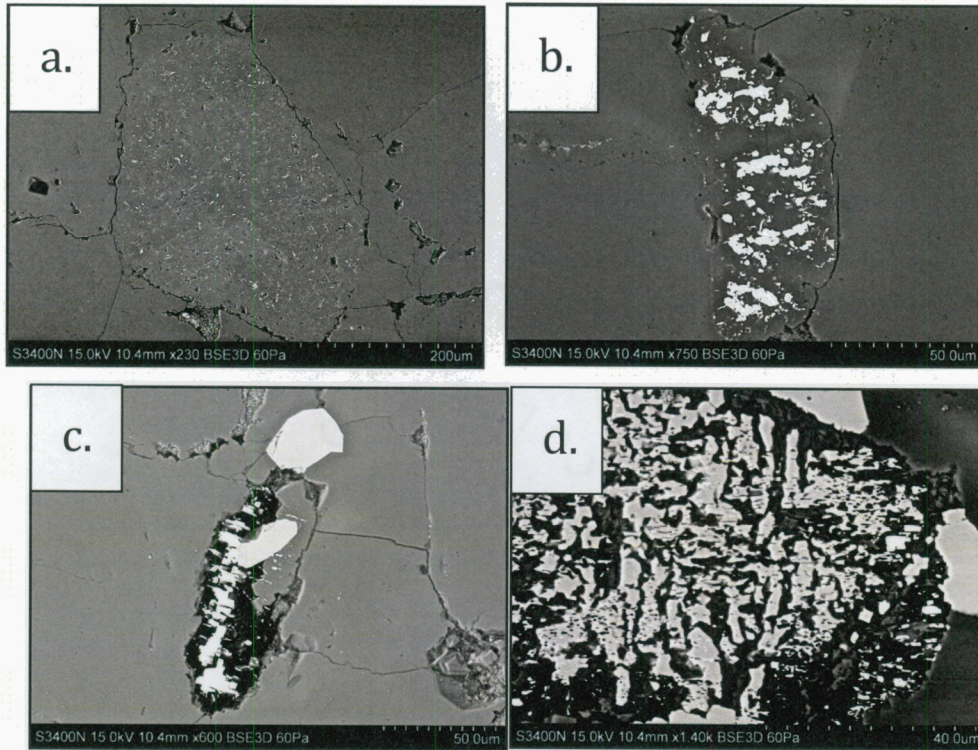


Figure 30. Sample S5-D3-B7.

**a.** and **b.** Magnetite inclusions within quartz grains. **c.** Light 'specks' are of titanomagnetite composition ( $\text{Fe}/\text{Ti} = 10$ ). The grey areas are rutile. The dark grey/black region above it is quartz. **d.** Magnetite found within cracks between quartz grains.

Figure 31. NBP01-01 S5-D3-B5

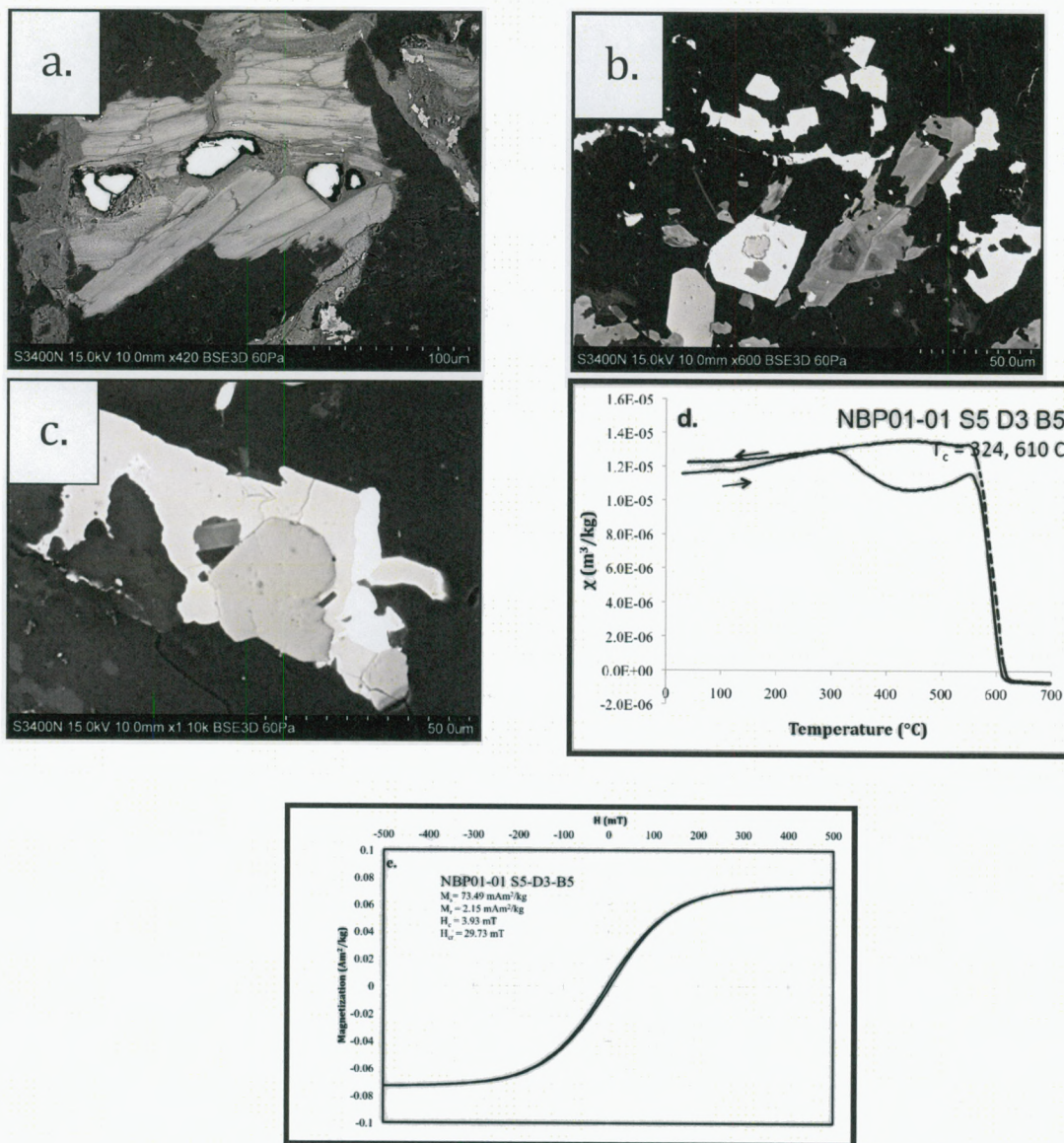


Figure 31. NBP01-01 S5-D3-B5.

**a.** Titanomagnetite grains ( $\text{Fe}:\text{Ti} = 30$ ) embedded within a cluster of micas. Rim around grains contains less iron. **b.** Iron sulfides. Core in grain in lower half of image = Cu-rich iron sulfide. **c.** Displays three phases of iron sulfide, one with a moderate Fe:S ratio, two that are more sulfur rich, and one that contains Cu. **d.**  $\chi(T)$  plot. The Curve displays Curie points of  $324 \text{ }^{\circ}\text{C}$  and  $610 \text{ }^{\circ}\text{C}$ . The  $324 \text{ }^{\circ}\text{C}$  Curie point it believed to be that of the iron sulfide. **e.** Hysteresis loop. The loop displayed is that of multidomain magnetic material.

Figure 32. Sample NBP01-01 S3-D1-B1 A

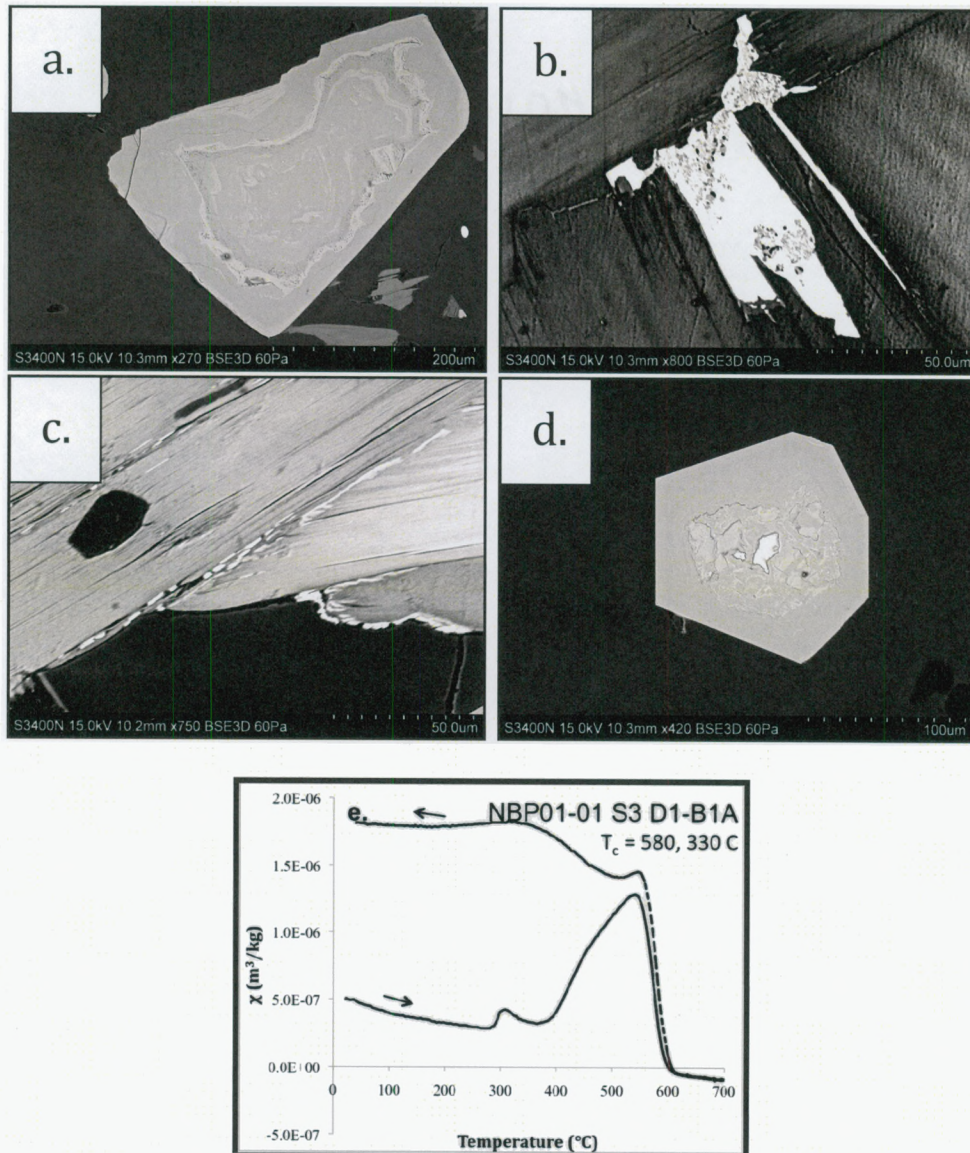


Figure 32. Sample NBP01-01 S3-D1-B1 A

**a.** Magnetite grain with pitted surface. **b.** and **c.** Ilmenite grains associated with potassium mica. **d.** Magnetite with sulfur rich core. **e.**  $\chi(T)$  plot displaying Curie temperatures of 330 °C and 580 °C. 580 °C Curie temperature is inferred to be that of magnetite. The 330 °C Curie temperature is that of the iron sulfide.

Figure 33: Sample NBP01-01 S3-D1-B10.

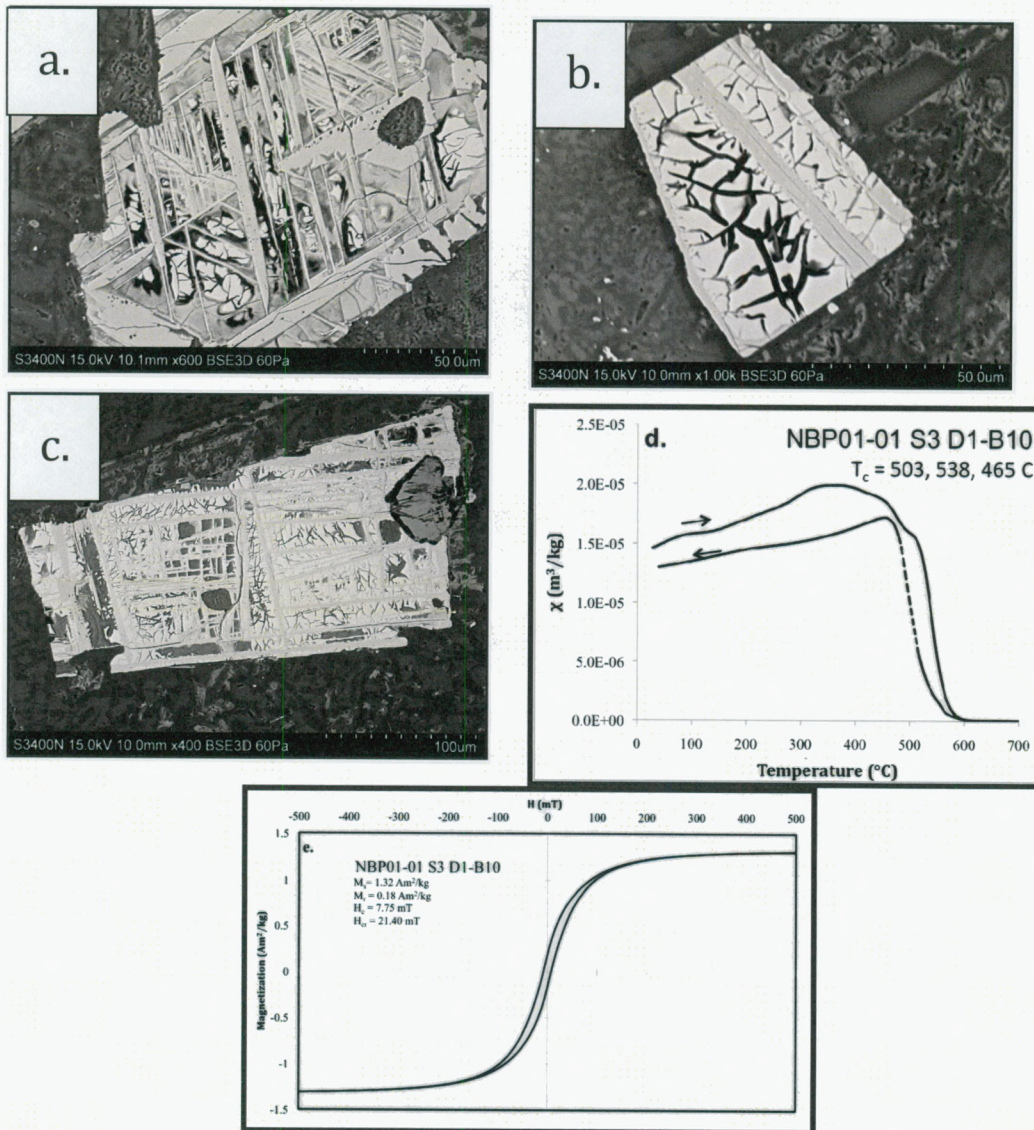


Figure 33. Sample NBP01-01 S3-D1-B10.

a. b. c. and d. Display titanomagnetite grains with laths of ilmenite dividing the grain into regions. Within these regions the grain is commonly fractured and rutile crystallization is common. This texture is more developed in larger grains.



Figure 34. NBP01-01 S-II Volcanics

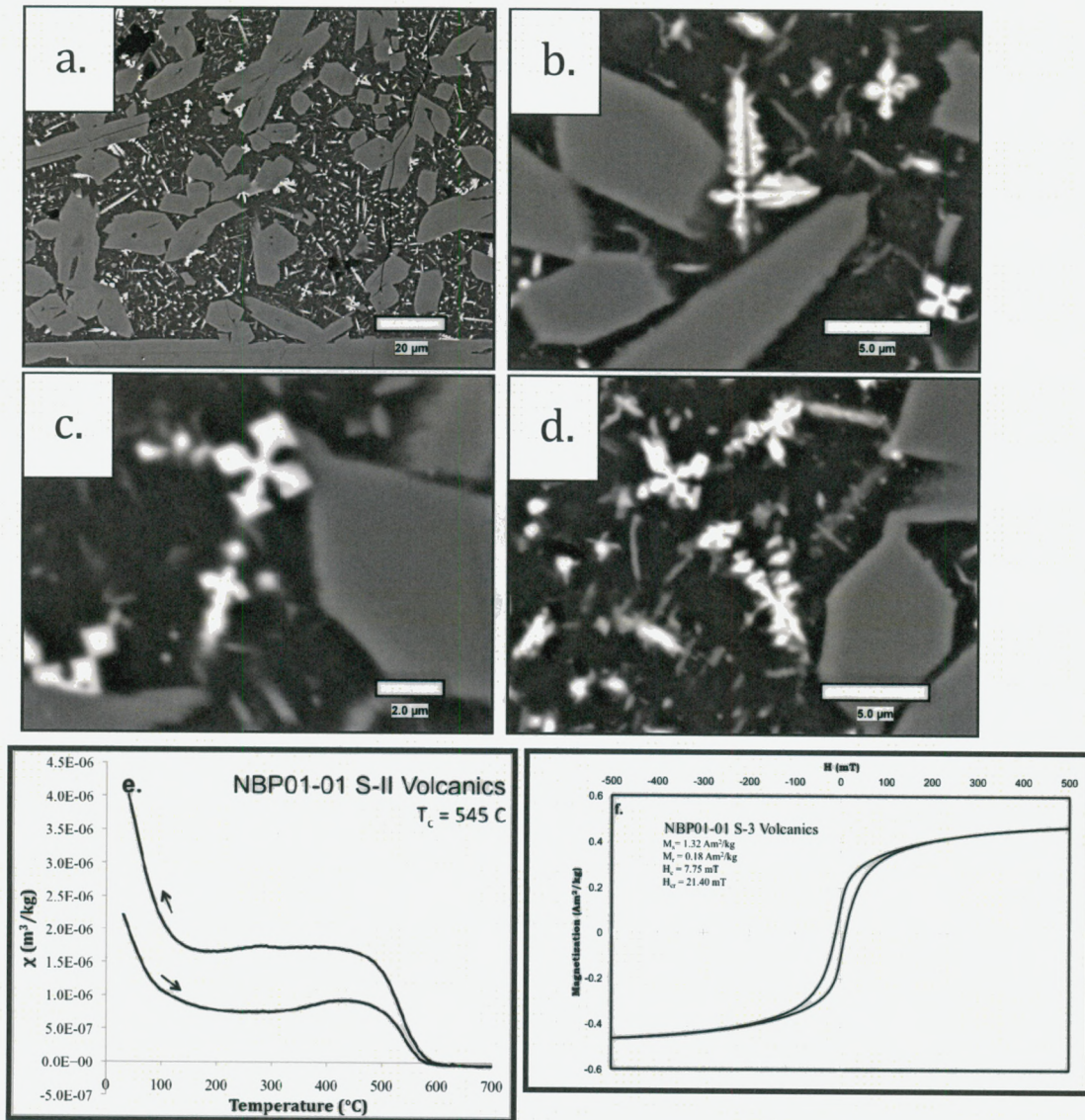


Figure 34. NBP01-01 S-II Volcanics

**a-d.** This sample contains abundant of titanomagnetite with a variety of cruciform morphologies. **e.**  $\chi(T)$  plot. The curve displays a Curie temperature of 545  $^{\circ}\text{C}$  believed to be the signal of titanomagnetite. **f.** Hysteresis loop displays stable single domain behavior and appears to be wasp-wasited, suggesting two minerals with different coercivities.

Figure 35. Dropstone Day Plot

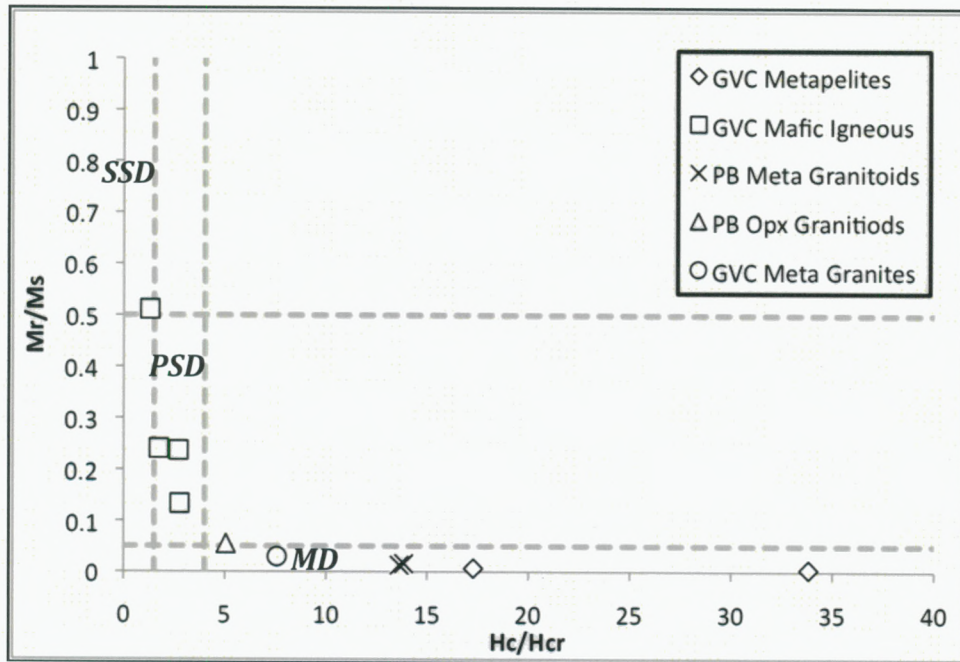


Figure 35. Dropstone 'Day Plot' (Day et al., 1977). The plot displays magnetic hysteresis parameters  $M_r/M_s$  plotted vs  $H_{cr}/H_c$ , which defines the magnetic domain state. Most samples plot in the multi-domain (MD) region below the horizontal dashed line. Mafic igneous samples plot in the pseudo-single-domain (middle region) and stable single domain regions (upper left region).

Figure 36. Distribution of Remanence and Susceptibility Values

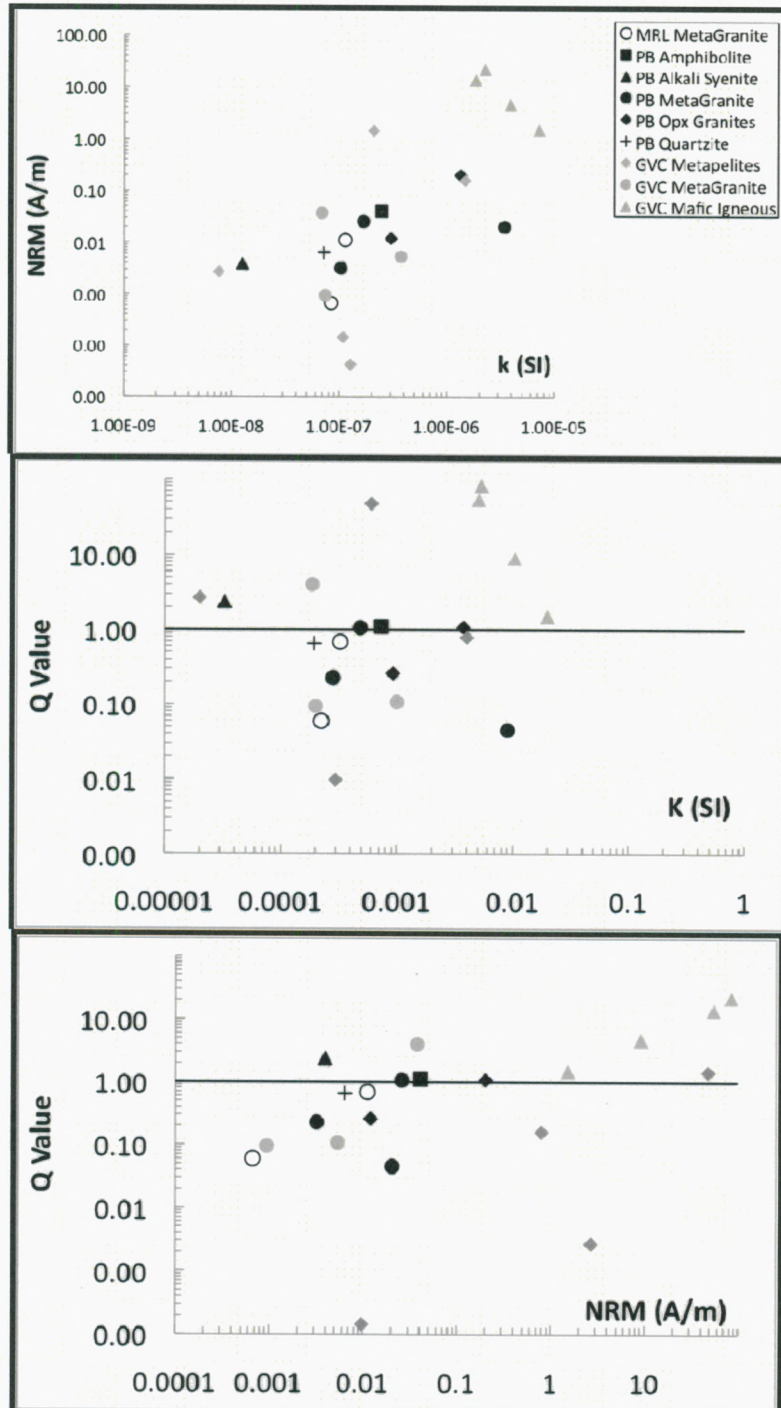


Figure 36. Distribution of NRM and k values. The figures shows the distribution of NRM and k values for dropstones. The horizontal line in each graph represent the division between induced (below) or remanent dominated (above) Q values.

Figure 37. Depths to the Curie Isotherm

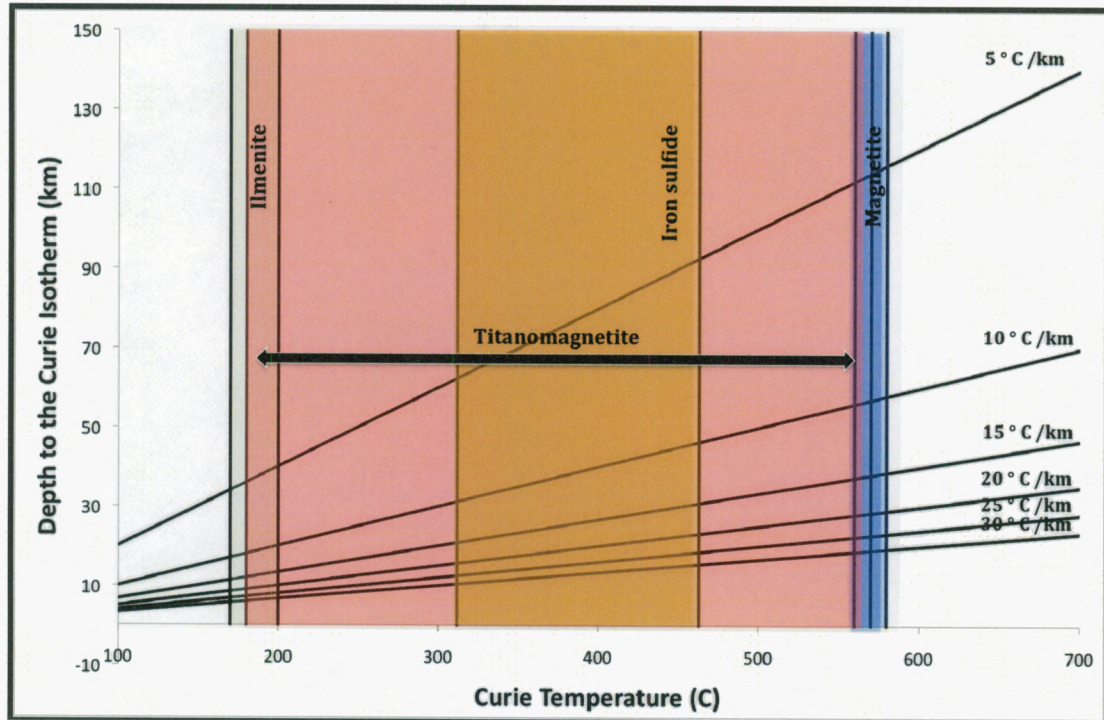


Figure 37. Depths to the Curie Isotherm. The above figure displays depth to the Curie isotherm vs Curie temperature as a function of geothermal gradient. Each line represents a different geothermal gradient from 5 – 30 °C/km, with 5 C/km typical of a passive margin, and 30 °C/km typical of a spreading ridge. The colors represent the range of Curie temperatures observed. Blue = Magnetite, Red = Titanomagnetite, Green = Ilmenite, Yellow = Iron sulfide.

**Table 4. Sample Locations of Dropstones**

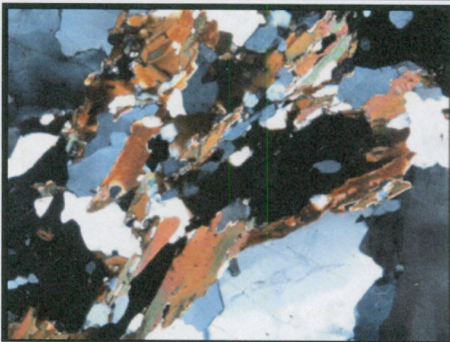
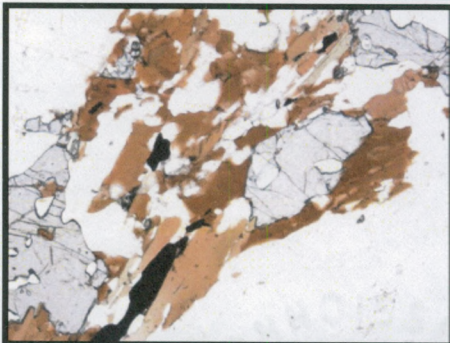
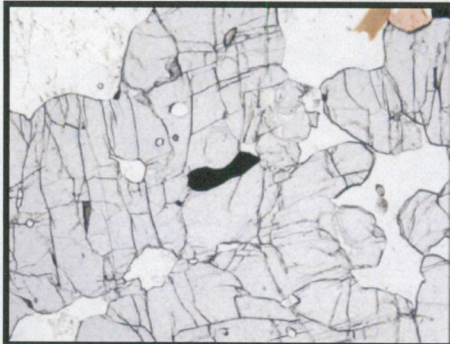
<b>NBP01-01 Sampling Site</b>	<b>Location</b>	<b>Latitude °S</b>	<b>Longitude °E</b>
<b>Dredge 3</b>	Mertz Glacier	66 55.989	145 09.901
<b>Dredge 4</b>	Mertz Glacier	66 48.976	145 21.787
<b>Dredge 5</b>	Mertz Glacier	66 42.492	145 36.730
<b>JPC11</b>	Mertz Drift	66 33.777	143 03.082
<b>JPC24</b>	Svenner Channel	68 41.637	76 42.712
<b>JPC34</b>	Prydz Channel	68 15.021	72 43.782
<b>JPC36</b>	Prydz Channel	68 03.956	72 16.428
<b>JPC40</b>	Nielsen Basin	67 10.619	65 44.323

**Table 5. Summary of Susceptibility, NRM and Q Values**

			Oxide %	Susceptibility SI	NRM A/m	Q
<b>MACROBERTSON LAND</b>						
<b>META-GRANITES</b>						
NBP01-01	JCP40	2272-2275 cm	0.75	3.2E-04	1.1E-02	0.69
NBP01-01	JPC40	2302-2305 cm	0.6	2.2E-04	6.7E-04	0.06
<b>PRYDZ BAY</b>						
<b>AMPHIBOLITE</b>						
NBP01-01	JPC34	72 cm		7.3E-04	4.0E-02	1.11
<b>QUARTZ ALKALI FELDSPAR SYENITE</b>						
NBP01-01	JPC36	424-427 cm		3.3E-05	3.9E-03	2.41
<b>META-GRANITES</b>						
NBP01-01	JPC24	1611-1612 cm	0.95	4.8E-04	2.6E-02	1.06
NBP01-01	JPC34	75-78 cm		9.0E-03	2.0E-02	0.05
NBP01-01	JPC34	75-83 cm	0.05	2.8E-04	3.2E-03	0.23
<b>OPX GRANITOIDS</b>						
NBP01-01	JPC34	59-62 cm	0.4	3.7E-03	2.0E-01	1.07
NBP01-01	JPC36	100-103 cm	3.43	9.3E-04	1.2E-02	0.26
<b>QUARTZITE</b>						
NBP01-01	JPC34	345-350 cm	0.04	1.9E-04	6.4E-03	0.66
<b>GEORGE V COAST</b>						
<b>METAPELITES</b>						
NBP01-01	S4	D2-B10	0.26	4.0E-03	1.6E-01	0.80
NBP01-01	S3	D1-B7 A	0.26	3.0E-04	1.4E-04	0.01
NBP01-01	S3	D1-B4 C	0.06	2.1E-04		
NBP01-01	JPC 11	2305 cm	0.81	6.0E-04	1.4E+00	47.61
NBP01-01	S4	D2-B7	0.22			
NBP01-01	S3	D1-B4 A	0.11	3.6E-04	4.3E-05	0.002
NBP01-01	S3	D1-B4 B	0.98	6.7E-02		
NBP01-01	S5	D3-B7	0.05	2.0E-05	2.7E-03	2.69
<b>METAGRANITE</b>						
NBP01-01	S5	D3-B5		1.0E-03	5.4E-03	0.11
NBP01-01	S5	Bag 2		1.9E-04	3.7E-02	4.02
NBP01-01	S3	D1-B1 A	0.08	2.0E-04	9.5E-04	0.10
<b>MAFIC IGNEOUS</b>						
NBP01-01	Station 3 II	Volcanics +		5.1E-03	1.4E+01	54.46
NBP01-01	S3 II	Volcanics		5.3E-03	2.2E+01	84.09
NBP01-01	S4	D2-B2		1.0E-02	4.7E+00	9.11
NBP01-01	S3	D1-B10		2.0E-02	1.5E+00	1.52

## MacRobertson Land Granite Gneiss

*NBP01-01 JPC40 2302-2305 cm*



Sample NBP01-01 JPC40 2302-2305 cm is a granitic gneiss. The sample contains quartz, plagioclase, garnet, and minor amounts of K-feldspar.

The images to the left display four photomicrographs that represent a typical field of view seen in petrographic analysis. The top image displays an ilmenite grain enclosed within a garnet seen in plain light.

The middle two photomicrographs display garnet and bitotite found within this sample and is a typical fields of view seen throughout the sample (top: plain light, bottom: transmitted light).

The bottom image displays what is interpreted to be a microvein of quartz. Notice the polygonal mosaic texture of this vein.

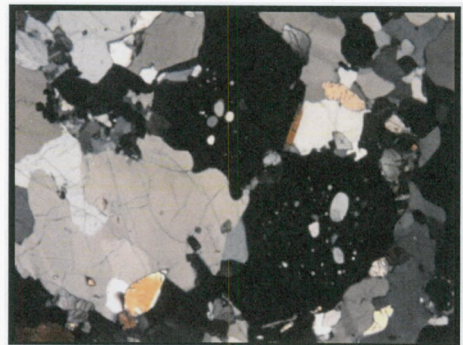
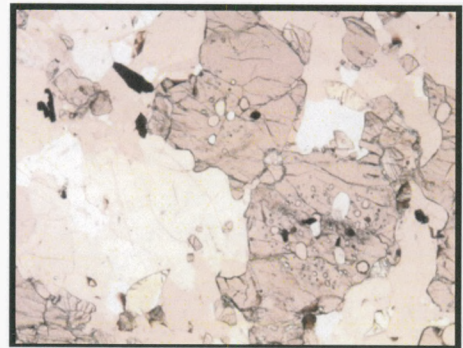
## MacRobertson Land Orthopyroxene-bearing Meta granitoid *NBP01-01 JPC40 2272-2275*

Sample NBP01-01 JPC40 2272-2275 cm is a orthopyroxene bearing metagranitoid.

The photomicrographs to the right display common fields of view seen in thin section of the sample. The top two images display quartz grains that contain inclusions of quartz.

The bottom image displays a pyroxene grain that possesses exsolution textures.

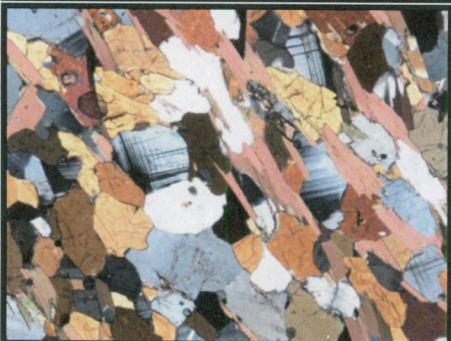
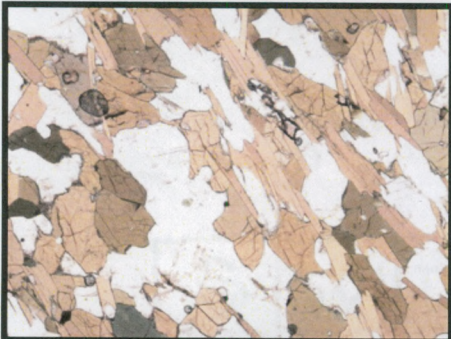
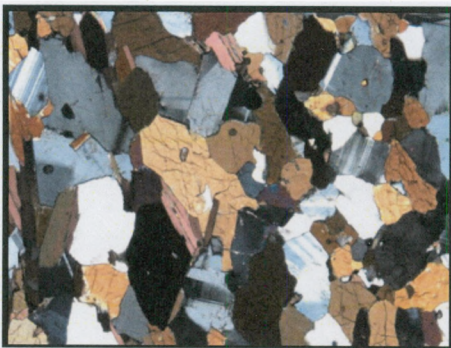
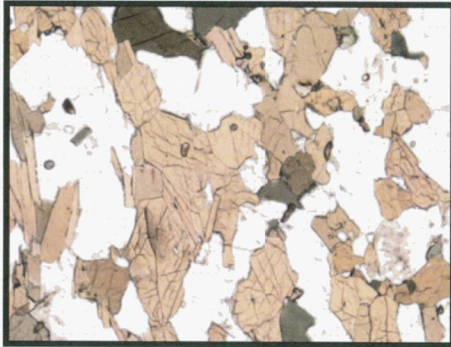
Also present within this sample is plagioclase, biotite, and garnet.





## Prydz Bay Amphibolite

*NBP01-01 JPC34 72 cm*



Sample NBP01-01 JPC34 72 cm is an amphibolite dominated by brownish-green amphibole. Also present within this sample is quartz, plagioclase, and biotite. The biotite appears pink in transmitted light and is best distinguished from amphiboles by its cleavage.

The photomicrographs to the right display two fields of view in plain light (top) and transmitted light (bottom)

Notice the fabric within the sample defined by the amphibole minerals, best seen in plain light.

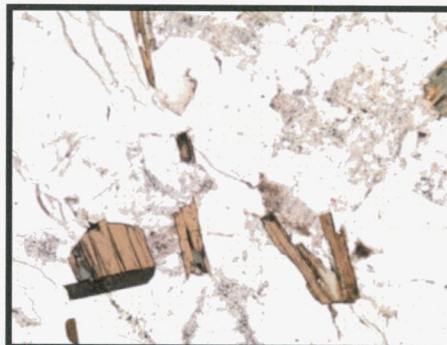
## Prydz Bay Quartz Alkali feldspar Syenite

*NBP01-01 JPC36 424-427 cm*

Sample NBP01-01 JPC36 424-427 cm is a quartz-alkali feldspar syenite.

The sample is dominated by potassium feldspar. The images to the right display microcline, which commonly contains quartz inclusions.

Also present within this rock is biotite, which stands out both in plain and transmitted light due to its higher relief.



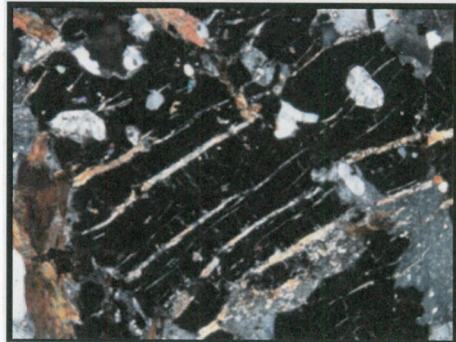
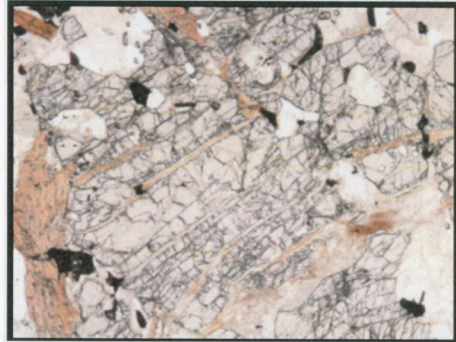
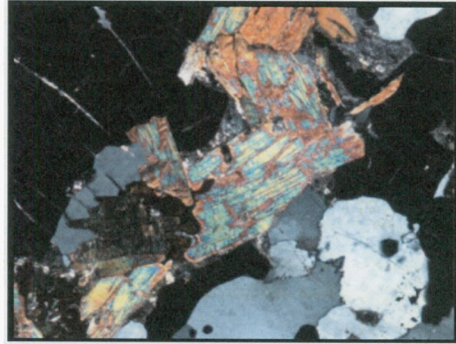
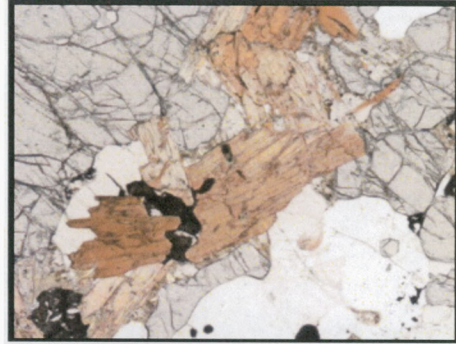
## Prdyz Bay Meta Granite

*NBP01-01 JPC24 1611-1612 cm*

Sample NBP01-01 JPC24 1611-1612 cm is a meta-igneous rock that has a high abundance of garnet, perthite, and an amphibole mineral of unknown composition.

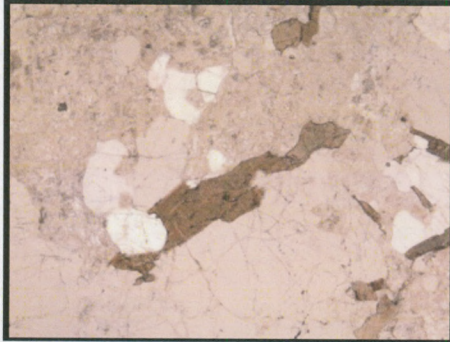
The two top images display the unknown amphibole seen in plain light (top) and cross polarized light (bottom). This mineral displays high-order interference colors and is pale brown in plain light.

The bottom two photomicrographs display a garnet grain that is highly strained and recrystallized with biotite within its cracks.

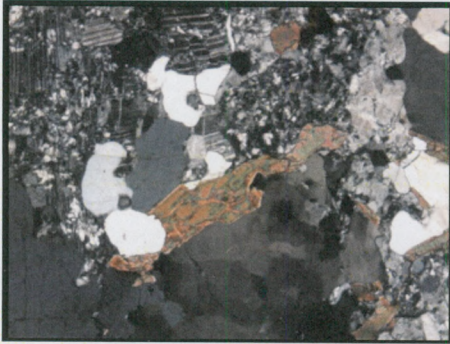


## Prdyz Bay Meta Granite

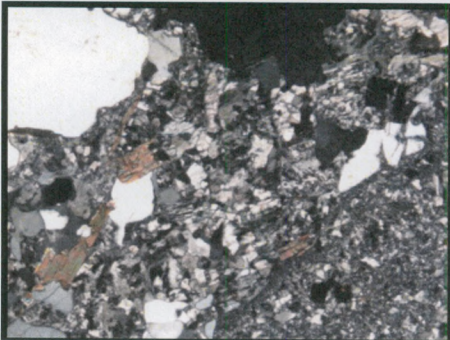
*NBP01-01 JPC34 75-78 cm*



Sample NBP01-01 JPC34 75-78 cm is a meta igneous rock that contains quartz, plagioclase, microcline, and amphibole.



The top two photomicrographs to the left display an amphibole of unknown composition. Above the amphibole are examples of feldspars with perthitic texture commonly found in this rock.



The bottom image shows fine grained regions of quartz and plagioclase that are seen in thin section as isolated regions or veins.

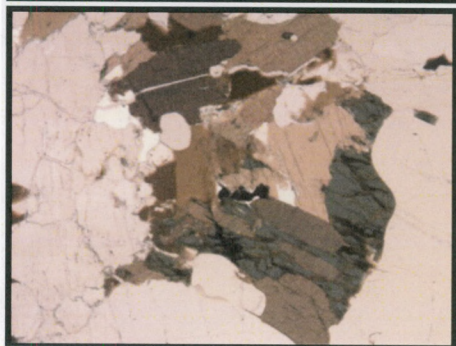
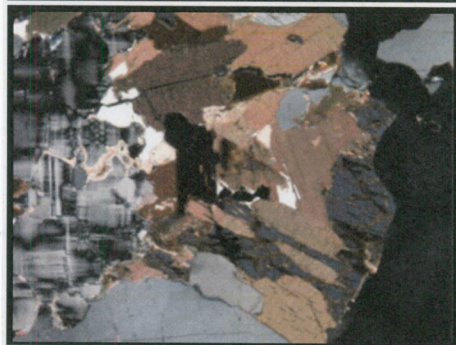
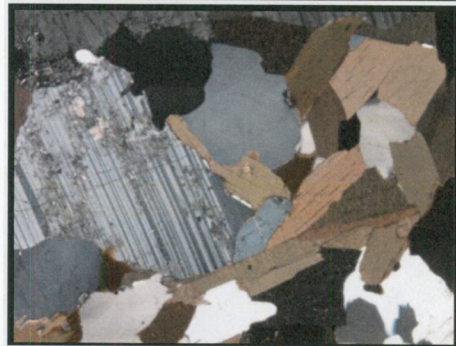
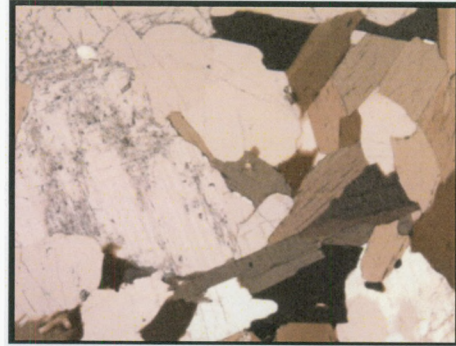
## Prdyz Bay Meta Granite

*NBP01-01 JPC34 75-83 cm*

Sample NBP01-01 JPC34 75-83 cm is a meta granitoid found in the Prydz Bay area. This rock differs from other meta-granites found in Prydz bay in that it is very coarse grained, has minor amounts of potassium feldspar, and has a high abundance of biotite.

The images to the right display typical photomicrographs of the sample. The top two photomicrographs display an average field of view within this sample. Notice the large grains, the abundance of biotite, and the alteration to plagioclase, which appears to be breaking down possibly to a clay mineral.

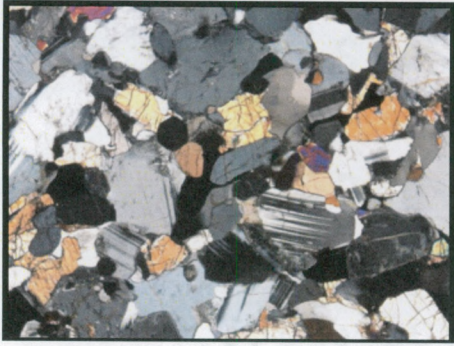
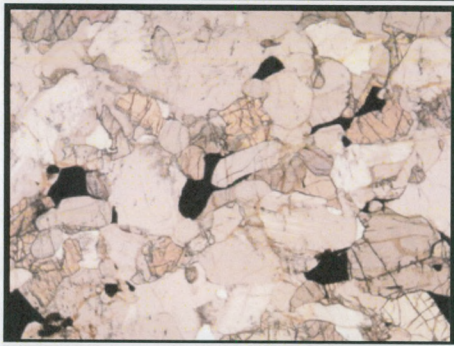
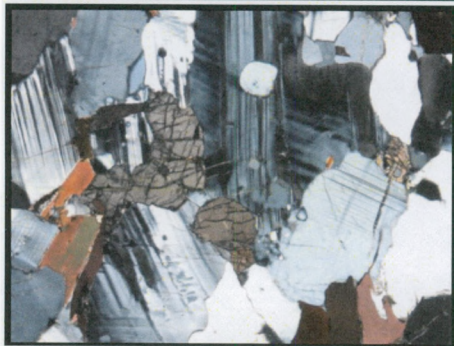
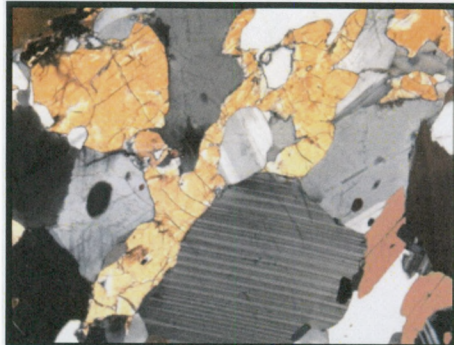
The bottom two photomicrographs are of biotite reacting to an iron-rich chlorite (inferred to be iron rich due to its blue color). Also present in this field of view is microcline, a mineral seen rarely in this rock.



## Prydz Bay Orthopyroxene Granite

*NBP01-01 JPC34 59-62 cm*

*NBP01-01 JPC36 100-103 cm*



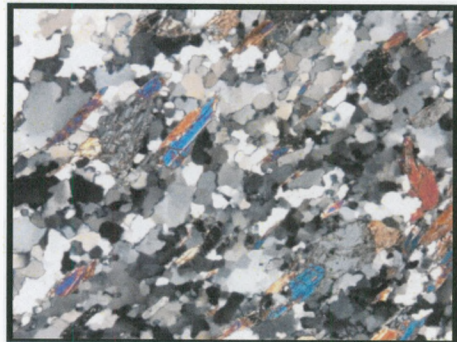
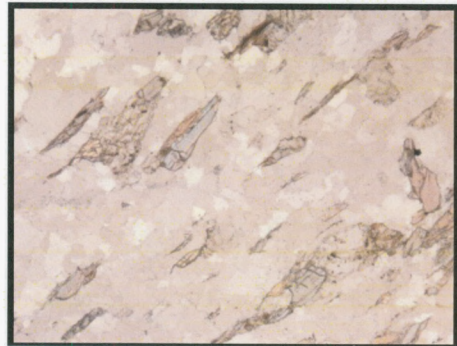
Samples NBP01-01 JPC34 59-62 cm and NBP01-01 JPC36 100-103 cm are orthopyroxene bearing granitoids. The top two images to the left are of sample NBP01-01 JPC34 59-62 cm and the bottom two images are of sample NBP01-01 JPC36 100-103 cm.

The dominant mineralogy in these rocks are quartz, plagioclase, orthopyroxene, clinopyroxene and biotite. Sample NBP01-01 JPC34 59-62 cm is coarser grained and does not contain clinopyroxene.

## Prydz Bay Quartzite

*NBP01-01 JPC34 345-350 cm*

Sample NBP01-01 JPC34 345-350 cm is a quartzite. The sample contains quartz and amphibole. There appears to be a fabric in this sample, interpreted to be the product of grain flattening. The fabric is best seen in plain light.



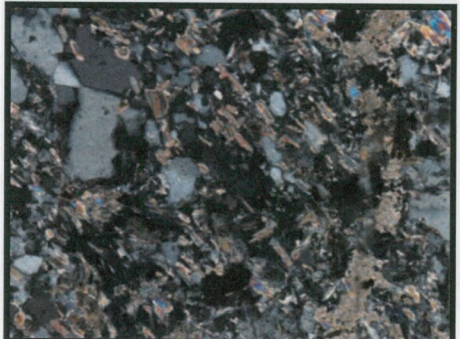
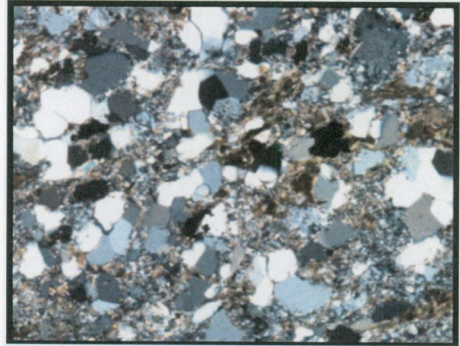
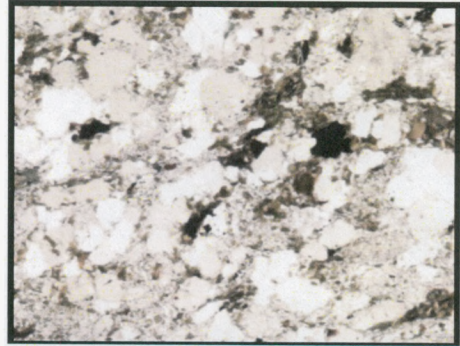
## Hornfels of the George V Coast

*NBP01-01 S4 D2 B10*

*NBP01-01 S3 D1 B7*

Sample NBP01-01 S4 D2 B10 (top two images) is a biotite hornfels dominated by coarser grained quartz. The matrix is composed of biotite and Fe-oxide minerals. The quartz grains display minor recrystallized textures.

Sample NBP01-01 S3 D1 B7 (bottom two photomicrographs) is a finer grade hornfels composed of smaller quartz grains. Located within the matrix is a mixture of biotite, chlorite, and amphibole. In the center of the above images are what appears to be chlorite. In the upper right corner of the field of view is an amphibole that displays high birefringence and appears to have yellow reaction halos surrounding it.

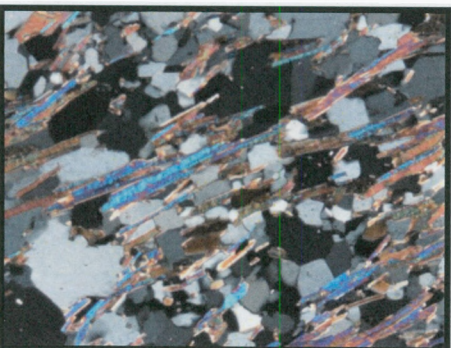
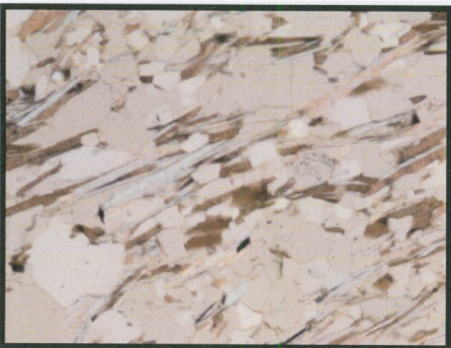
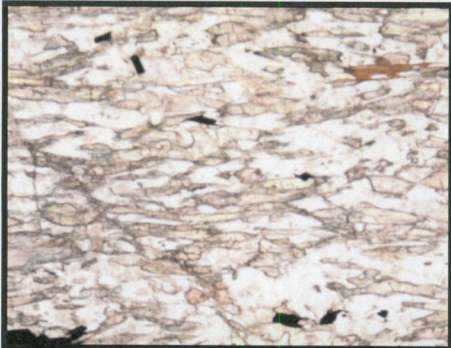




## Two Mica Schists from the George V Coast

*NBP01-01 JPC11 2305*

*NBP01-01 S3 D1 B4 C*



The top two photomicrographs displayed to the left are of sample NBP01-01 JPC11 2305 cm. The sample is a muscovite schist with a dominant mineralogy of muscovite, quartz and plagioclase and minor amounts of Fe-oxide.

The bottom two photomicrographs are of sample NBP01-01 S3 D1 B4 C. The sample is a biotite muscovite schist. Biotite is clearly the dominant mica in this sample. Also present in this rock is an abundance of quartz.

## **Biotite Magnetite Schist from the George V Coast**

*NBP01-01 S3-D1-B4 A*

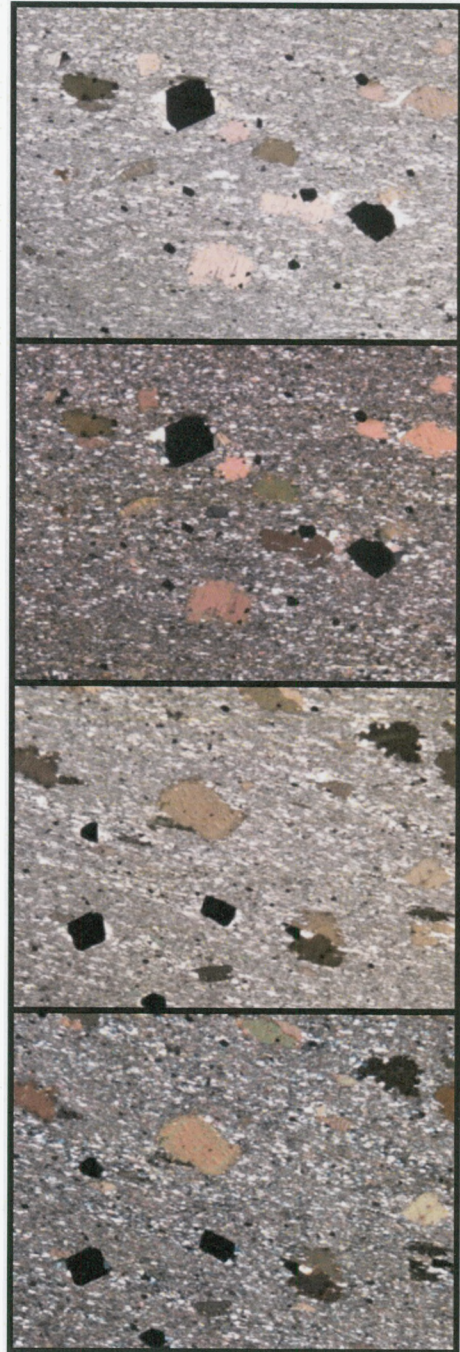
*NBP01-01 S3-D1-B4 B*

Two biotite schists were recovered that contain porphyroblasts of biotite and Fe-oxide within a fine grained matrix composed of quartz and biotite.

Sample NBP01-01 S3 D1 B4 A (top) and sample NBP01-01 S3 D1 B4 B (bottom).

The Fe-oxide grains do not appear to follow the same orientation as the fabric, suggesting they are post tectonic, however most grains are equidimensional.

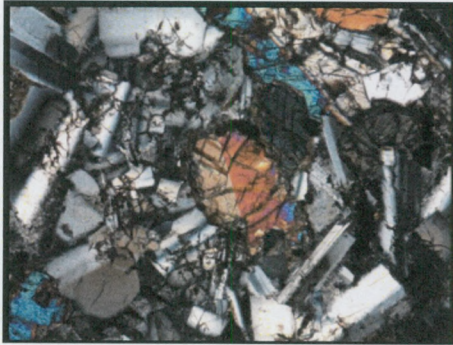
Elongated biotite grains appear to have a preferred orientation parallel to the fabric displayed in the rock.



## Mertz Glacier Dolerite from the George V Coast

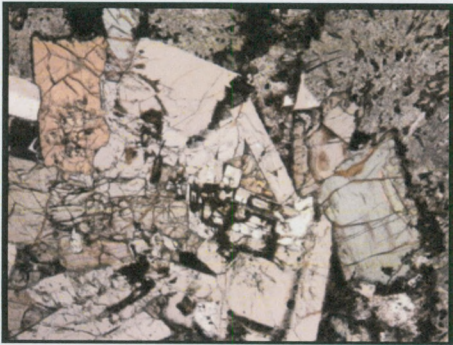
*NBP01-01 S4-D2-V 4-2-2*

*NBP01-01 S3-D1-B10*



Two doleritic samples were found in dredges off the coast of the Mertz glacier. These samples are dominated by plagioclase, clinopyroxene, and orthopyroxene.

The top figure is sample NBP01-01 S4-D2-V 4-2-2, in the center of the photomicrograph is a twinned clinopyroxene grain commonly found in these rocks.



The bottom two photomicrographs show a typical field of view of sample NBP01-01 S3 D1 B10 in plain and cross polarized light on the top and bottom, respectively. The field of view displays orthopyroxene to the left and clinopyroxene to the right as well as some brown alteration that is commonly found within the plagioclase.



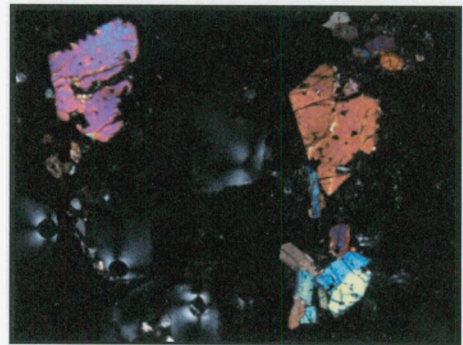
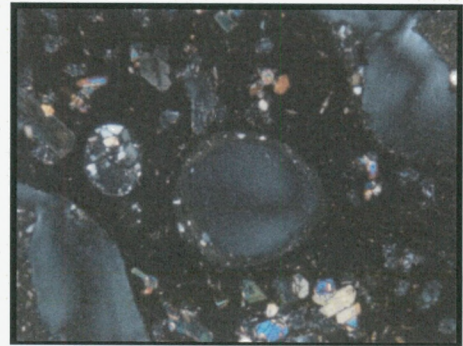
## Basalt from the George V Coast

*NBP01-01 S3-II volcanics*

One dropstone of volcanic origin was recovered from the Mertz Glacier Dredges, sample NBP01-01 S3-II. The sample is vesicular basalt that contains porphyroblasts of clinopyroxene and orthopyroxene in a fine matrix most likely composed of plagioclase, apatite, and pyroxene.

In the center of the top photomicrograph is a vesicle that displays secondary mineralization around the rim of the cavity, seen best in plain light.

The bottom photomicrograph displays the porphyroblasts of pyroxenes found within this rock in cross polarized light.



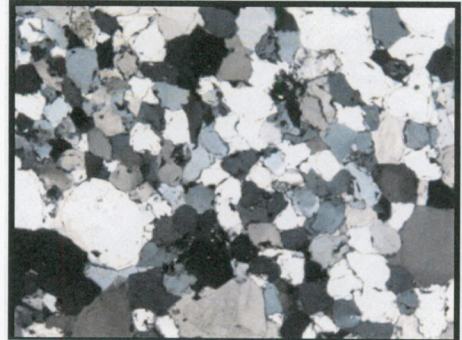
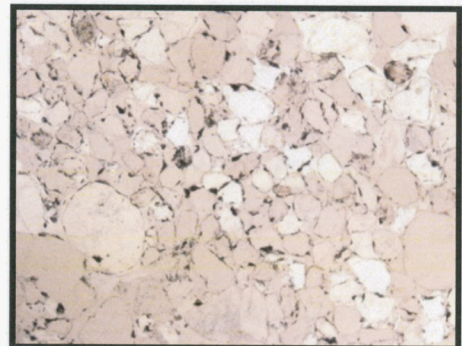
**Biotite Schist from the George V Coast**  
*NBP01-01 S4 D2 B7*



The dominant mineralogy in this rock is biotite. There appears to be two phases of biotite; euhedral grains that have a preferred orientation creating a fabric and subhedral grains that have no preferred orientation. A weak fabric can be seen best under plain light and higher magnification.

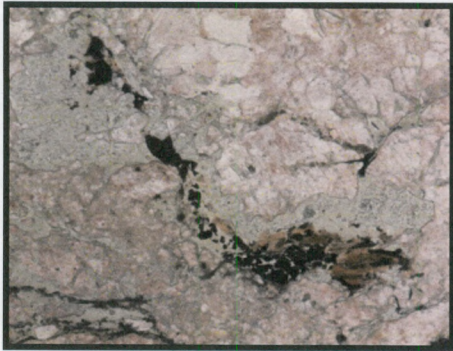
## Meta-sandstone from the George V Coast *NBP01-01 S5 D3 B7*

The sample is a metasandstone that contains subrounded quartz grains and minor amounts of biotite. Some quartz grains contain several inclusions. The quartz grains display some recrystallized textures suggesting this rock experienced low-grade metamorphism. There appears to be opaque minerals found within the cracks between quartz grains believed to be Fe-oxides.

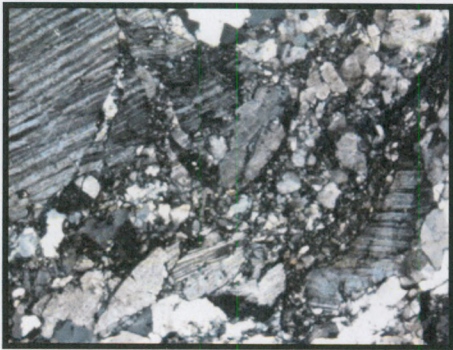


## Meta Granitoids from the George V Coast

*NBP01-01 S5 D3 B5*



The rock contains highly deformed plagioclase grains, which have several cracks and quartz with recrystallized textures.



The top photomicrograph displays an antigorite / Fe-rich chlorite (seen pale green in plain light). Enclosed within the chlorite is Fe-oxide minerals (opaque). As well as an unknown brown mineral that appears to be a mica.



The middle photomicrograph displays deformed plagioclase and quartz grains. These appear as regions or veins within the sample that have finer grain quartz and fractured feldspars.

The bottom photomicrograph is a feldspar grain with poikiloblastic texture. Cutting the grain is a chlorite (extinct). Above is a grain of quartz and below the grain is biotite. The opaque mineral to the right is a mixture of iron oxide and rutile.

## Meta Granitoids from the George V Coast *NBP01-01 S5-B2*

Sample NBP01-01 S5 B2 contains quartz plagioclase, biotite, muscovite and minor amounts of potassium feldspar and chlorite.

The quartz and feldspars crystals are highly fractured and clay minerals have recrystallized in the cracks (top photomicrograph).

The bottom photomicrograph displays a biotite grain altering to an Fe-rich chlorite. To the right is a white mica.

The image above displays an altered plagioclase feldspar grain where the plagioclase is altering to a clay mineral.





## Meta Granitoids from the George V Coast

### *NBP01-01 S3-D1-B1 A*

Sample NBP01-01 S3-D1-B1 A contains a dominant mineralogy of quartz and plagioclase with biotite and chlorite as well as accessory rutile, garnet and amphibole.

The top two photomicrographs to the right display biotite reacting to chlorite. The blue color of the chlorite suggests it to have a high concentration of iron.

The bottom two photomicrographs are of a garnet grain with a biotite corona seen in plain light, and a quartz grain, presently extinct, but showing alteration to most likely clay minerals.

